Master Thesis

Investigation of inland ship resistance, propulsion and manoeuvring using literature study and potential flow calculations

Author:
Erik Rotteveel

Supervisor:
Frans Quadvlieg

Graduation report
MSc Marine Technology
Science Track, Ship Hydromechanics
Student number: 1508342
E-mail: erik.drw@gmail.com

Graduation Committee:
Prof.dr.ir. R.H.M. Huijsmans
Dr.ir. H.J. de Koning Gans
Dr.ir. R.G. Hekkenberg
Dr.ir. S.L. Toxopeus

Submitted to the Department of Maritime Engineering on September 24, 2013 in partial fulfilment of the requirements for the degree of Master of Science in Ship Hydromechanics

Abstract

Manoeuvring simulations can be of good use in determining whether an inland ship may be allowed access to a certain channel/river or not. The SURSIM mathematical model is able to predict the necessary manoeuvres and can therefore be used to determine the acceptance of ships on fairways. However, the SURSIM program is mostly developed for use with sea-going ships, and therefore effort is put in investigating how the SURSIM model should be adjusted to be useful for inland ship manoeuvring simulations. This report particularly focuses on the shallow water corrections for resistance, propulsion and manoeuvring forces. It is chosen to carry out a literature study into inland ship resistance and propulsion, while for manoeuvring potential flow calculations using DelKelv are carried out. The performance of DelKelv calculations in the field of ship manoeuvring is tested using a validation study, and afterwards shallow water corrections for an inland ship are computed using potential flow theory. Chapters 5 to 7 discuss the literature study into inland ship resistance, propulsion and manoeuvring. Chapter 8 discusses the validity of potential flow calculations, while chapter 9 gives a review on the performance of the SURSIM model for inland shipping. Conclusions emerging from the study are given in chapter 10. I would like to thank Frans Quadvlieg and Serge Toxopeus from MARIN for providing me with great assistance on the project. Also, I would like to thank my graduation committee - René Huijsmans, Robert Hekkenberg and Henk de Koning Gans - for providing me with useful feedback on the study and the report itself. Finally, thanks go out to my girlfriend Ariënne who helped me a lot on writing this report in correct English.

Nomenclature

β	Drift angle of ship (angle between heading and course)
π	Pi number, 3.14159265.....
ρ	Water density, 1000 kg/m^3 for fresh water $[kg/m^3]$
A_m	Area of submerged part of midship cross-section $[m^2]$
B	Ship breadth $[m]$
C_b	Block coefficient $\frac{\nabla}{LBT}$
C_L	Lift coefficient
C_p	Prismatic coefficient $\frac{\nabla}{A_m L}$
$C_{m_{yy}}(h, x)$	Added mass distribution correction factor
C_{WD}	Keel clearance to water depth ratio $(h - T)/h$
F_x	Lift force, acting in positive x-direction $[N]$
F_y	Lift force, acting in positive y-direction $[N]$
$F_{lat,\beta}$	Sway force divided by the sine of the drift angle $[N]$
F_{lat}	Sway force acting on ship $[N]$
g	Gravity acceleration, $9.81 m/s^2$ $[m/s^2]$
h	Water depth $[m]$
$k(h)$	Double aspect ratio, $2T/L$

L_{pp}	Ship length between perpendiculars $[m]$
L_{wl}	Ship length at the waterline $[m]$
$M_{rr}(h)$	Total yaw added mass $[kgm]$
$M_{yy}(h)$	Total sway added mass $[kg]$
m_{yy}	Longitudinal distribution of added mass $[kg/m]$
$N_{uv}(h)$	Lateral hull moment coefficient $[Ns^2/m]$
p	Pressure $[N/m^2]$
r	Rate of turn [rad/s]
$R_T(\infty)$	Resistance at deep water [N]
$R_T(h)$	Resistance at shallow water [N]
S_W	Wetted surface of ship hull $[m^2]$
T	Ship mean draught $[m]$
U_R	Return flow velocity $[m/s]$
$V_s(h)$	Ship speed, eventually depending on water depth $[m/s]$
W_C	Channel width
$w_P(h, \beta)$	Propeller wake fraction, eventually depending on drift angle or water depth
x	Longitudinal position in the earth-fixed coordinate system $[m]$
y	Lateral position in the earth-fixed coordinate system $[m]$
$Y_{uv}(h)$	Lateral hull force coefficient $[Ns^2/m^2]$
z	Vertical position in the earth-fixed coordinate system $[m]$
Z_s	Sinkage of the ship $[m]$

Contents

List of Figures

List of Tables

Chapter 1

Introduction

Mathematical models are frequently used to simulate the manoeuvring behaviour of ships. Most of the models consist of a set of empirical formulas to estimate the forces acting on the ship. These forces are then used to determine the dynamical behaviour of the ship, which by itself will result in a new set of forces. These are then used in a following time step to determine the movements again. In this way, a simulation is made of the ship carrying out a specific manoeuvre or navigating through a river. This simulation can be carried out in fast-time or in a real-time simulator.

At the moment, there is interest to use these mathematical models to determine if a specific inland ship type should be allowed to navigate on a certain channel or river. Whether a ship is authorized to sail on a certain fairway or not, usually depends its ability to carry out specific manoeuvres. A mathematical model can - if it is correctly adjusted for the considered ship type - give an accurate prediction on how the ship will perform a specific manoeuvre, without executing expensive model tests or even real-world tests.

Usually, a mathematical model such as described above is implemented in a software program. An example of such a program is SURSIM. SURSIM is a manoeuvring simulation program developed by MARIN. The software is dedicated to the simulation of the manoeuvrability of mainly twin-screw ferries, cruise ships and motor yachts. In SURSIM, a modular approach is used. Forces on the hull, rudder and propellers are calculated separately. In the case of inland ships - which often encounter shallow water environments - the forces are first determined for deep water and are then corrected for shallow water environments by a set of correction formulas.

This study will mainly focus on these correction formulas. A disadvantage of the

correction formulas implemented in SURSIM is that their development is based on sea-going ships primarily. Because inland ships are significantly different from sea going ships with respect to design, the methods used to correct forces acting on the ship for shallow water may not perform sufficiently when applied to inland ships.

The study consists of two parts. The first part gives a review on methods found in literature to determine resistance, propulsive performance and manoeuvring hull forces in shallow water. The second part investigates possibilities of applying potential flow theory in the field of ship manoeuvring, and describes the application of numerical potential calculations to determine linear hull forces for ships sailing in shallow waters.

The goals of this study are:

- Reviewing the available literature on ship resistance, propulsion and manoeuvring forces.
- Investigating the possibilities of potential flow theory for estimating linear hull forces for ships under certain motion.
- Using numerical potential flow calculations to determine linear hull forces on inland ships in deep as well as in shallow water, and using the corresponding results to improve the shallow water correction implemented in SURSIM.

Following the study, information is available on how to improve the mathematical model in SURSIM for application to inland ships. Certain improvements can be applied to give the possibility to determine if a ship is accepted or not on a certain fairway, based on both fast-time simulation as well as real-time simulations using a simulator.

Chapter 2

Problem description

In the introduction, it is already mentioned that the development of methods to correct forces acting on the ship for shallow water is mainly based on research on sea-going ships. This gives reason to improve the methods so that they provide more accurate results for inland ships. This chapter will give an overview of the problems that need to be overcome in this study.

2.1 Differences between two shipping worlds

There are many differences between sea-going ships and inland ships. Not only do they differ in design, the parameters that influence the manoeuvring behaviour are also different. The following lists some important aspects of inland ships which are not observed in sea-going ships.

- **Dimensions.** As inland ships need to be able to navigate at shallow water, the ships are designed for little draught, especially when compared to their length and breadth. This results in high B/T ratios and low T/L ratios. Also, length and breadth is limited due to maximum lock dimensions, regulations considering the crew numbers or size restrictions on certain fairways. To still have a load capacity as high as possible, block coefficients are usually high compared to sea going ships.

- **Appendages.** Inland ships are frequently equipped with various types of appendages. Tunnels are usually found at the aft ship section. These tunnels are

required to keep the propellers from ventilating, which occurs because the propellers are not far below the free surface. This is due to maximizing propeller diameter at relatively low draught. Other appendages are skegs for course stability and gondolas for engine placement and decreasing the space required for the engine room.

- **Restricted waters.** All inland ships are often subject to shallow waters and narrow channels. These affect the flow around the ship significantly, usually increasing resistance and hull lift forces, and decreasing propulsive efficiency due to an increased wake fraction. Also, the sinkage and trim of the ship are increased, resulting in a different submersed hull shape which then affects the hull forces again.

- **Current flow.** In rivers and channels, flow of water is always present. Even up to speeds of 2 km/h, which is high given that inland ships do not often exceed speeds of 20 km/h. Sailing against the current increases resistance, but also increases manoeuvrability. Sailing along with the current results in a less manoeuvrable ship, which means less safe navigation.

Ideally, all of the effects above should be taken into account in order to develop a method that determines forces acting on an inland ship in an inland waterway environment. However, this would lead to a very complex method, and a very extensive study to test the influence of all these effects. In chapter 3, the scope and limitations of the study are described.

2.2 Fast-time simulations

CFD (Computational Fluid Dynamics) calculations can give a very accurate estimate of the forces that act on an inland ship in various environments and situations. However, the time required for a single CFD calculation is still too much to use CFD for real-time or fast-time simulations. Therefore, one should stay with empirical formulas to determine the forces acting on a ship. Still, CFD can be used to conduct a systematic series of calculations in order to develop empirical formulations.

In this study, effort is thus made to investigate the possibilities to accurately estimate the manoeuvring behaviour of inland ships based on empirical methods.

Chapter 3

Objectives and scope

This chapter describes the objectives of the study, it presents the limitations of the study and describes the questions that should be answered after this study.

3.1 The SURSIM program

The study is focused on improving the SURSIM program. SURSIM is a simulation software program developed at MARIN. It's development was dedicated to the simulation of the manoeuvrability of mainly twin-screw ferries, cruise ships and motor yachts. The theory in the program is based on the slender body theory, see [32], and the cross flow drag theory, see [14], [15] and [13]. Example validation studies of the SURSIM program can be found in [34].

3.2 Objectives

The study has two main objectives. These objectives are:

- **First objective: improving the mathematical model of SURSIM to obtain accurate simulation of inland ship manoeuvring.** The first objective is to improve the formulations implemented in SURSIM so that the software can be applied to inland ship manoeuvring. Resistance, propulsion and manoeuvring hull forces are considered. Formulations will be derived from both literature study and systematic computational research.

- **Second objective: determine if DelKelv is able to determine the linear manoeuvring behaviour of ships sufficiently accurate.** The second objective is to test the usability of the potential flow program DelKelv for prediction of ship manoeuvring. This will include a study on the application of the Kutta condition using a wake model, and it will be researched how this model should be applied to a ship geometry.

3.3 Scope of study

The scope of this study includes conventional inland ships only, meaning push-barge convoys are not included. For conventional inland ships, methods will be proposed to determine hydrodynamic hull forces, moments and added mass in shallow water. Further, propulsion forces are also considered. Forces due to wind are excluded, and forces due to rudder action are treated in research at MARIN and are therefore no part of this study. The following sums up the limitations of this study:

- Channel width variations are not included. Although some model experiments need to be validated including channel width, the effect of width on hull forces is not investigated. For some situations - as for sailing on the Amsterdam-Rhine channel - this may have a significant effect. However, for vessels sailing at the river Rhine or other wide waters, the effect of width is assumed to be small.

- Ship-to-ship interactions are excluded. When ships pass each other, there is a significant amount of suction between these ships. However, including ship-to-ship interactions is of less importance when investigating shallow water corrections or sway force for a ship under drift. Therefore, ship-to-ship interactions are excluded from this study.

- Shallow water effects on resistance and propulsion are only investigated using literature study. More research is still needed in this field, however it is not possible to include extensive research on resistance and propulsion in this study.

- The study to determine correction methods for manoeuvring hull forces will only investigate linear forces. Non-linear forces are determined by the cross-flow drag theory [13]. In earlier work on shallow water manoeuvring, only

corrections for linear forces are given and the shallow water effect on non-linear forces is considered to be an effect of higher order.

- Only motions in the horizontal plane are considered. This means that the influence of heave, pitch and roll on ship manoeuvring performance is not taken into account in the present study. It is known that these quantities have an effect on ship manoeuvring. For example, the lateral area of the ship is altered due to heave and pitch, resulting in different lift forces for a ship under drift, especially for very shallow water. These effects are not taken into account in the present study, however.

- Only straight forward sailing is considered in this study. Backing, stopping or sidewards motion ($\beta = 90$) are not considered.

3.4 Questions to be answered

Based on the goals of the study and its limitations, the following main research question will be answered during this study:

"How should a mathematical model that is based on empirical methods for manoeuvring simulation be improved for application to inland ships in their normal operational conditions, using both literature study and potential flow calculations?"

The main question is split up in several sub-questions. Each sub-question will answer part of the main question. The first question involves the literature study into inland ship resistance and propulsion.

"Which methods are available to estimate resistance and propulsion performance for inland ships, and how do these compare to the methods currently implemented in the mathematical model?"

After answering this question, ship manoeuvring in shallow water is investigated. As this part of the study also involves numerical potential flow calculations, the following question needs to be answered first:

"Is potential flow theory, combined with the panel method, an accurate method to predict ship manoeuvring forces acting at the ship hull for deep water, as well as shallow water?"

This question will be answered by carrying out a validation study for various hull shapes of which model test results are available. Then, if potential flow theory proves

successful in estimating the forces, we can see how the results compare to the methods implemented in the mathematical model:

"How do results from numerical potential flow calculations compare to values obtained from methods implemented in the mathematical model or found in literature?"

Then, it should be possible to derive improved versions of the shallow water corrections implemented in the mathematical model. To be able to derive these equations, we have to know which parameters are of importance here.

"Which parameters are of importance when considering inland ship resistance, propulsion and manoeuvring in shallow water?"

Answers to the questions are included in the parts of this report from which the answer to a certain question should be clear. At the end of this report, a sum-up of all the questions with their corresponding answers is given.

Chapter 4

Work plan

This chapter presents the work plan during the study. The work plan is set up in such a way that a good sequence in answering the questions is found.

4.1 Literature study on resistance and propulsion

A literature study on inland ship resistance and propulsion is conducted. The main focus of this literature study lies on the correction of resistance and propulsion performance for shallow water. Various methods found in literature will be compared with the methods implemented in the mathematical model.

4.2 Investigation into inland ship hull forces and moments

This part of the study consists of several steps. First, literature is studied to find methods to determine manoeuvring hull forces acting on inland ships. Then, DelKelv - a program that implements the panel method to numerically solve a potential flow problem - is used to determine hull forces at various ships at various water depths. The program results are first validated with model experiments for various ship hull forms. Then, computational results are compared to methods found in literature and the method implemented in the mathematical model considered.

4.3 Derivation of new methods

Based on the literature study into resistance and propulsion, methods are proposed to use in the mathematical model. For manoeuvring forces, potential flow calculations are executed to investigate how the methods currently implemented in SURSIM should be modified.

4.4 Build-up of the report

Chapters 5 and 6 covers the literature study described in 4.1. These chapters also cover the propositions for methods to be used in the mathematical model. Chapter 7 covers the literature study into methods to estimate the manoeuvring performance of inland ships, while chapter 8 covers an explanation of the DelKelv software, validations studies and comparison of DelKelv results with methods found in literature and the method implemented in the mathematical model. After that, chapter 9 covers a study using DelKelv for various inland ships to see how the methods currently being used in the mathematical model should be improved for use with inland ships.

Chapter 5

Inland ship resistance

This chapter covers a literature research into inland ship resistance. This literature study is included since the resistance of an inland ship can significantly influence the manoeuvring behaviour of a ship. For example, a higher resistance will result in a higher propeller thrust to maintain speed. Larger thrust results in stronger flow about the rudder, which increases the rudder forces. Therefore, a good estimate of ships resistance can improve the overall quality of the manoeuvring simulation. The chapter will mainly focus on shallow water resistance estimation methods found in literature. Deep-water resistance can already be estimated sufficiently accurate using Holtrop and Mennen, also for inland ships since this type of ships is added to the database and thus included in the updated method.

5.1 Resistance determination in SURSIM

As the goal of the study is to find an improved method to determine inland ship resistance for the SURSIM simulation software, the method for resistance determination SURSIM is described here. SURSIM determines the resistance in two steps; first, the deep water resistance is estimated using the method of Holtrop & Mennen [11], or any other method if preferred. It is also possible to directly use a trend derived from model experiments. Once the deep water resistance is known, a correction is applied for shallow water using equation 5.1. It is not known exactly where this correction formulate originates from, but graphs in this chapter show that it is probably based on the method of Lackenby [20].

$$\frac{R_T(h)}{R_T(\infty)} = 0.125 + 0.875\left(K_{WD0} + 0.4\frac{B}{T}K_{WD1}\right) \tag{5.1}$$

In which:

$$\begin{aligned} K_{WD0} &= 1.0 + 0.97\exp\left(-2.74C_{WD}\right) \\ K_{WD1} &= 0.75\exp\left(-4.875C_{WD}\right) \\ C_{WD} &= \tfrac{h-T}{T} \end{aligned}$$

The method for resistance correction for shallow water implemented in SURSIM thus relies on the fraction between keel clearance $(h - T)$ and the water depth h, as well as on the B/T ratio. The method does not take squat (sinkage and trim) effects into account. The method described by equation 5.1 is compared to various methods described in the next section.

5.2 Literature on inland ship resistance

A variety of work is available on ship resistance estimation methods, for deep water as well as for shallow water. Even some methods specifically developed for inland ships are available. This section gives an overview of methods for resistance estimates found in literature.

5.2.1 Deep water resistance estimates

Although it is mentioned already that the method of Holtrop & Mennen is probably sufficient for deep water resistance determination, a short description of other methods found in literature is given here. The method of Holtrop & Mennen [11] is the most well-known method for resistance estimation of a wide variety of ships. The method requires quite a lot of input parameters, but it also gives an advice on which values to choose for some parameters, based on the other parameters given by the user.

A main remark on this is that the method is primarily based on sea-going ships, which are significantly different from inland ships. Inland ship dimensions lie in the outer regions of the application range of the method. The advised values for some parameters may thus be inaccurate as they are determined using statistical information that mainly consists of data from sea-going ships. The advised *half entrance angle* is an example for this, the advised value is usually too high for inland ships. This parameter has a relatively strong impact on the wave resistance estimation.

Holtrop also developed a method for use with barges [12]. This method requires only little input, and is validated with a variety of barge-shaped hull forms with high block coefficients, such as is usual for inland ships. This method is therefore interesting to investigate somewhat further. Looking at the range of validity for the method, the L/B ratio of the ships in the used dataset is between 2.5 and 7.5. Typical inland ships have higher L/B ratios (Kempenaar 7.6, 110 m 'standard' inland ship 9.6). Another drawback of the method is that appendage resistance is not included. According to Holtrop, a large skeg (used for increasing course stability) may result in a 50 percent resistance increase.

Another method is that of Latorre & Ashcroft, described in Terwisga's literature research on barge resistance [31]. It's purpose is to estimate the resistance of a barge in deep water. The method's range of application is for L/B ratios between 4 and 5, and B/T ratios between 2 and 3. Although an average inland ship will not have dimensions within this region, the method of Latorre & Ashcroft is developed based on tests with various bow and stern shapes, among which are also shapes typically seen at inland vessels.

Terwisga [31] also describes the method of Dai. The method of Dai applies for a wider range of L/B and B/T ratios, however the bow and stern shapes used during tests do not resemble those seen at typical inland ships. The method will therefore not be considered further in this report.

Pompeé [26] advises to use the method of Holtrop & Mennen or that of Guldhammer & Harvald [37, p.177]. This last method gives results comparable to the method of Holtrop & Mennen, and may, according to Pompeé, be used to estimate deep water resistance of inland ships. A main drawback of the method is that the range of prismatic coefficients C_p (for inland ships; $C_p \approx C_b$) goes from 0.50 to 0.80, while a value of 0.85 is not uncommon for inland ships.

Verheij [36] advises the formula of Gebers, which is a very simple formula for resistance estimation. The method is advised by Graewe [4], who carried out various tests with inland ships, at deep as well as at shallow water. Due to it's simplicity, various hull details are not taken into account, and also the magnitude of the two coefficients (which are determined from a table given by Verheij) will affect resistance estimation significantly.

Altogether, various methods are available to estimate the deep-water resistance of ships. Figure 5.1 shows a comparison of four different deep-water resistance estima-

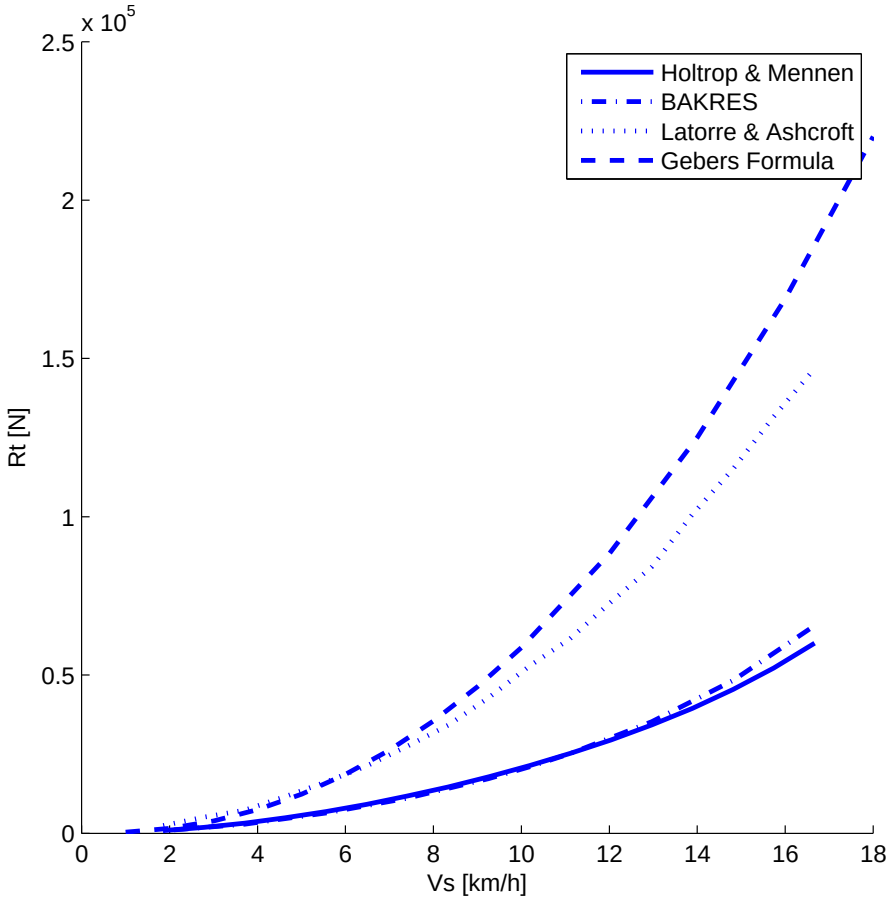

Figure 5.1: Deep water resistance for 110 m inland ship

tion methods. The legend entry 'BAKRES' refers to the barge resistance estimation method from Holtrop, Mennen and van Terwisga [12].

The figure shows that the methods from Holtrop & Mennen and that of BAKRES give very similar results. The methods of Gebers and Latorre & Ashcroft give much higher results. The differences between the methods may lie in the effect of the wave and frictional resistance coefficients (read from graphs or tables), as the advice on which coefficient to used is described somewhat vaguely. For example, the residual resistance coefficient in the method of Latorre & Ashcroft is chosen from a graph with quite large bandwidth. In the present study, the mean value of the bandwidth is chosen, but it could be that for the 110 m inland ship, the lowest values in the

bandwidth had to be chosen.

The methods of BAKRES and Holtrop & Mennen are developed more recently, and although more input variables are required, the methods are based on a wider variety of ships and also inland ships are added to the database from which the Holtrop & Mennen method estimates the ship resistance. Thus, these methods are considered sufficient for determination of inland ship resistance in deep water. Still, the difference between the various methods shown in figure 5.1 is remarkable. A difference of ten to twenty percent may be expected, but these large difference clearly give reason to investigate the resistance of inland ships more deeply, especially since the method of Gebers is based on research on inland ships.

5.2.2 Shallow water resistance

The previous section described some methods available in literature to determine the deep-water resistance of ships, and resistance estimates for a 110 m inland ship where compared using a graph. Since inland ships usually navigate in restricted (shallow and/or narrow) waters, this section will describe methods available in literature that can be used to determine the resistance in shallow water, usually in combination with results from deep-water resistance estimates.

Basically, the shallow water resistance estimation methods give a speed correction or a resistance correction. For the methods that correct the resistance, some methods only correct frictional resistance, while other methods also correct for wave resistance.

The method of Lackenby [20] is probably the most widely known method to correct for shallow water effects. Lackenby extended the work of Schlichting, who created a diagram from which the velocity correction could be read for shallow-water situations. Lackenby derived a formula that can be used to determine the speed loss in shallow water compared to the speed in deep water:

$$\frac{\nabla V_s}{V_s(\infty)} = 0.1242 \left(\frac{A_m}{h^2} - 0.05 \right) + 1 - \left(\tanh \left(\frac{gh}{V_s^2(\infty)} \right) \right)^{\frac{1}{2}} \tag{5.2}$$

Equation 5.2 is meant to be used for determination of speed loss relative to deep water speed. However, for resistance estimation, one would want to determine deep water velocity from the actual ship speed to use as input for a deep-water resistance estimation method. This can be done by rewriting equation 5.2 into:

$$V_s(h) = V_s(\infty) - \left(0.1242\left(\frac{A_m}{h^2} - 0.05\right) + 1 - \left(\tanh\left(\frac{gh}{V_s^2(\infty)}\right)\right)^{\frac{1}{2}}\right) V_s(\infty) \quad (5.3)$$

And solving for $V_s(\infty)$. $V_s(\infty)$ can then be used to estimate resistance using the method of Holtrop & Mennen, for example. The method of Lackenby is frequently used to correct ship speed or resistance for shallow water effects. However, it is very important to notice that the original method of Schlichting was only developed on basis of three warship hull forms, and only for slight shallow water effects. Lackenby only modified the method on theoretical basis, keeping the same experimental test results. The formula of Lackenby, equation 5.2, can be split in a part corresponding to wave resistance and a part corresponding to viscous resistance. Research at MARIN [29] already pointed out that using the Lackenby method for resistance correction gives a relatively high correction for wave resistance, as well as a too high overall resistance estimate. The idea arises that a single correction factor is not sufficient.

Hekkenberg [9] chooses to use the method of Karpov. The method is desribed in [31]. Contrary to Lackenby, Karpov gives a separate correction for wave resistance and viscous resistance. Both the resistance components are corrected by reading a velocity increasing factor from two graphs. The method does not give a correction for h/T values lower than 1.5, which decreases its range of applicability. Unfortunately, the work written by Karpov on this method is not available anymore.

Another single-correction-factor method is developed by Jiang [16]. Jiang's method is based on the so-called effective speed. The effective speed can be seen as a combination of ship speed and return velocity. The formula for the effective speed (denoted here as $V_s(\infty)$) is as follows:

$$V_s(\infty) = V_s(h)\sqrt{\left(1 + \frac{2gZ_s}{V_s^2(h)}\right) / \left(1 - \frac{Z_s}{h}\right)} \quad (5.4)$$

The effective speed determined with equation 5.4 should be used as input for deep-water resistance estimation methods. Since sinkage also occurs at deep water, the effective speed should be determined for deep water as well in order to give a resistance correction for shallow water. Jiang validated his method with two ships, a containership and a 110 m inland ship. For both ships, the method showed to give good results. Still, Jiang's method is not widely used or further validated. Research

at MARIN [29] showed that using this method gives a too low shallow water resistance estimate.

Pompeé proposed a new method to estimate shallow water resistance. His method is primarily developed for inland ships, and depends on the equations of Schijf and the squat prediction method of Romisch. The formulations of both Schijf and Romisch are given in the work of Blaauw and van der Knaap [5]. Separation is made between wave resistance and viscous resistance, similar to the method of Karpov. The method of Pompeé is based on literature research only, so validation is not available at this moment.

Different from the methods given above, the formula of Gebers (described in [4]) gives a resistance estimate without corrections. The shallow-water resistance depends on the return flow velocity only, which can be determined by the equations of Schijf in combination with a squat prediction method. The formula of Gebers is:

$$R_T = \rho g \left(C_1 A_M + C_2 S_W\right) \left(V_s(h) + U_R\right)^{2.25} \tag{5.5}$$

In which C_1 and C_2 are coefficients of which advices are given by Verheij [36]. The method of Gebers is already discussed in the previous section, but it is only used for deep-water resistance estimation there. For shallow water, the method mainly acts as an velocity correction, since the last part $(V_s(h) + U_R)^{2.25}$ is the only part affected by shallow water. It is therefore also a single-factor correction, similar to the method of Lackenby and Jiang.

Various methods for shallow water resistance correction are mentioned. In literature, many more methods can be found to correct shallow water effects. However, a significant part of these methods is developed to correct the resistance of fast ships, which are subject to much more wave resistance than inland ships. Application of these methods to inland ships would thus be useless. It is already seen that for methods that give a separate correction of wave and viscous resistance, the wave resistance correction is very small for inland ships.

This directly leads to an important note on methods that do not give a separate correction for wave resistance; shallow water resistance corrections will be too high for ships that are subject to a significant amount of wave resistance, since the wave resistance correction appears to be small in case of inland ships. The resistance correction thus also depends on the method used to determine deep-water resistance. For example, Holtrop & Mennen and BAKRES give a similar total resistance magnitude,

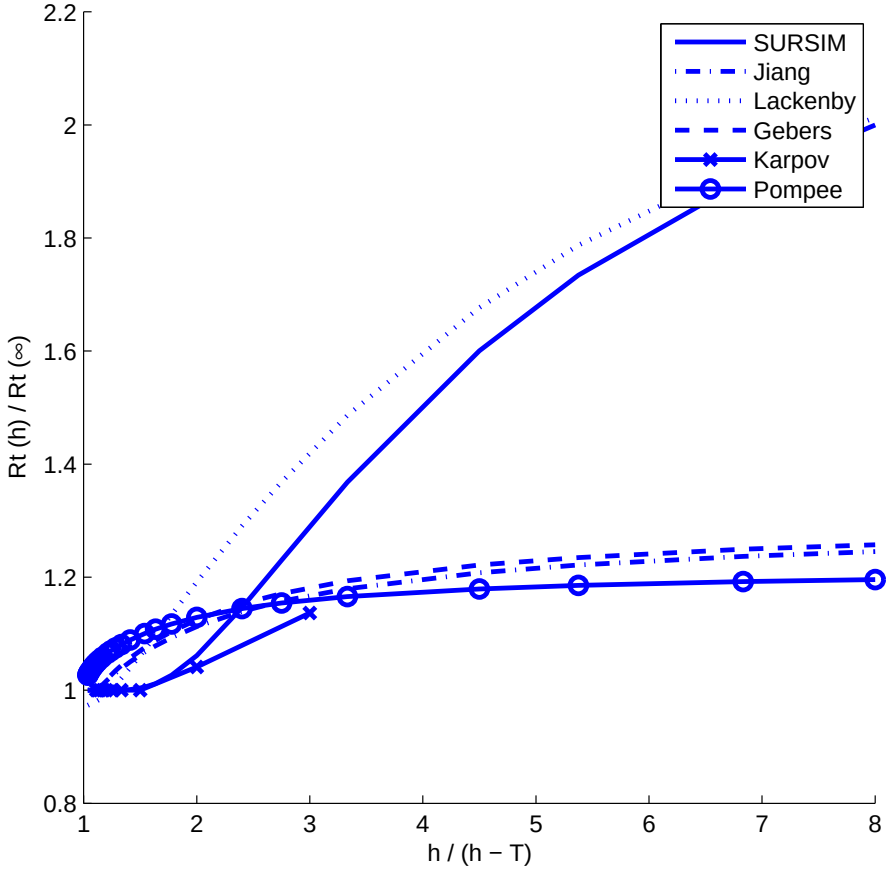

Figure 5.2: Comparison of various resistance corrections

but the composition of both methods is different; BAKRES gives a much higher wave resistance, while viscous resistance is higher in the method of Holtrop & Mennen.

Also for methods that do separate between wave and viscous resistance for shallow water corrections, the method that is used for deep water resistance estimation can affect the shallow water resistance correction. Since different corrections are used for viscous and wave resistance, a different composition of the total resistance will then also yield a different resistance correction for shallow water.

Altogether, there exist numerous methods to determine the shallow water correction of ship resistance. A comparison is given in figure 5.2.

From the figure, it is clearly seen that the method used in SURSIM is derived from

Lackenby's method in some way. The difference between the two curves probably occurs because the calculation method used in this report differs from how it is used to derive the empirical formula in SURSIM. Another observation is that the correction from Lackenby is significantly higher than the methods of Pompee, Gebers or Jiang. Research at MARIN already pointed out that the method of Lackenby gives too high correction for resistance. This same research also showed that inclusion of squat effects for the resistance correction is important. Methods from Pompee, Jiang and Gebers include the effects of squat, indicating that these methods are probably a better option to implement in SURSIM.

At MARIN, research [29] also pointed out that the method of Jiang gives a relatively low resistance estimate, compared to results from CFD calculations and towing tests. The research conducted at MARIN was - however - only aimed at correction of tank towing tests for not too extreme shallow water effects. For that region, the method of Jiang appeared to give too low corrections.

5.3 Conclusion on resistance estimations

The previous sections described various methods to estimate deep-water resistance, as well as methods to correct deep-water resistance estimates for shallow water. For deep-water resistance estimates, the method of Holtrop & Mennen is probably a good method to use. Still, the method is primarily aimed at resistance estimates for sea-going ships that have lower B/T and C_b values, more streamlined appendages and a less full bow section. More research into the resistance of inland ships may significantly improve the quality of a deep-water resistance estimate. For shallow water, it is clear that the method currently implemented in SURSIM gives too high corrections, since its results are similar to those of the Lackenby method, which is known to give too high corrections (apart from the fact that the method gives paradoxial results when it comes to the resistance composition) by research. Methods such as that of Jiang, Pompee or Gebers are known to give too low results. Which also shows that more research is needed in this field as well.

Chapter 6

Inland ship propulsion

The previous chapter discussed the resistance of inland ships. Various methods for deep-water resistance estimation and shallow water corrections from literature are mentioned and compared to each other. In that chapter, it is mentioned that resistance is relevant for a ship manoeuvring simulation because a higher resistance results in higher thrust and consequently a higher velocity along the rudders. Together, this gives a better manoeuvring performance. The mentioned thrust needs to be provided by the engine. In shallow water, the wake fraction is usually increased, while propeller efficiency is decreased. This means that in some cases, the engine may not be able to provide the required amount of thrust, which results in a decreased manoeuvring performance. A brief discussion on propulsion in shallow water is given here.

6.1 Propulsion performance in SURSIM

In SURSIM, propulsion parameters (thrust, torque, etc.) can be determined in various ways. One could use a set of propeller series formulations, but it is also possible to just put in a table of thrust value for certain situations. Thus, it is possible to use Wageningen B-series, Kaplan series or Meyne VBD series (a ducted propeller series that is specifically designed for inland ships, giving higher efficiency at low speeds and heavy propeller load), but also custom propeller performance data. (if a ship is known to have a custom propeller, for example). For shallow water, no method is implemented to correct wake fraction, thrust deduction or propeller efficiency.

6.2 Literature on inland ship propulsion

From literature, it is clear that there is an effect on propulsion from shallow water, for the wake fraction as well as for the thrust deduction factor. Unfortunately, there is no empirical method derived yet due to the lack of data. This by itself is a consequence of the fact that real-world wake field or thrust deduction measurements are still very complex. The following mentions some literature on both wake fraction and thrust deduction in shallow water.

6.2.1 Shallow water effect on wake fraction

Harvald [8] carried out model tests with a bulk carrier model equipped with pitot tubes behind it in order to determine the wake field at several water depths. His results show that the wake factor increases by 40 percent at a water depth to draught ratio of 1.5.

Raven [27] carried out a research into the effects of restricted water on the viscous resistance and propulsion factors of a ship. Experiments have been carried out with an inland ship of the type "Kempenaar" and it is found that the wake fraction even increases up to 0.6 at h/T values of 1.3. A significant change of the wake fraction was found at h/T values below 3.

Raven also mentions the formula from Basin and Miniovich to determine the wake fraction for inland ships. The method does not include water depth, while other research clearly shows that there is a certain effect of water depth on the wake fraction of a propeller.

At MARIN, the wake fraction of various ships at shallow water is studied using CFD calculations. The advantage of CFD calculations is that it gives good possibilities to determine the wake fraction in shallow water. A good trend is not yet found for the wake fraction at shallow water, but a decrease of 5 to 25 percent for the advance velocity $(1 - w_P)$ is found. This is significantly lower than what is found in earlier research.

Górski [3] carried out calculations with a push-barge train to show the effect of limited width and depth of channels on propeller performance. The subject push boat is a very specific one, equipped with one centre propeller and two, smaller, side propellers. The paper written based on this research shows the results from the calculations, which are carried out at model scale. The results show an increase

of wake fraction at decreasing water depth. At certain point the increase of wake fraction stalls and it seems a certain limit for the wake fraction is reached.

Altogether, very little accurate information is available on the ship wake fraction at shallow water. Much more research is still needed in this field. The data from Raven's research with the "Kempenaar" type vessel can be used to estimate the increase of wake fraction for inland ship simulations at shallow water. The wake values from this research are plotted against $h/(h-T)-1$ in figure 6.1. Wake fraction factors for the KVLCC2 are also included. It is interesting to notice that the wake fraction correction of both the KVLCC2 and the kempenaar approximately lie on the same line when plotted against $h/(h-T)$. A trendline is derived from the results and shown in same figure. The equation for this trendline is:

$$\frac{w_P(h,0)}{w_P(\infty,0} = 0.0356\left(\frac{h}{h-T}-1\right)^2 + 0.3356\left(\frac{h}{h-T}-1\right)+1 \tag{6.1}$$

In the figure as well as for the trendline, the value of $h/(h-T)-1$ is chosen as input or x-axis value, instead of $h/(h-T)$. This is done to obtain a trendline more easily. Despite the little basis equation 6.1 can be used to determine the wake fraction at shallow water.

6.2.2 Shallow water effect on thrust deduction

Contrary to the effects on the wake fraction in shallow water, the effects on thrust deduction may not be significant according to Raven [28]. In very shallow water, the suction of the propeller may extend to further upstream, but this is not yet found in literature.

6.2.3 Drift angle effect on propulsion

Apart from shallow water propulsion is also affected by the ships' drift angle. For inland ships, drift angles are relatively large, also for straight sailing. This is due to the low draught, large wind area (lateral area above the water) and low speeds. Hirano showed this in his research [10], and also derived an estimation formula for it:

$$w_P(\beta,h) = w_P(0,h)\exp\left(K_1\beta^2\right) \tag{6.2}$$

Where $K_1 = -4.0$. The method is validated by three sets of model tests and

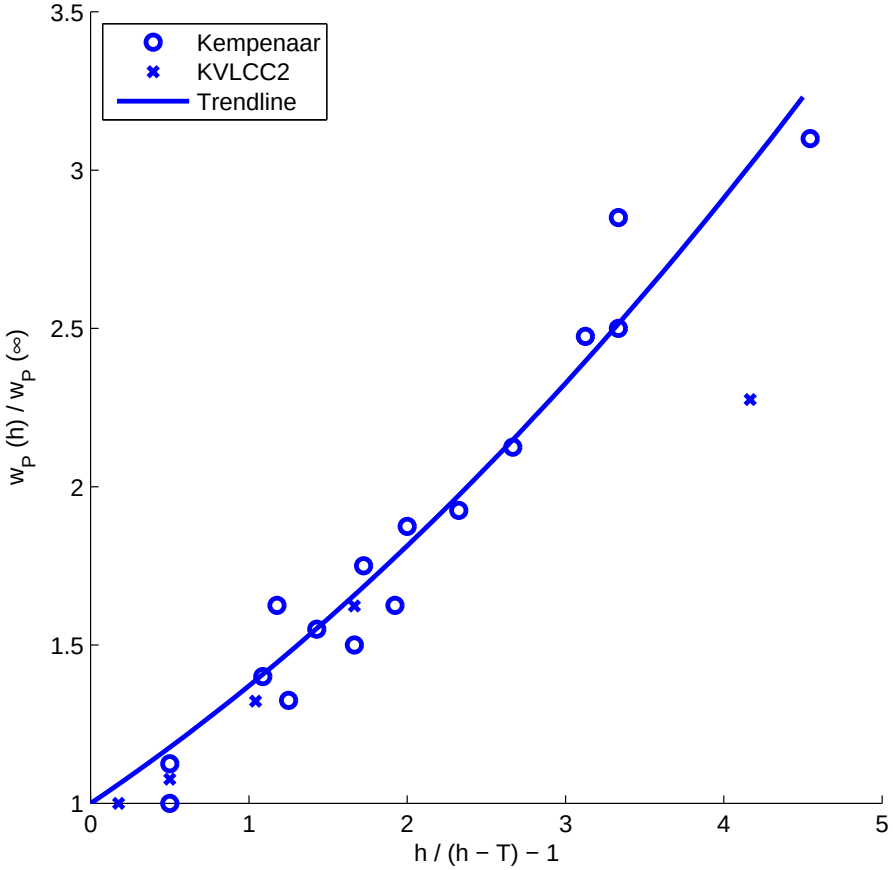

Figure 6.1: Wake fraction values for Kempenaar and KVLCC2 compared to the trendline

real world manoeuvring tests (by comparing these tests to manoeuvring simulations), giving a good agreement between the estimation formula and the test results. Drift angles included in the tests are up to 20 degrees. The tests were carried out for sea-going ships only, but the method may still be used (probably with another value for K_1) to take the drift angle into account for inland ship propulsion.

6.3 Conclusions on inland ship propulsion

From literature, it is clear that much more research is needed in this field. Not only for inland ships, but also for sea going ships, very little information on shallow water effects on propulsion performance is available. However, from the research done with the Kempenaar [27], it is possible to derive a trend which can be used to estimate the increase of wake fraction in shallow water. This trend is given by equation 6.1. The effect on thrust deduction is negligible, according to [28]. Further, there is an effect of drift angle on the wake fraction, which can be estimated by equation 6.2. At this moment, no method is implemented in SURSIM to correct propulsion performance for shallow water. Using the wake fraction trendline and the method to estimate the drift effect on wake fraction from Hirano, an improvement on this can be achieved.

Chapter 7

Inland ship manoeuvring

The previous two chapters discussed the resistance and propulsion of inland ships. Methods for propulsion determination in deep as well as for shallow water are mentioned, and compared to each other. Recommendations were given which methods would be best to use in the SURSIM program. This chapter will deal with the most important part of a manoeuvring simulation program; methods to determine hull forces for ships under drift or rotational motion. The formulations given by Inoue [30] are probably the most simple and widely known formulations to determine hull forces for manoeuvring ships, however SURSIM implements a different approach to determine hull forces. An overview of the methods available is given in this chapter.

7.1 Manoeuvring hull forces estimation in SURSIM

As mentioned in this chapters' introduction, SURSIM does not implement the coefficients given by Inoue. SURSIM uses the slender body method [32] to derive linear hull force coefficients (Y_{uv}, N_{uv}, Y_{ur}, N_{ur}), while for non-linear forces, the cross-flow drag theory is applied [13]. This is different from the well-known MMG model that gives a lateral force composition similar to an Taylor-expansion. A main advantage of the SURSIM model is that the hull forces remain realistic even for very high (90 degrees) drift angles, as well as the ability to take hull details into account for determination of sway forces, for example.

As the main purpose of this study is to improve shallow water hull force estimates,

the method for this currently implemented in SURSIM is given here:

$$\begin{aligned} \frac{Y_{uv}(h)}{Y_{uv}(\infty)} &= K_{WD0} + \frac{B}{T}K_{WD1} + 0.5\left(\frac{B}{T}\right)^2 K_{WD2} \\ \frac{N_{uv}(h)}{N_{uv}(\infty)} &= K_{WD0} + \frac{2}{3}\frac{B}{T}K_{WD1} + \left(\frac{B}{T}\right)^2 K_{WD2} \end{aligned} \tag{7.1}$$

In which:

$$\begin{aligned} K_{WD0} &= 1.0 + 0.97 \cdot \exp\left(-2.74 C_{WD}\right) \\ K_{WD1} &= 0.75 \cdot \exp\left(-4.875 C_{WD}\right) \\ K_{WD2} &= 0.663 \cdot \exp\left(-6.07 C_{WD}\right) \\ C_{WD} &= \frac{h-T}{T} \end{aligned}$$

Comparing to the formulations in section 5.1, SURSIM thus uses similar methods to correct for resistance and linear hull forces. The following section will discuss manoeuvring force correction methods found in literature. For lateral added mass, obviously the same correction is used as for $Y_{uv}(h)$, because the slender body method is used to estimate $Y_{uv}(\infty)$, the scaling of added mass and lateral force must be the same. There is no method implemented in SURSIM to correct for rotational added mass.

7.2 Literature on manoeuvring force correction for shallow water

Various methods have been derived to correct hull forces and added mass for shallow water. Especially for linear forces, a wide variety of methods is available. The following will discuss some of the methods and compare them with the method implemented in SURSIM. First, the methods for force and moment corrections are discussed, and after that some methods for shallow water added mass corrections are given.

7.2.1 Shallow water corrections for forces and moments

Hirano [22] gives a method to specifically correct the force and moment estimates given by Inoue. The correction is simply a modification of the aspect ratio, k, used in the empirical formulas of Inoue. The correction is given by the following formula:

$$k(h) = \frac{k(\infty)}{\frac{Tk(\infty)}{2h} + \left(\frac{\pi T}{2h}\cot\left(\frac{\pi T}{2h}\right)\right)^{\lambda}} \tag{7.2}$$

Where lambda is a factor that needs to be estimated experimentally. Hirano also gives some values for quick usage of his method.

A more widely applicable method is developed by Kobayashi [18]. His method returns a correction factor for the overall lateral force or moment, instead of giving a effective value of a parameter used within a deep-water force estimation method. He validated his method using model tests for three different sea-going ships. His research was based on the MMG model, but the correction of linear forces will apply to the SURSIM model as well. The correction given by Kobayashi is as follows:

$$\begin{aligned} \frac{Y_{uv}(h)}{Y_{uv}(\infty)} &= \frac{\frac{\pi}{2}\left(\frac{1}{\frac{T}{2h}\left(k+\pi\cot\left(\frac{\pi T}{2h}\right)\right)}\right)^{Q_1} + \frac{pC_bB}{L}}{\frac{\pi}{2}k + \frac{pC_bB}{L}} \\ \frac{N_{uv}(h)}{N_{uv}(\infty)} &= \left(\frac{1}{\frac{T}{2h}\left(k+\pi\cot\left(\frac{\pi T}{2h}\right)\right)}\right)^{Q_2} \end{aligned} \tag{7.3}$$

For the value of p, 1.4 can be taken when we compare the lower part of the fraction to the equations of Inoue. For values of Q_1 and Q_2, Kobayashi gives values in his work. All three coefficient can be determined experimentally as well.

Kijima [17] uses a different approach to correct linear hull forces for shallow water. Basically, his method states:

$$D(h) = f\left(\frac{T}{h}\right) D(\infty) \tag{7.4}$$

In which D should be replaced by the hull force of interest. The function f is described as follows:

$$f\left(\frac{T}{h}\right) = \frac{1}{\left(1-\frac{T}{h}\right)^{n}} - \frac{T}{h} \tag{7.5}$$

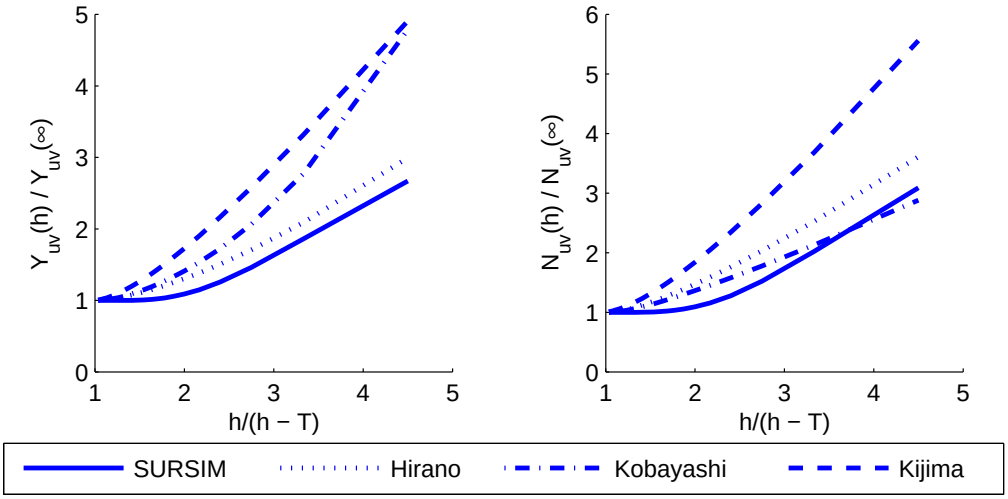

Figure 7.1: Comparison of shallow water corrections of manoeuvring forces for a 110 m inland ship

Where

$$n = \begin{cases} 0.40 C_b(B/T) & \text{if} \quad D(h) = Y_{uv}(h) \\ 0.425 C_b(B/T) & \text{if} \quad D(h) = N_{uv}(h) \end{cases}$$

So far, three methods from literature have been discussed. The methods are all developed for use with the MMG model, but since SURSIM uses the same linear coefficients as the MMG model, the methods described above can also be used for the SURSIM model. In figure 7.1, the methods given above are compared with each other and the formulations implemented in SURSIM. The corrections are computed based on a 110 m inland ship, which was also used for the comparison of resistance correction methods in chapter 5.

The figure shows that the method of Kijima gives the largest correction for shallow water, for both the force and the moments. Hirano and SURSIM give a very similar correction for shallow water. In chapters 8 and 9, the estimation methods will be compared to corrections obtained from potential flow calculations. These calculations are then carried out for the considered 110 m inland ship as well, to see how the methods - developed for use with sea-going ships, perform for an inland ship.

7.2.2 Shallow water corrections for added mass

For lateral and rotational added mass, Li & Wu [21] derived the following methods:

$$\begin{aligned} \frac{M_{yy}(h)}{M_{yy}(\infty)} &= \frac{0.413 + 0.032\frac{B}{T} + 0.0129\left(\frac{B}{T}\right)^2}{(h/T-1)^{0.82}} \\ \frac{M_{rr}(h)}{M_{rr}(\infty)} &= \frac{0.413 + 0.0192\frac{B}{T} + 0.00554\left(\frac{B}{T}\right)^2}{(h/T-1)^{0.82}} \end{aligned} \tag{7.6}$$

Further, Sadakane [7] developed the following method:

$$\begin{aligned} \frac{M_{yy}(h)}{M_{yy}(\infty)} &= 1 - \left(-0.02\frac{T}{B} + 0.07C_b + 0.0098\right) \times \\ &\quad \left(1 - \exp\left(\frac{T}{h}\left(-1.1\frac{T}{B} - 2.2C_b + 7.0\right)\right)\right) \\ \frac{M_{rr}(h)}{M_{rr}(\infty)} &= 1 - \left(-0.02\frac{T}{B} + 0.001C_b + 0.0232\right) \times \\ &\quad \left(1 - \exp\left(\frac{T}{h}\left(-0.75\frac{T}{B} + C_b + 4.405\right)\right)\right) \end{aligned} \tag{7.7}$$

In figure 7.2, the two methods for added mass correction are compared to the method of SURSIM. It is seen that for M_{rr}, the estimation methods found in literature estimate a rotational added mass increase factor between 2.0 and 2.5, while SURSIM does not correct for rotational added mass. A better quality of simulations may be achieved if a correction for rotational added mass is included. The relation between added mass and water depth for inland ships is investigated in chapter 9.

7.3 Conclusions on ship manoeuvring estimation

From the comparisons of various methods, it is clear that SURSIM gives relatively low correction estimates. The difference between the correction estimates is probably due to the fact that the methods are developed for use with sea-going ships, indicating that inland ships may have dimensions outside of the range of application of the methods. Chapters 8 and 9 will show the results of potential flow calculations for inland ships, for lateral forces as well as for added mass coefficients. Since the manoeuvring forces are further investigated by potential flow calculations, no conclusions are given here on the methods discussed in this chapter. Chapter 10 will give conclusions on which

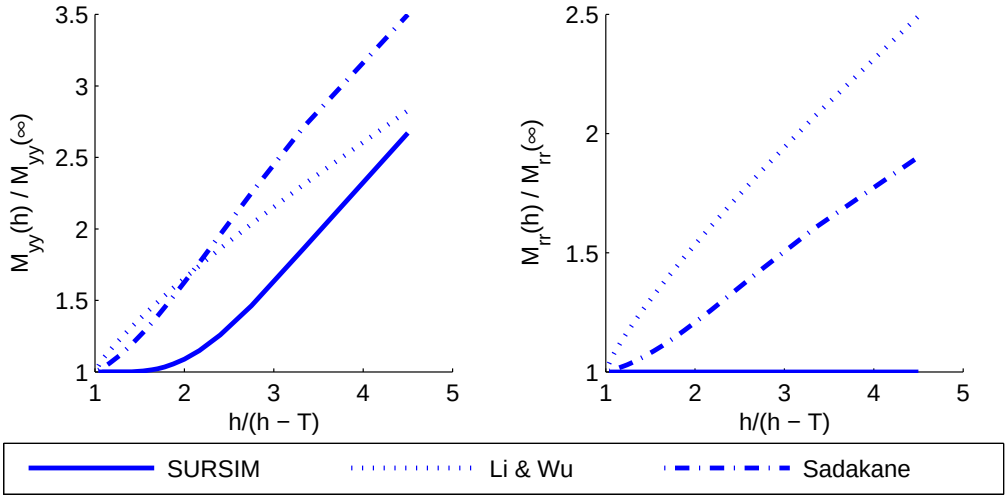

Figure 7.2: Comparison of shallow water corrections added mass coefficients for a 110 m inland ship

method may be sufficient for inland ship manoeuvring estimates.

Chapter 8

Potential flow theory in ship manoeuvring

Up to now, empirical methods for estimation of resistance, propulsion performance and manoeuvring forces in shallow water have been discussed. Various methods were compared to each other, and for resistance and propulsion, an advice was given on which is the best method to use for inland ship manoeuvring simulations. For manoeuvring forces, no advice was given yet, as this chapter will investigate manoeuvring forces in shallow water further by use of potential flow calculations. In the next chapter, manoeuvring force correction methods from literature and SURSIM are compared to values obtained by potential flow calculations.

Potential flow calculations are in fact CFD calculations where viscosity is neglected. This greatly simplifies the calculation, reducing the required amount of computational time and power. Computational time is further decreased by the fact that the equations only need to be solved on the boundaries instead of throughout the whole fluid domain. Normally, it is not possible to use potential flow theory to determine forces acting on a certain body (paradox d'Alembert). But with some adaptations (see appendix A), potential flow can be used to determine lateral hull forces and yaw moments acting on a ship hull. That, together with much faster and less complex calculations, makes potential flow theory a promising tool to predict ship manoeuvring forces, like lateral forces and yaw moments acting on the hull.

For potential flow calculations, the program DelKelv is used. The program is used as it was obtained from Dr. ir. De Koning Gans, with no further adaptations. DelKelv implements the panel method to solve a potential flow problem, and wake

surfaces can be included to capture lift forces and yaw moments acting on the ship hull. The free surface - which can normally be modelled as well to capture forces due to wave formation - is omitted in the present study, since this would introduce non-linear effects such as a drift angle dependent shallow water corrections.

The next section gives an overview of literature that describes potential flow approaches to determine forces acting on ships or other bodies. A detailed description of the DelKelv program can be found in appendix A, while a descrption of the application of DelKelv for ship manoeuvring is given in 8.2. Validation of the DelKelv program is presented in 8.3 for three different cases. Conclusions on potential flow for application to ship manoeuvring are given in the last section of this chapter.

8.1 Literature on potential flow for ship hull forces

De Koning Gans applied the panel method for solving a potential flow problem involving passing ship events [6]. A wake was applied to the passing ship in order to give a more accurate estimation of the forces acting on moored ships. It appeared, however, that the difference in forces on the moored ship was small after a wake surface was modeled behind the passing ship. It is mentioned that for better force estimates, the wake surface should be connected to the ship from keel to free surface.

A 2D-potential flow method was developed by Huet Muñoz to estimate the forces on a moored ship when another ship is passing by [23]. The work is similar to the work of De Koning Gans described above, however Muñoz also validated forces acting on a 2-D van Vooren profile (wing shape), showing good validation with known results. Lift (comparable to lateral manoeuvring force on a ship hull) force on the foil was in good agreement with the force calculated using the method developed by Muñoz. He recommends extending his passing ship code to 3D, since the results of validation between tests and 2D calculations for passing ship events looked promising.

8.2 Application of potential flow to ship manoeuvring

In the introduction it is already mentioned that DelKelv - a software program that implements the Panel Method to solve a potential flow problem - is used for the

potential flow calculations in the present study. For a description of the program as well as for a description of potential flow theory and the panel method, the reader is referred to appendix A. There, an explanation is also given on how the Kutta condition can be enforced in potential flow calculations. This is done by modelling a wake surface. The wall boundary condition is applied to this wake surface, which means that the flow must leave the ship along with the modelled wake surface, at the location where this surface is attached to the ship.

8.2.1 Wake surface construction methods

As the wake surfaces ensures that the flow leaves the ship at a certain position, it is important that the wake surface is constructed such that it is attached to locations where a real flow would also leave the ship. One of these locations is the trailing edge, at the aft end of the ship. Another position may be the bilge at the lee-side (which is portside in the present study), as one can imagine that for a drifting ship, the total wake left behind by the ship gets larger for increasing drift angle. Other locations are tunnels (usually applied to inland ships to prevent propeller ventilation), bilge keels, windward side bilge in the aft ship region and the edge of a submersed transom (also usually seen at inland ships).

In the present study, two different wake surface modelling methods are applied. Both methods are visualized in figures 8.1 and 8.2. The following gives a brief description of the wake models:

- **Wake only at trailing edge**: A wake surface is attached only at the trailing edge of the ship. The surface will extend from the ship's keel ($z = -T$) to the free surface ($z = 0$). No other wake surfaces are modelled.

- **Wake surface at trailing edge and lee-side bilge**: Apart from the wake surface attached to the trailing edge (which is the same as for the description above), wake surfaces are attached to the lee-side bilge as well. The wake surface at the bilge is attached at $z = -T + R_b$, where R_b is the bilge radius and T is the ship draught. Longitudinally, the wake surface reaches from the aft end of the bow (from where the ship is at maximum breadth) towards the trailing edge of the ship. There, the two wake surfaces are connected to each other geometrically.

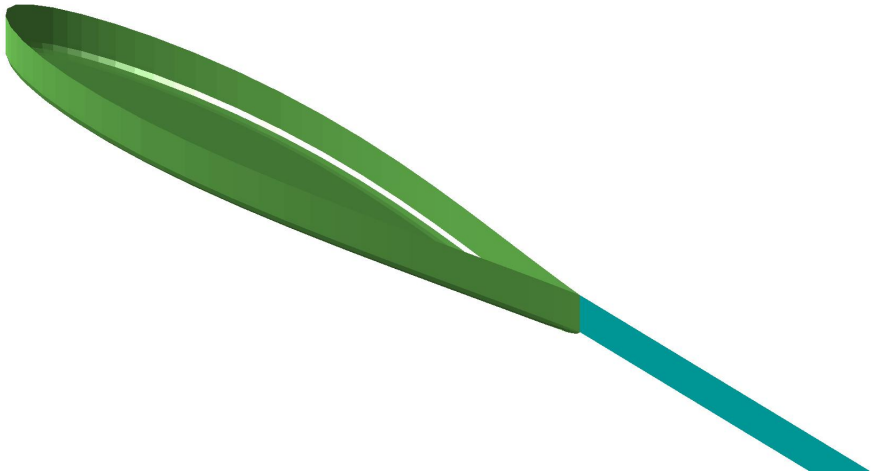

Figure 8.1: Beukelman wing ($\beta = 4$) with a wake surface attached to the trailing edge of the wing only

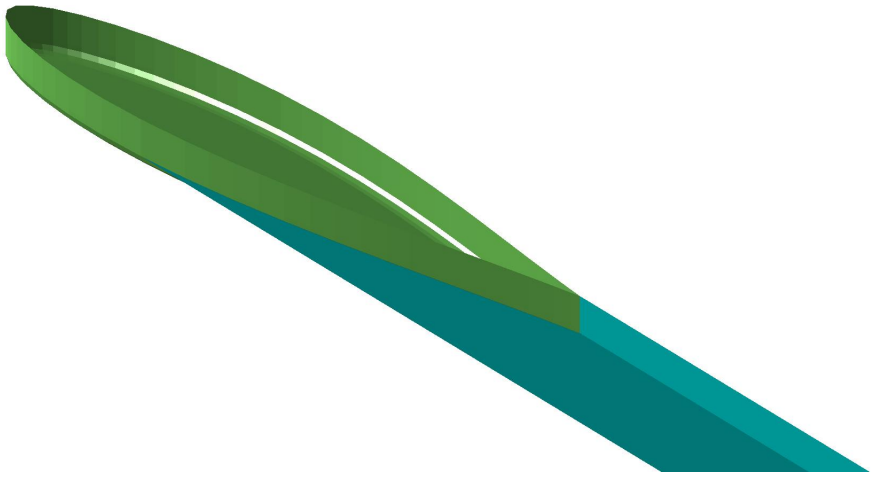

Figure 8.2: Beukelman wing ($\beta = 4$) with wake surfaces at the trailing edge as well as at the lee-side bilge. The lee-side bilge extends from the point where the maximum breadth is reached towards the trailing edge, positioned at the upper border of the bilge

Each of the wake surfaces are modelled such that they are parallel to the direction of the flow (thus parallel to the x-axis). This introduces a small error, as ships usually do not have a straight line trailing edge. The wake surface is attached to the ship with a certain angle, resulting in a slightly curved wake surface. Preferably, one would use a flat wake surface, but the difference due to deformation is small ($< 2\%$), as appeared from testing calculations.

For the wake surface construction including a wake surface attached to the lee-side bilge, lateral force and yaw moments are not zero at zero drift angle. This is due to the fact that the lee-side bilge wake surface only captures the vortex leaving from lee-side. In the aftship region, a vortex may also leave the ship from the windward side bilge. As this vortex (which normally produces a compensating force for the portside bilge vortex) is not modelled by a wake surface at the windward side, the computed force is too high for small drift angles. At higher drift angles, this problem is not present as the flow will stick to the windward side over the entire ship length.

8.2.2 Coordinate systems

During the calculations, an earth-fixed and right-handed coordinate system is used, with the following properties for a ship at zero drift angle:

- X is positive towards the bow, $X = 0$ at midship (ordinate 10).
- Y is positive towards portside, $Y = 0$ at the ship's centerline.
- Z is positive upwards, with $Z = 0$ at the free surface, and $Z = -h$ at the channel bottom.
- β, the drift angle, is positive if the ship bow turns to portside.

The forces and moments determined from DelKelv are defined in the earth-fixed coordinate system as well. This means that for a certain drift angle, equation 8.1 needs to be evaluated to obtain the lateral force, F_{lat}.

$$F_{lat} = F_y cos(\beta) - F_x sin(\beta) \tag{8.1}$$

Moments are determined with respect to midship. Depending on the experimental set-up used, the moments need to be corrected in order to be compared to experimental results. These corrections are described for each case DelKelv is validated for.

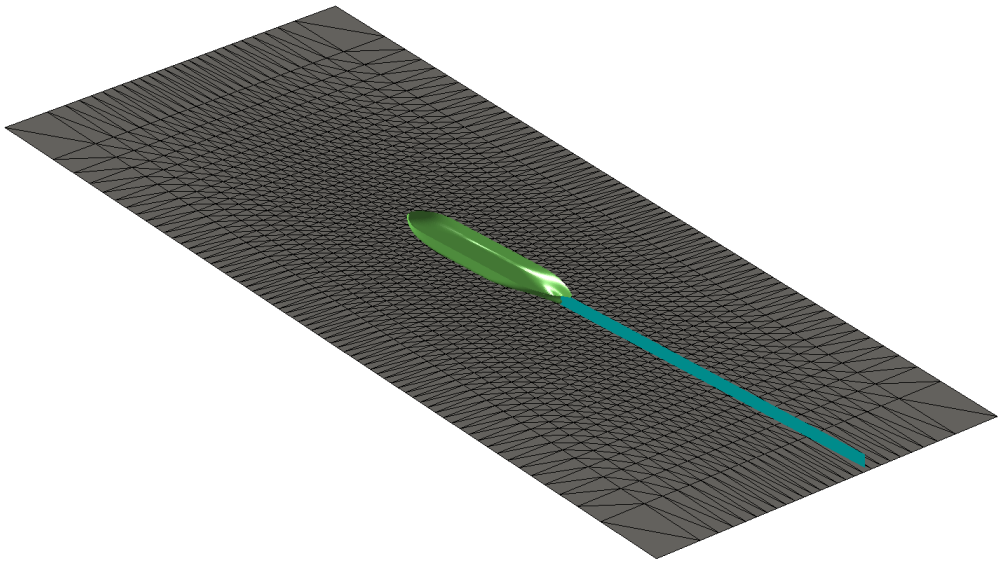

Figure 8.3: Overview of KVLCC2 including a coarse gridded channel for $h/T = 1.5$, $\beta = 4$

Furthermore, the ship hull is located in the middle of the channel, in x-direction as well as in y-direction. This is shown in figure 8.3

8.3 Validation of DelKelv program

The previous section described how DelKelv is used to determine manoeuvring forces. This section will describe the validation of the DelKelv program, which will give an idea on how accurate potential flow calculations are in the field of ship manoeuvring. Validation is carried out for three different test cases:

- **Beukelman surface piercing wing**: Beukelman conducted measurements at the TU Delft towing tank for a simple wing model [1]. He included various water depths, drift angles, draughts and speeds. This is off course not a ship model, but due to the simplicity of the model (from here on called 'Beukelman Wing') is a very good test case for various wake constructions and grid studies. Also, it is an extension of two-dimensional potential flow calculations for foils towards a three-dimensional domain.
- **KVLCC2**: KVLCC2 stands for 'Korean Very Large Crude Carrier, version

2'. This is a so-called benchmark ship. Various models are build of it, but a full scale version was never constructed. The purpose of this benchmark ship is to have a model for which many measurements and CFD calculations are conducted (and of which the results are published), so that more knowledge becomes available on the validation of certain CFD methods, shallow water effects, etcetera. INSEAN conducted model experiments for the KVLCC2 [2] at various drift angles, water depths and speeds. Therefore, it is a very interesting test case to validate DelKelv with.

- **Marin Inland Ship**: The Marin Inland Ship (often referred to as MIS) serves practically the same purpose as the KVLCC2, but in this case it offers possibilities to generate more knowledge on inland ships. At MARIN, tests are conducted at various drift angles and water depths, providing a very good method to validate DelKelv.

The validation studies are described in the order as presented above, thus starting with the highly conditioned Beukelman Wing. For each of the validation cases, a numerical verification study is carried out to determine the required channel length, channel grid density and hull grid density.

8.3.1 Beukelman Wing validation

As stated, the Beukelman Wing offers a very good test case to validate DelKelv with. Not only a lot of tests were conducted, the model itself is a very simple one, providing a straight line trailing edge and a vertically constant hull form (apart from the bilge). This makes it very easy to attach wake surfaces at various locations. Table 8.1 gives the main dimensions of the beukelman wing.

Table 8.1: Main dimensions of beukelman wing

Name	Beukelman Wing	
Length	2.2577	m
Breadth	0.3385	m
Draught	0.1, 0.3	m

The tests were carried out in the towing tank basin of the TU Delft, subject to the parameters given in table 8.2.

Table 8.2: Main dimensions of beukelman wing

Basin length	142	m
Basin width	4.22	m
Basin depth	0.6, 0.75, 2.2 and 2.4	m
Drift angles	4, 8, 12, 16 and 20	deg
Model velocity	0.9412	m/s

The rest of this section will discuss the DelKelv preparations, the comparison method between computational and measurement results and the results them selves. At the end of the section, conclusions on the Beukelman Wing validation study will be given.

Preparations for DelKelv

The Beukelman Wing is given a panel distribution consisting of 3040 panels, which is sufficient according to the grid study described in the next section. The panel size and length of the channel are chosen according to the grid study described in the next paragraph. Near the wing body, the panel size is 0.25 meter, increasing towards the domain ends by an inverse consine function. The length of the channel is 10 meter. The width of the channel is the same as the TU Delft towing tank, namely 4.22 meter.

The wake models for the Beukelman Wing are constructed as shown in figures 8.1 and 8.2. For the second method (where wakes are connected to the bilges as well), some extra research is done by extending the bilge wake to further upstream towards the point where $y = y_{max}$ *after* applying the drift angle. This results in the whole longitudinal projection of the model being covered by wake surfaces.

Numerical verification study

It is mentioned in the previous paragraph that the panel distribution over the Wing body and the channel, as well as the required channel length, are to be determined by a grid study. For the investigation of the panel distribution over the Wing itself, five different panel distributions are applied to the wing. Using a Richardson-extrapolation in the way described by [19] on each combination of three out of the five distributions, the minimum and maximum lateral force in case of infinite panel number is determined. The results of this grid study are shown in table 8.3.

Table 8.3: Wing body grid study for Beukelman Wing in deep water

Number of panels on body	F_Y [N]	e_{F_Y} [%]	N_{ZZ} [Nm]	$e_{N_{ZZ}}$ [%]
800	1.62559	0.00	1.86013	26.63
1800	1.43329	0.00	2.23709	11.77
3040	1.33053	6.21	2.40521	5.14
6960	1.27470	5.03	2.50755	1.10
12160	1.26283	3.25	2.52608	0.37
Extrapolated (coarse grids)	1.25556	0.00	2.76869	0.00
Extrapolated (fine grids)	0.93987	0.00	2.53541	0.00

The minimum and maximum extrapolated values show large difference. The minimum estimated value, however, is obtained when using the three most coarse grids in the Richardson Extrapolation. When a triplet of finer grids is used, the extrapolated value for lateral forces and moments approaches the maximum value given in table 8.3.

It was not possible to increase the amount of panels used even more due to memory allocation problems. As the validation study also includes the use of a channel grid, a less dense grid must be chosen. The estimated error for the grid consisting of 3040 panels is six percent, which is considered as sufficient. For the validation study, the Beukelman wing geometry is thus divided into 3040 panels.

The required grid density of the channel is also investigated. Grid panel sizes are reduced from 0.5 m down to 0.06 m. Within this range, the resulting forces did not significantly change (less than one percent), as shown by figure 8.4. This indicates that a panel size of 0.5 m is already sufficient. Calculations to determine channel grid density was conducted for the case in which T = 0.3 m and h = 0.75 m, resulting in the smallest keel clearance among the available test results. The influence of the wing body on the bottom surface is maximized then, meaning a sufficient grid for this case will also be sufficient for other situations. In further calculations, a grid panel size of 0.25 m is used.

For determination of the required channel length, the length of the channel was increased from 4 to 13 meters, while the channel grid panel size was kept constant at 0.25 meters. The convergence of the lateral hull force is shown in figure 8.5. The graph shows that from a channel length of 10 meters, the error for both yaw moment and lateral force is below one percent. A channel length of 10 meters is therefore considered sufficient. In further calculations, a channel length of 10 meters is used.

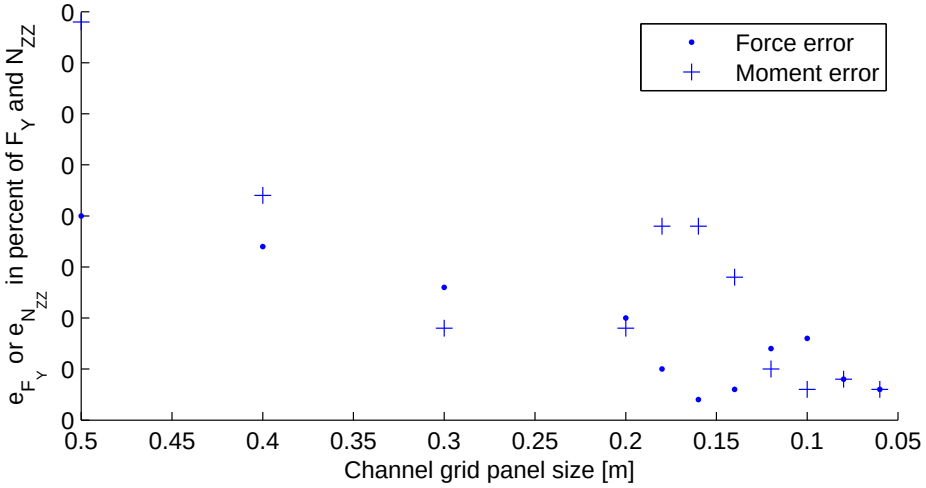

Figure 8.4: Convergence of lateral force on Beukelman wing for decreasing channel panel size, T = 0.3, h = 0.75

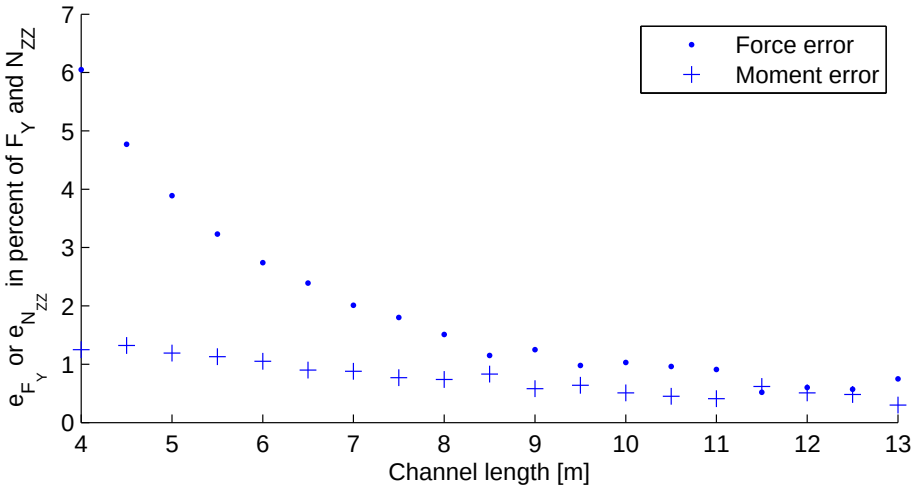

Figure 8.5: Convergence of lateral force on Beukelman wing for increasing channel length, T = 0.3, h = 0.75

Comparison method

Beukelman presents his results in a non-dimensional way, by giving the lift coefficient and the non-dimensional moment about the wing model's leading edge. From DelKelv, the lift force is obtained in Newtons, thus for comparison of lift force, equation 8.2 is evaluated:

$$C_L = \frac{F_y}{0.5\rho V_S^2 LT} \tag{8.2}$$

For comparison of the moment about the mid-ship location (which is obtained from DelKelv), some extra effort is required. Beukelman presents the non-dimensional moment about the leading edge of the wing (C_{M_e}). Equation 8.3 is used to convert C_{M_e}, given by Beukelman, to C_{M_0}. In this equation, e is the distance from the lift force point of action to the wing leading edge.

$$C_{M_0} = \frac{(0.5L - e)\, C_{M_e}}{e} \tag{8.3}$$

The values of C_L and C_{M_0} can be used to compare the results from calculations and measurements with each other.

Results comparison for wake surface only at trailing edge

This section shows the comparison of calculated values with measurement results for the case where a wake surface is only attached to the trailing edge. It is important to note here that it is not expected (or required) that the computational results are exactly the same as the experimental results. For larger drift angles, non-linear and viscous effects influence the results significantly, while in DelKelv the forces and moments increase practically linear with an increase of drift angle. At low drift angles, the results from experiments and calculations should, if the modelling method is correct, approximate each other. The best comparison can therefore be made by comparing the derivatives $\partial C_L/\partial\beta$ and $\partial C_{M_0}/\partial\beta$ at $\beta = 0$. The results from Beukelman and DelKelv are compared graphically in figures 8.6 to 8.9.

From the graphs, it is seen that the forces determined by Delkelv are approximately 50 percent lower than the results obtained from the experiments. The moments from DelKelv, on the other hand, are too high for all calculations. Further, the measurements show a slightly non-linear behaviour which starts from approximately 10 degrees. It appears that only attaching a wake surface at the trailing edge of the wing is not sufficient. The next sections shows the lift force and moment comparison for a more complex wake model, including a wake at the bilge of the wing model.

Results comparison for the wake model at trailing edge and lee-side bilge

Here, a comparison of forces and moments is shown (figures 8.10 to 8.13) for calculations including a wake surface at the lee-side bilge of the wing. For comparison between experiments and calculations, the same method as described in the previous section should be used.

Including the wake at the bilge significantly increases the agreement between the experiments and calculations, as can be seen from the graphs in figures 8.10 to 8.13. For all situations tested, the steepness of the force/moment curves at $\beta = 0$ is nearly equal for calculations and experiments. The explanation for this lies in the vortices leaving the wing model from the bilge in real fluid. Using CFD calculations, it can be shown that a vortex leaves a ship not only at the trailing edge of the ship, but also from the bilge at some point. By attaching a wake at the ship bilge, this vortex can also be 'captured' in potential flow calculations. The influence of this vortex on the integral force depends on the ship's dimensions, and it appears that for the Beukelman Wing, this influence was approximately 50 percent of the total force.

Extending the wake surface to further upstream

In the previous section, the bilge wake starts at the point of maximum width and ends at the trailing edge. For large drift angles, this may cause an inaccuracy in the

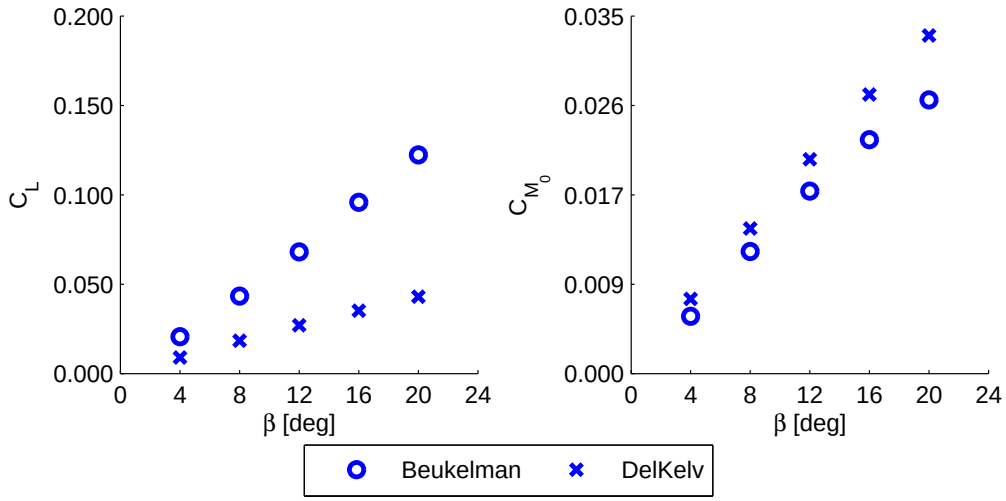

Figure 8.6: Comparison for Beukelman Wing with only a trailing edge wake, $T = 0.1$ m and $h = 0.6$ m

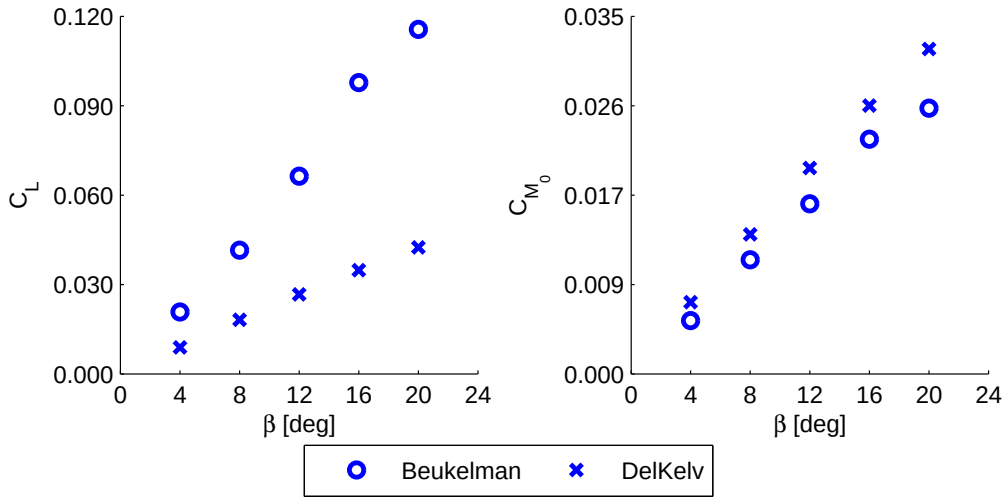

Figure 8.7: Comparison for Beukelman Wing with only a trailing edge wake, $T = 0.1$ m and $h = 2.2$ m

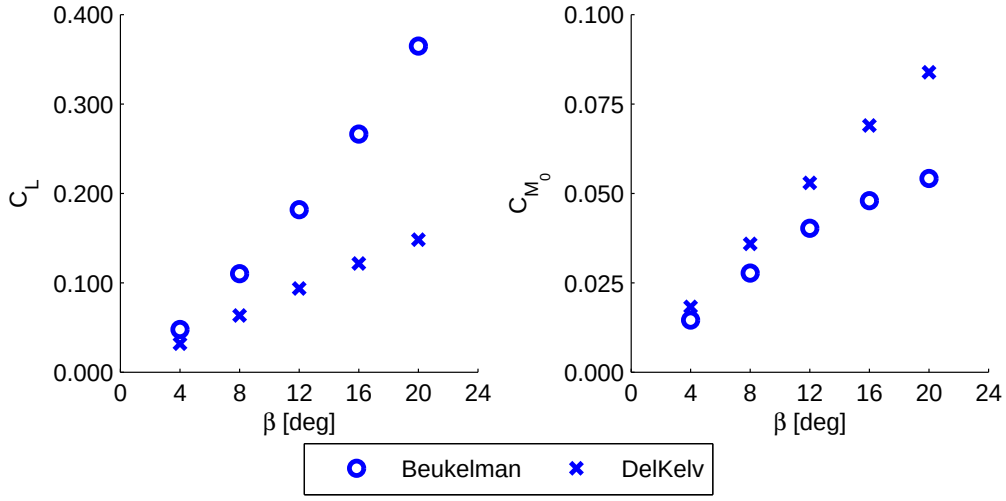

Figure 8.8: Comparison for Beukelman Wing with only a trailing edge wake, $T = 0.3$ m and $h = 0.75$ m

determined forces and moments, since one may assume that a real wake is generated by the full projection of the wing at the y-z plane. The vortex leaving the wing from the bilge may thus separate from the wing closer to the fore point. In order to still capture the influence of the vortex on the integral force, the wake surface should be extended to further upstream.

Calculations described in this section include a wake that does not start at the point of maximum width, but start at the point where the y-position is maximum

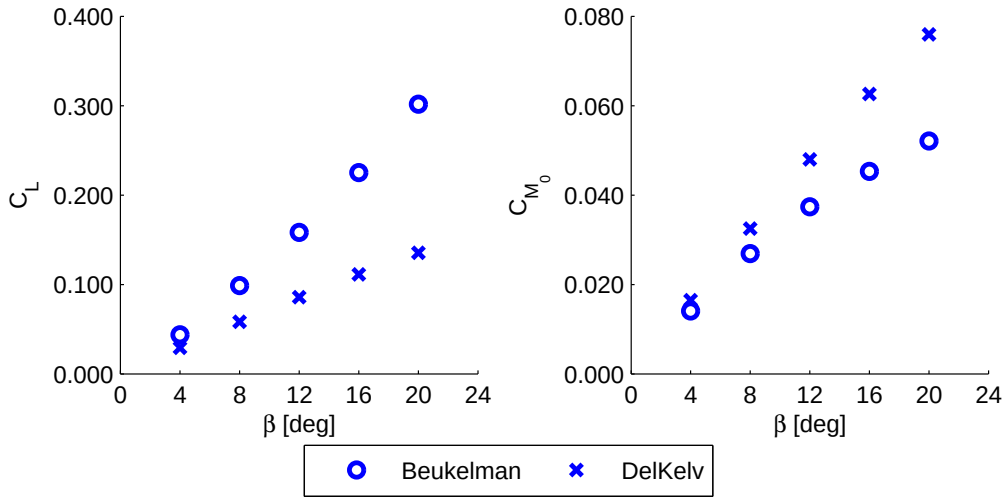

Figure 8.9: Comparison for Beukelman Wing with only a trailing edge wake, $T = 0.3$ m and $h = 2.4$ m

after rotating the wake to account for the drift angle. For zero drift, this y-position is equal to the point of maximum width, but at higher drift angles, a point further upstream may exceed the y-position at maximum width. The wake surface will then start from that point.

From calculations done at drift angles of 8 and 12 degrees, it became clear that extending the wake surface to further upstream slightly increased the resulting forces,

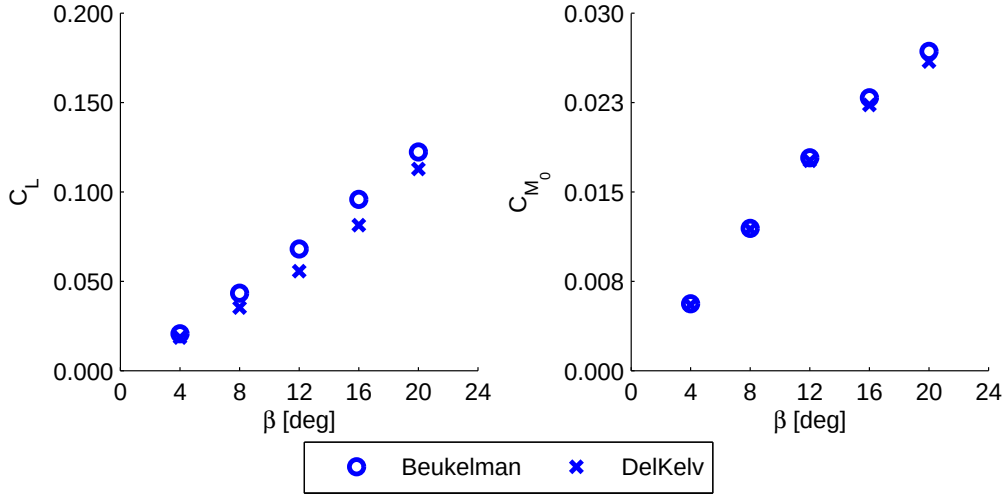

Figure 8.10: Comparison for Beukelman Wing with wake at trailing edge and bilge, $T = 0.1$ and $h = 0.6$

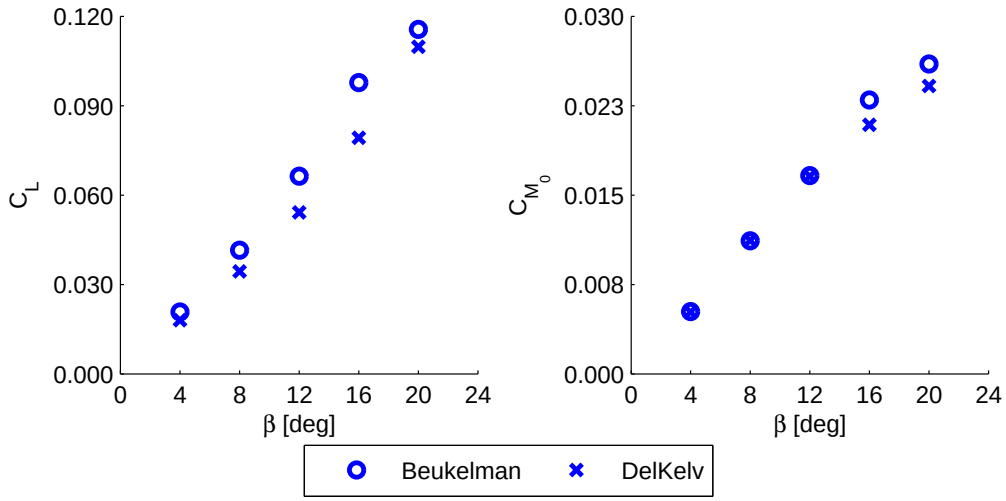

Figure 8.11: Comparison for Beukelman Wing with wake at trailing edge and bilge, $T = 0.1$ and $h = 2.2$

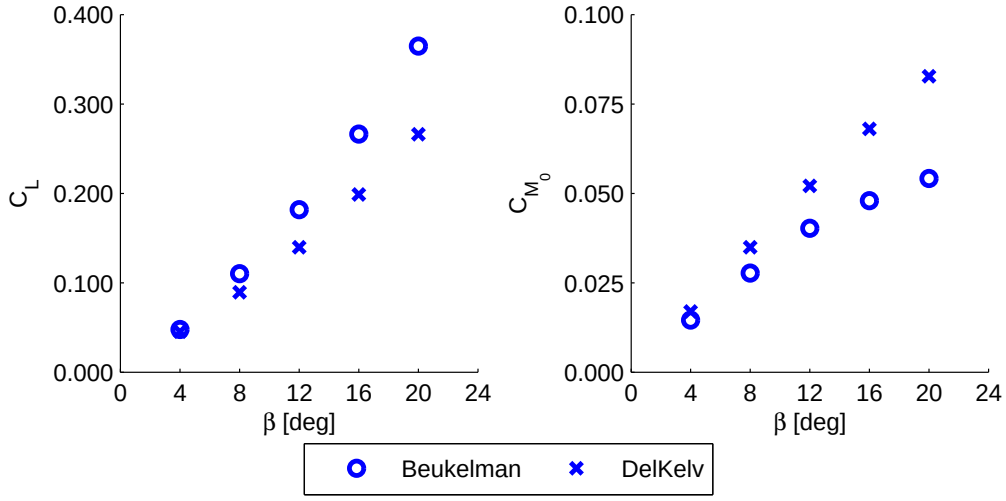

Figure 8.12: Comparison for Beukelman Wing with wake at trailing edge and bilge, $T = 0.3$ and $h = 0.75$

but only by one or two percent. Graphs are therefore not shown for these calculations. Since the complete Wing grid model needs to be rebuilt to apply a wake extending to further upstream, and as using a bilge wake from the maximum width to the trailing edge already shows sufficient results, it may not be worth the effort to apply bilge wakes starting from the location of maximum y-position. Especially for real ships, the amount of forward extension is small compared to the length of the bilge wake, so the effect will be even smaller.

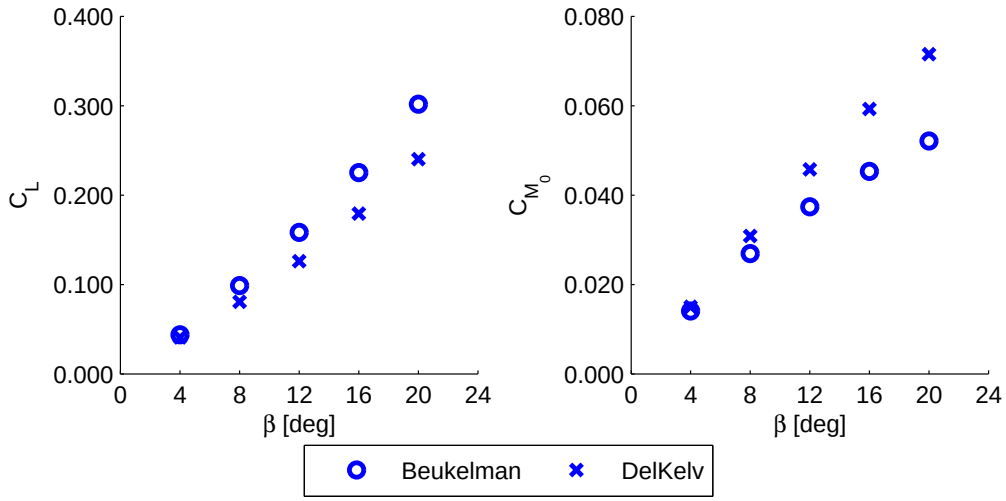

Figure 8.13: Comparison for Beukelman Wing with wake at trailing edge and bilge, $T = 0.3$ and $h = 2.4$

Conclusions on Beukelman Wing validation

In the previous sections, the Beukelman Wing was described, an overview of the calculations is given and the grid dimensions used in the calculations was described. Also, comparison between results from computations with three different wake models and experimental results was described as well. The following conclusions can be drawn on the validation of DelKelv for the Beukelman Wing:

- Using only a wake surface attached to the trailing edge of the wing, computed forces are approximately 50 percent too low, while moments are too high. The explanation for this is that apparently, a vortex leaves the wing from the bilge, which is not captured by the trailing edge wake.

- It is remarkable that for both wake models, better agreement between experiments and calculations is found for $T = 0.1$ than for $T = 0.3$. It is expected that flow about the wing at $T = 0.3$ has a larger two dimensional behaviour, which would lead to better DelKelv results. The good agreement for $T = 0.1$ can be a small error as well. Perhaps, forces are overestimated by DelKelv for $T = 0.1$ since the bilge wake will enforce two-dimensional flow behaviour.

- Applying a wake to the trailing edge as well as to the suction side bilge of the wing results in very good agreement between computational and experimental

results. The vortex leaving the wing from the bilge appears to have a 50 percent influence on the integral forces.

- Extending the wake to further upstream does not result in significantly increased forces, so it is not worth the effort doing this for calculations with real ships, since amount of forward extension is even smaller for ships.
- Altogether, potential flow theory shows to be able to capture lift forces reasonable accurate for a three-dimensional wing model.
- Beukelman also conducted experiments with square wing tips. For this situation, no calculations are done in this study. However, it is an interesting extension of the present validation.

It appears that DelKelv is able to capture lift forces and corresponding moments qualitatively good for a wing model like the Beukelman Wing. The next section will discuss the DelKelv validation for a ship hull, the KVLCC2.

8.3.2 KVLCC2 validation

The KVLCC2 is a 320 meter long very large crude carrier (VLCC). The ship is an interesting test case for DelKelv validation, since a great amount of data is available on this ship. This is due to the fact that the KVLCC2 is a so-called benchmark ship. The ship itself is never built at full scale, but the design of the ship is used by various organizations to conduct model experiments or carry out CFD calculations. Experimental or computational results for this ship Have been published, so that large knowledge is generated on this ship. At INSEAN, the italian ship model basin, model experiments at various water depths and drift angles are conducted. [2] Yaw rates at forward speed were also included. This section describes the KVLCC2 model, the experiment data, a convergence study for domain grid size and domain length. Then, the results from experiments are compared to DelKelv results.

description of ship model and experiments

Table 8.4 shows the main dimensions of the ship.

The ship is scaled down by a scale factor of 45.71. The resulting model dimensions are given in table 8.5, together with the parameters applied during the experiments.

Table 8.4: Main dimensions of KVLCC2

Name	KVLCC2	
Length	320.00	m
Breadth	58.00	m
Draught	20.80	m
Block Coefficient	0.810	
Midship section coefficient	0.998	

Table 8.5: Model dimensions and test description of KVLCC2

Basin length	240.00	m
Basin width	9.00	m
Basin water depth	0.546, 0.683, 1.365 and 3.777	m
h/T ratios	1.2, 1.5, 3.0 and 8.3	
Model scale factor	45.71	
Model length	7.00	m
Model width	1.27	m
Model draught	0.455	m
Drift angles	0, 2, 4, 6 and 8	deg
Yaw rates	0.0, 0.2, 0.4 and 0.6	
Ship velocity	0.533	m/s

The yaw rates in table 8.5 are given in non-dimensional form, where the yaw rate is made nondimensional using $r' = (rL)/V_S$.

Preparations for DelKelv

A three-dimensional ship model was received from MARIN. The model obtained was at full scale, this does not affect the validation results since experimental results and calculation results will be compared on a non-dimensional basis. The ship model file was converted into a useful format using Matlab, resulting in the three-dimensional ship model shown in figure 8.14. A grid study was carried out, as described in the next section, for the three-dimensional ship model to see which number of panels over the ship hull is sufficient.

The grid panel size and channel length were determined based on a grid study, described in the next section. The width of the channel is given the scaled value of the towing tank width, $W_C = 9 \cdot 45.71 \approx 410$ meter. The depth of the channel is also taken as the scaled towing tank water depths.

Two different wake models are tested for this ship. These are the same two wake

models as used in the Beukelman Wing validation (see section 8.3.1) study. First, a wake only connected to the ship trailing edge is applied, extending from the ship trailing edge towards the channel aft end where the boundary condition at infinity, $\phi = 0$, is applied. Second, a wake at the ship bilge is added to the calculation, in order to capture the vortices leaving the ship from the bilge. When using this wake model on a ship, the trailing edge wake surface is no longer a flat surface (like it is for the Beukelman Wing). The effect of this on the resulting forces is however smaller than 1 percent, as was found from testing calculations using the different wake types. The effect of the ship trailing edge wake surface deformation due to drift angles is therefore neglected.

Calculations for three different yaw rates are carried out as well. Although it is no main part of the scope for this study, it is interesting to see how DelKelv calculations perform for yaw rates at different water depths, especially considering the fact that only little research is done in the field of forces and yaw moments for a ship under rotary motion, see [33]. In table 8.5, non-dimensional yaw rates are presented, made non-dimensional by equation 8.4.

$$r' = \frac{rL_{pp}}{V_S} \tag{8.4}$$

Grid study

As mentioned above, the panel size of the ship and the channel as well as the channel length are to be determined by a grid study. For the grid of the ship itself, three

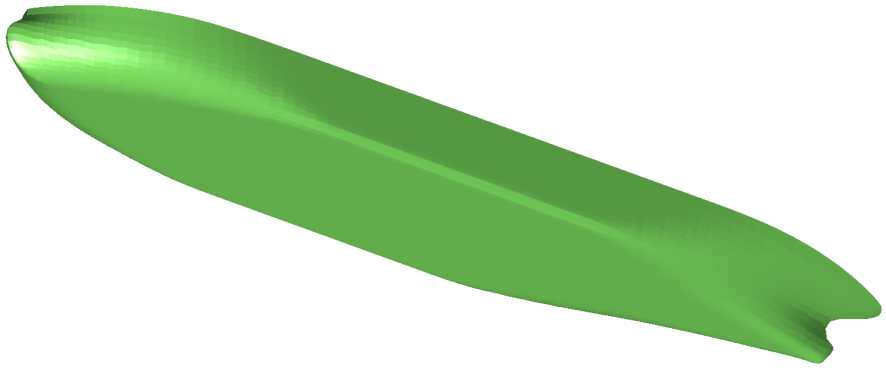

Figure 8.14: 3D model of the KVLCC2 as used in DelKelv

different panel distributions are applied to the ship hull. The results for lateral force and yaw moment are then extrapolated using a Richardson-extrapolation as described in [19], to estimate the lateral force and yaw moment if the panel size approaches zero. The forces and moments for the three grids are given in table 8.6, along with the extrapolated value. The hull grid study for the KVLCC2 is done for deep water only. From this study, a sufficient grid will be chosen which is then used to carry out the grid study for the channel grid, as well as the channel length.

Table 8.6: Hull grid study for KVLCC2 in deep water

Grid type	F_Y [N]	e_{F_Y} [%]	N_{ZZ} [Nm]	$e_{N_{ZZ}}$ [%]
101×27	43498	6.21	13957268	1.55
121×33	42958	5.03	14110661	0.44
143×39	42166	3.25	14155948	0.12
Extrapolated	40795	-	14173020	-

The results show that for a grid of 101×27 panels, the numerical error in the lateral force is 6.21 percent of the total force, which is acceptable for the present study. For yaw moment, the error is 1.55 percent of the total moment, which is lower than the error in lateral force, and therefore also acceptable. The error could be reduced by using a finer grid, however this would come at the cost of a significantly increased computational time and might pose memory allocation problems on the computer used for the computations.

The panel size of the channel grid is investigated as well. Systematic calculations are done using a decreasing grid panel size, starting from $L_{pan} = 20$ down to $L_{pan} = 6.0$. Taking a smaller panel size is not possible due to the memory limits on the used computer. Theoretically, the panel size should be smaller than the distance between panels to obtain sufficiently accurate results. From the grid study it appears however that the numerical error is already sufficiently small for larger panel size. The grid study was conducted for the situation of smallest h/T ratio, since in this case, the bottom is maximally influenced by the ship, resulting in large pressure gradients and thus large errors if a too coarse grid is chosen. For other h/T ratios, the bottom is less influenced and thus the panel size chosen from this convergence study is sufficient as well.

Figure 8.15 shows the convergence of lateral force for decreasing panel size. The graph shows significant scatter around the converging trend, thus it was chosen to use a least-squares approach to estimate the lateral force if the panel size approaches

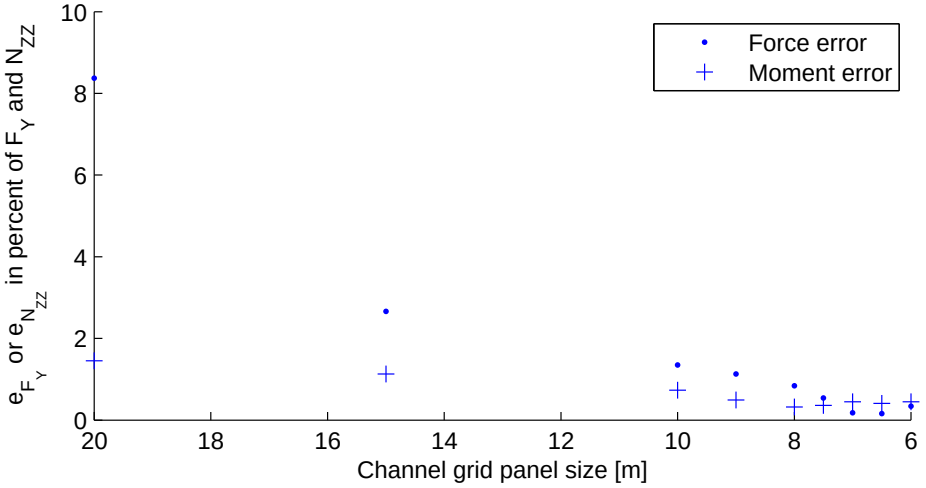

Figure 8.15: Convergence of grid panel size for the KVLCC2 at $h/T = 1.2$

zero. The method used is that found in [19]. The values and estimated errors are given in table 8.7.

Table 8.7: Least squares extrapolation for KVLCC2 channel grid at $h/T = 1.2$

Value type	F_Y [N]	e_{F_Y} [%]	N_{ZZ} [Nm]	$e_{N_{ZZ}}$ [%]
Values at panel size = 8.0	110602	0.84	46417422	0.32
Extrapolated values	111198	-	46585877	-

A similar study is done to investigate the required length of the domain. The domain length was increased from 500 meter up to 1750 meter, while the grid density was set at a panel size of 8 meter. Based on the results, the lateral force and yaw moment are estimated for infinite length using the least squares approach. The error for lateral force and yaw moment relative to the estimated values at infinity are shown in figure 8.16. Based on the errors, a channel length of 1500 m is chosen to be sufficient. Table 8.8 shows the forces and yaw moments for this channel length as well as the extrapolated value for infinite channel length.

Table 8.8: Least squares extrapolation for KVLCC2 channel length at $h/T = 1.2$

Channel length [m]	F_Y [N]	e_{F_Y} [%]	N_{ZZ} [Nm]	$e_{N_{ZZ}}$ [%]
1500	110265	0.63	46437114	0.69
∞ (Estimation)	110968	-	46758307	-

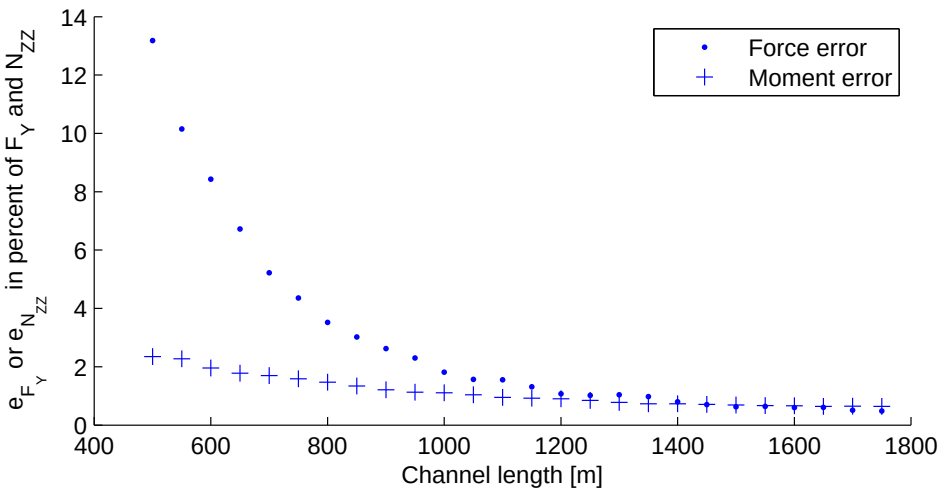

Figure 8.16: Convergence of channel length for the KVLCC2 at $h/T = 1.2$

Summarizing, the grid study resulted in the following values to be used for the validation study for the KVLCC2:

- From a comparison of various panel distributions applied to the ship hull, a panel distribution of 101×27 panels is chosen to be sufficient.
- From a series of calculations with increasing channel grid density, a panel size of 8 meter is chosen to be sufficient. This panel size is applied to the channel surface near the ship, while panel size increases towards the end of the domain by an inverse cosine function.
- From a series of calculations with increasing channel length, a length of 1500 meters is chosen to be sufficient. The ship is located at the half length of the channel.

Method of comparison

The coordinate system used in the results from INSEAN is different from that used in DelKelv. INSEAN uses a ship-fixed coordinate system, while the DelKelv results are given in an earth-fixed coordinate system. To transform the computational results into the same coordinate system as the measurements, equation 8.5 is applied.

$$F_{lat} = F_Y cos(\beta) - F_X sin(\beta) \tag{8.5}$$

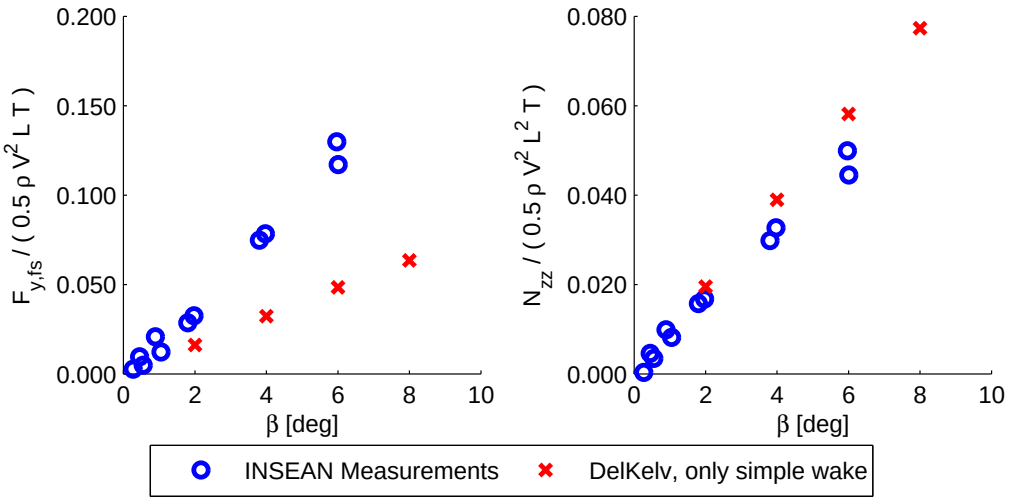

Figure 8.17: Comparison between DelKelv and measurements for the KVLCC2, static drift angles and $h/T = 1.2$. Wake surface only applied at the trailing edge

Forces and moments will be compared on a non-dimensional basis, since the DelKelv results are computed at full scale, and measurement results are determined for model scale. For removing the dimension of the values, equation (8.6) is used.

$$\begin{aligned} F'_{lat} &= \frac{F_{y,sf}}{0.5\rho V_S^2 LT} \\ N'_{yaw} &= \frac{N_{zz}}{0.5\rho V_S^2 L^2 T} \end{aligned} \tag{8.6}$$

Now, the grid is completely described, as well as the method of comparison. The following section will then describe the comparison between calculations and experiments.

Static drift angle tests for the KVLCC2 for a wake surface only attached to the trailing edge

This section shows the comparison between DelKelv and calculation results for the KVLCC2 static drift tests. For the calculations presented here, a wake surface was only attached to the trailing edge of the ship. A wake model including wake surfaces at the bilge are considered in the next section. Figures 8.17 to 8.20 show the graphical comparison between DelKelv and experiments.

Overall, yaw moments show good agreement between calculations and measure-

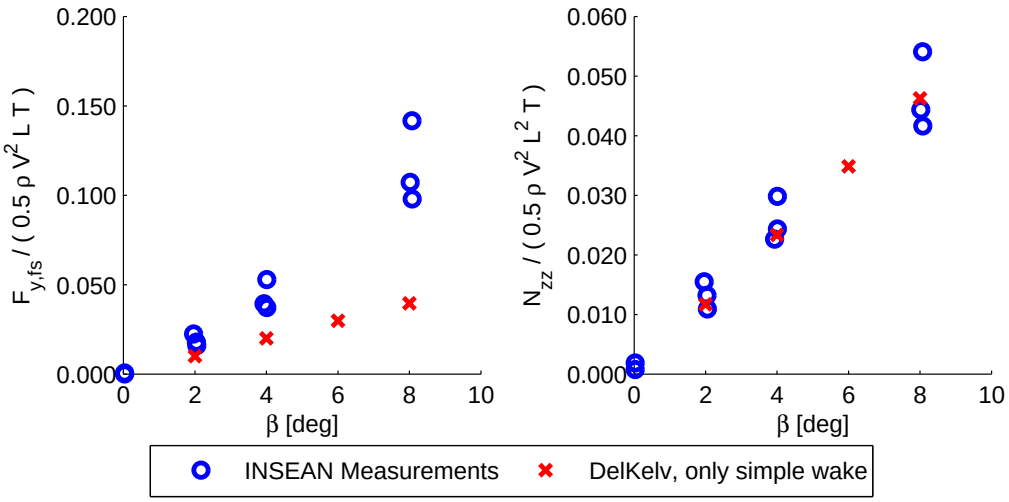

Figure 8.18: Comparison between DelKelv and measurements for the KVLCC2, static drift angles and $h/T = 1.5$. Wake surface only applied at the trailing edge

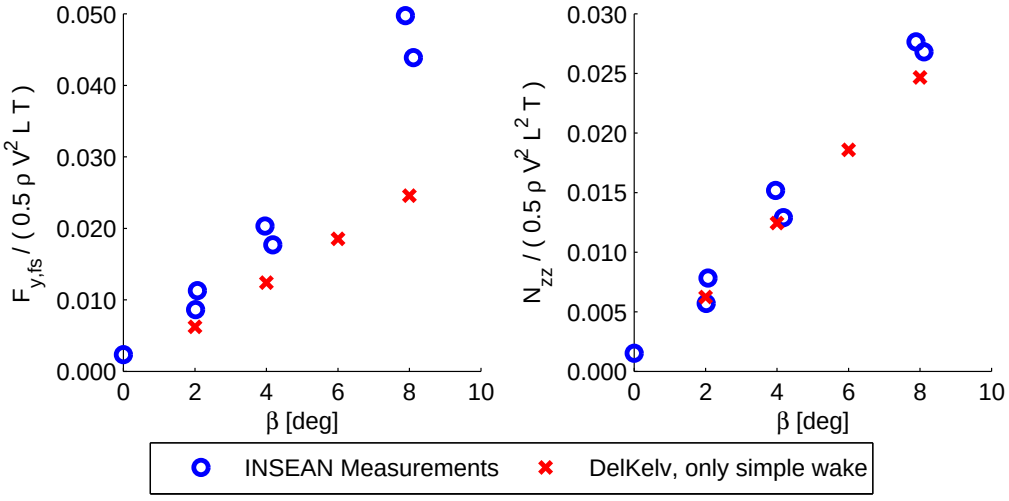

Figure 8.19: Comparison between DelKelv and measurements for the KVLCC2, static drift angles and $h/T = 3.0$. Wake surface only applied at the trailing edge

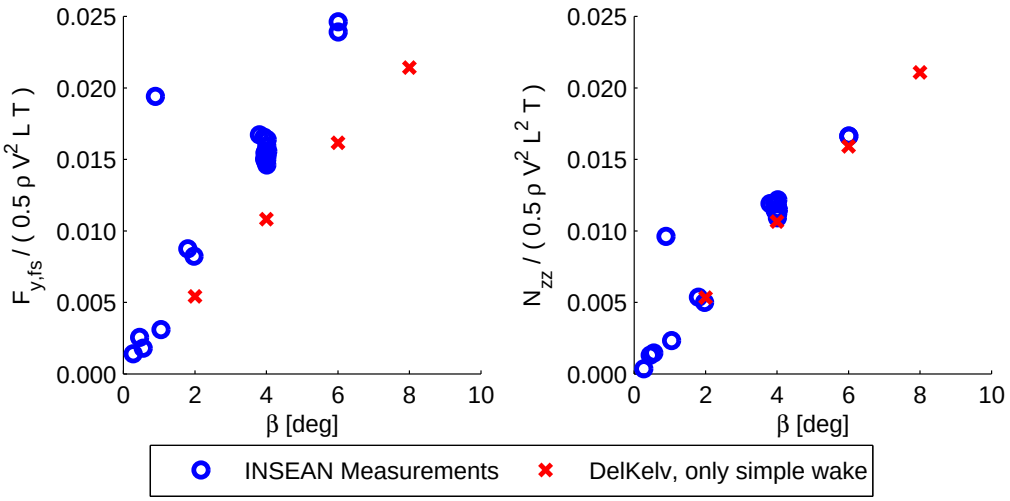

Figure 8.20: Comparison between DelKelv and measurements for the KVLCC2, static drift angles and $h/T = 8.3$. Wake surface only applied at the trailing edge

ments for the wake model that only includes a wake surface at the trailing edge. For lateral forces, significant differences between experiments and calculations are observed. Some remarks are to be made:

- For shallow water, figures 8.17 and 8.18 show a difference of approximately 50 percent between experiments and calculations.
- In less shallow water, the differences become smaller, as can be seen in figures 8.19 and 8.20.
- It appears that for shallow water, attaching a wake surface only at the trailing edge is not sufficient. For $h/T = 8.3$, the computational results is closer to the experimental results, but still a significant difference is seen.
- Yaw moments show good agreement for all h/T ratios, with only a slight over-estimation at $h/T = 1.2$.

Static drift angle tests for the KVLCC2 for a wake surface attached to the trailing edge and lee-side bilge

As mentioned, a wake model including a wake surface at the lee-side ship bilge is also investigated for the KVLCC2. The previous section described the validation

results for only including a wake surface attached to the trailing edge, and significant differences were observed between experimental and computational results, especially at low h/T ratios. Figures 8.21 to 8.24 show a comparison between measurements and calculations, where a wake surface is attached to both the trailing edge and the lee-side bilge (portside in this case).

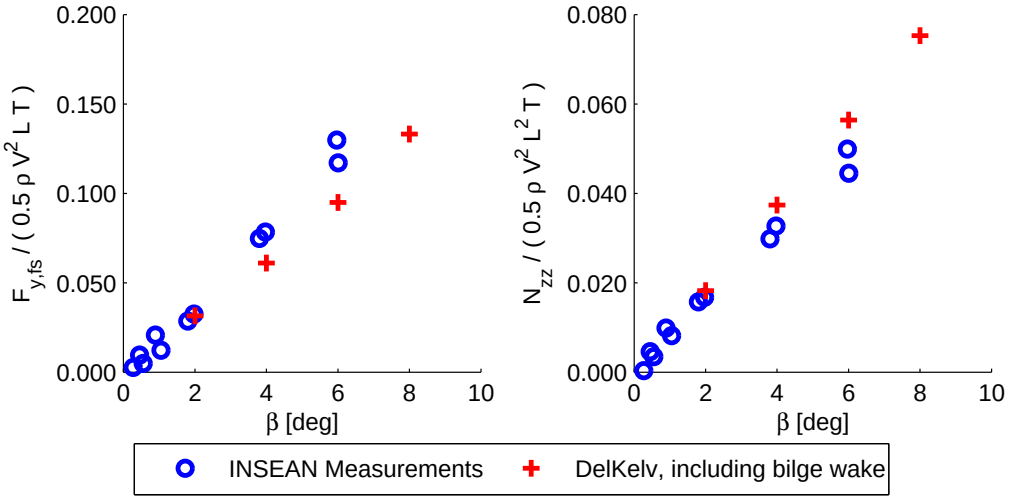

Figure 8.21: Comparison between DelKelv and measurements for the KVLCC2, static drift angles and $h/T = 1.2$. Wake surfaces are attached to trailing edge and lee-side bilge

The following observation are made from the figures showing the comparison between measurements and computations including bilge wakes:

- For h/T values of 1.2 and 1.5, very good agreement is found between experimental and computational results, for both the lateral force and the yaw moment.
- For h/T values of 3.0 and 8.3, the calculated lateral force is higher than the experimental results, especially for $h/T = 8.3$. Interestingly, in the previous section on comparison for trailing edge wake surface only, it is observed that the results from experiments and calculations become more similar at high h/T ratios. The explanation for overestimation of lateral forces is that the wake surface attached to the ship bilge enforces the flow to more two-dimensional, as it prevents flow in vertical direction. The wake surface thus 'simulates' shallow water effects, resulting in larger lateral force.

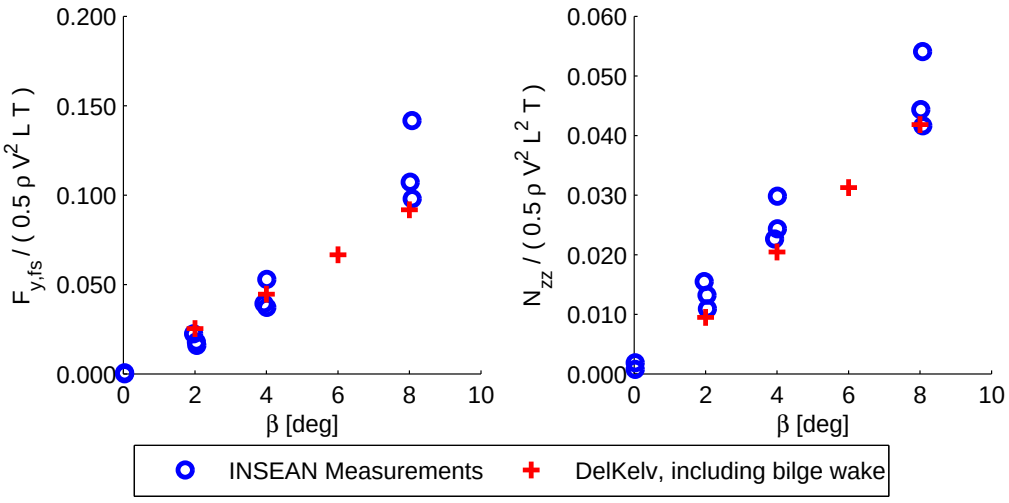

Figure 8.22: Comparison between DelKelv and measurements for the KVLCC2, static drift angles and $h/T = 1.5$. Wake surfaces are attached to trailing edge and lee-side bilge

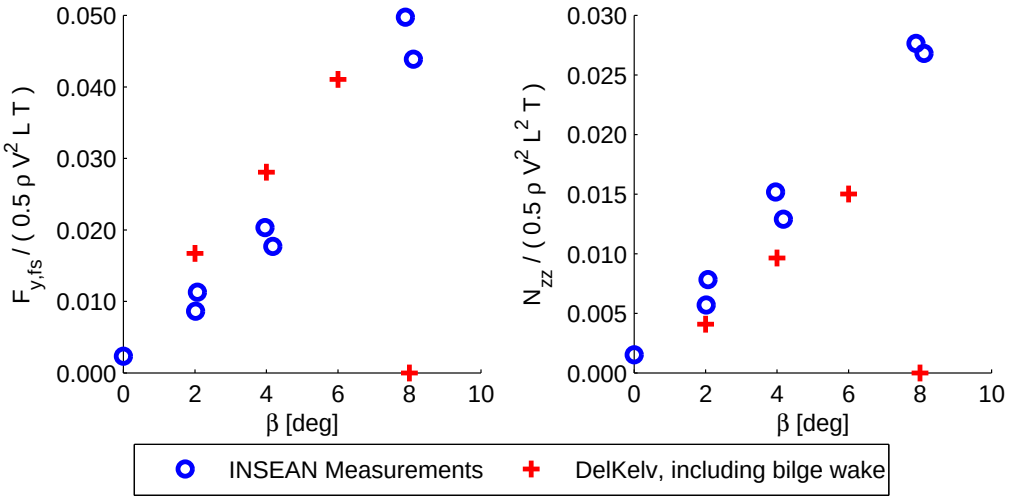

Figure 8.23: Comparison between DelKelv and measurements for the KVLCC2, static drift angles and $h/T = 3.0$. Wake surfaces are attached to trailing edge and lee-side bilge

- If one would draw a trendline based on the computational results, this trendline would not cross the vertical axis at $y = 0$. This is due to the fact that the bilge wake is only modeled on portside. At small drift angles, vortices may also leave the ship at starboard, and would then reduce the total lift force acting on the ship. For high drift angles, the effect of starboard bilge vortices becomes

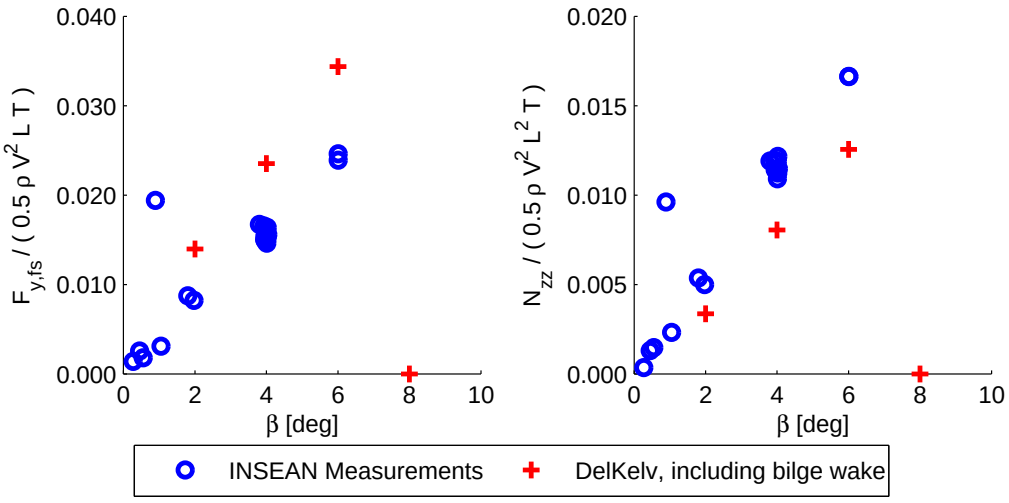

Figure 8.24: Comparison between DelKelv and measurements for the KVLCC2, static drift angles and $h/T = 8.3$. Wake surfaces are attached to trailing edge and lee-side bilge

negligible.

- For yaw moments, very good agreement is found for $h/T = 1.2$ or 1.5, while for larger h/T ratios, the yaw moments are slightly underestimated by DelKelv when a bilge wake is included. The explanation for this is the same as for the overestimated lateral forces in deep water.

Static yaw rate tests for the KVLCC2 for a wake only attached to the trailing edge

It was mentioned already that yaw rates are no part of the study, however conducting a small systematic study to compare computational results with experiments is worth the effort. For three different yaw rates, figures 8.25 to 8.28 show the comparison between non-dimensional forces and moments derived from experimental and computational results. For comparison between DelKelv and yaw rate measurements, no calculations are done using a wake attached to the bilge. The wake construction would become very complex, since a (given that the ship turns to portside) starboard wake needs to be attached to the fore half of the ship, while a portside wake should be attached to the aft half of the ship. This type of wake construction is no part of the present study.

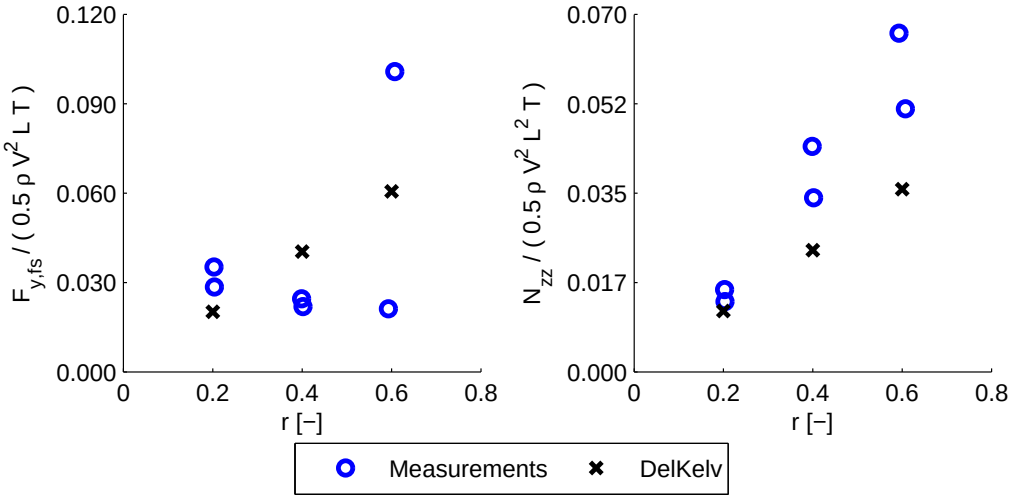

Figure 8.25: Comparison between DelKelv and measurements for the KVLCC2 equipped with a single wake at the trailing edge, static yaw rates and $h/T = 1.2$

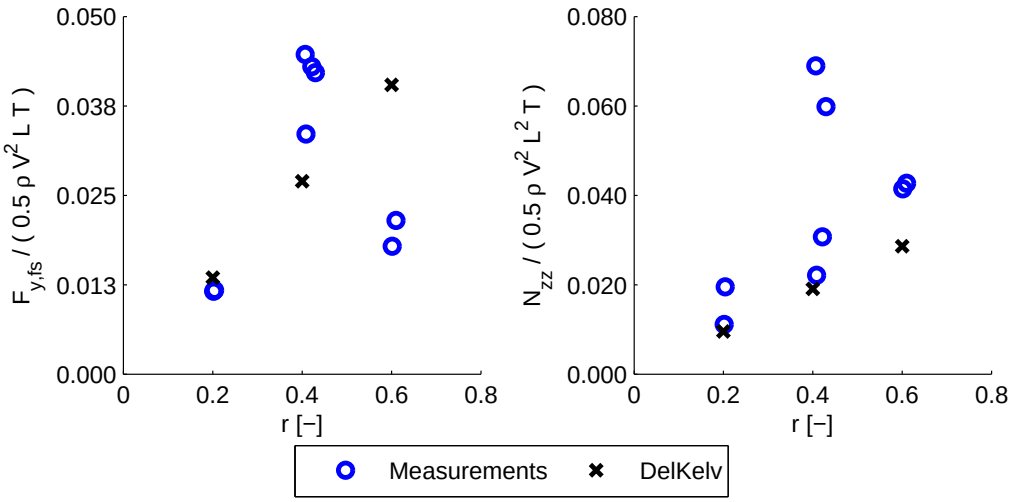

Figure 8.26: Comparison between DelKelv and measurements for the KVLCC2 equipped with a single wake at the trailing edge, static yaw rates and $h/T = 1.5$

A first note that needs to be made on graphs showing agreement for yaw rates is that the measurement results show a great amount of scatter. Especially the lateral forces do not show any clear trend with increasing rate of turn r'. For moments, the measurement results are of the same order as the computational results. For shallow water ($h/T = 1.2$ and $h/T = 1.5$), the DelKelv results are somewhat lower than experimental results. For deep water ($h/T = 8.3$), good agreement is observed

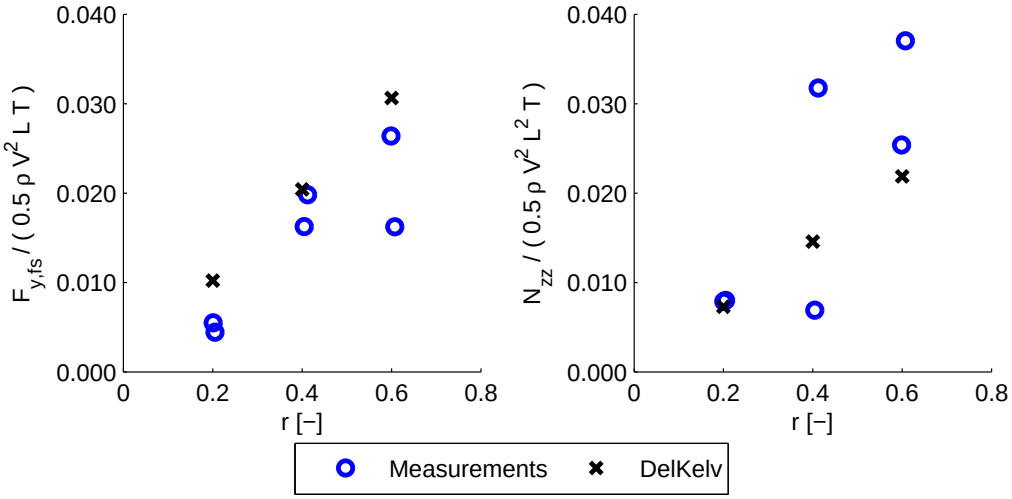

Figure 8.27: Comparison between DelKelv and measurements for the KVLCC2 equipped with a single wake at the trailing edge, static yaw rates and $h/T = 3.0$

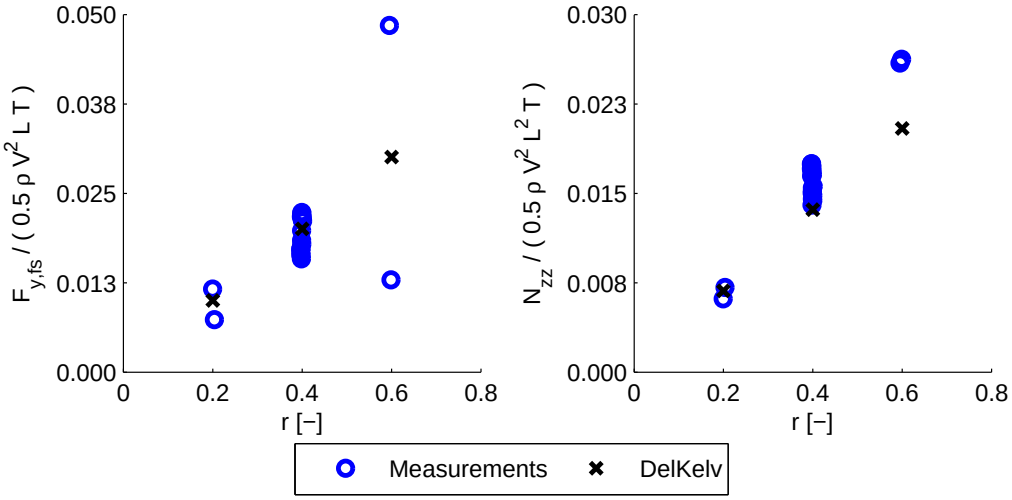

Figure 8.28: Comparison between DelKelv and measurements for the KVLCC2 equipped with a single wake at the trailing edge, static yaw rates and $h/T = 8.3$

between DelKelv and experimental results.

Comparison of Potential flow and CFD calculations

For the KVLCC2, CFD calculations have been conducted at MARIN [35]. The calculations were validated for the same experiments as presented in this section, showing good agreement between the CFD results and the measurement results. As compar-

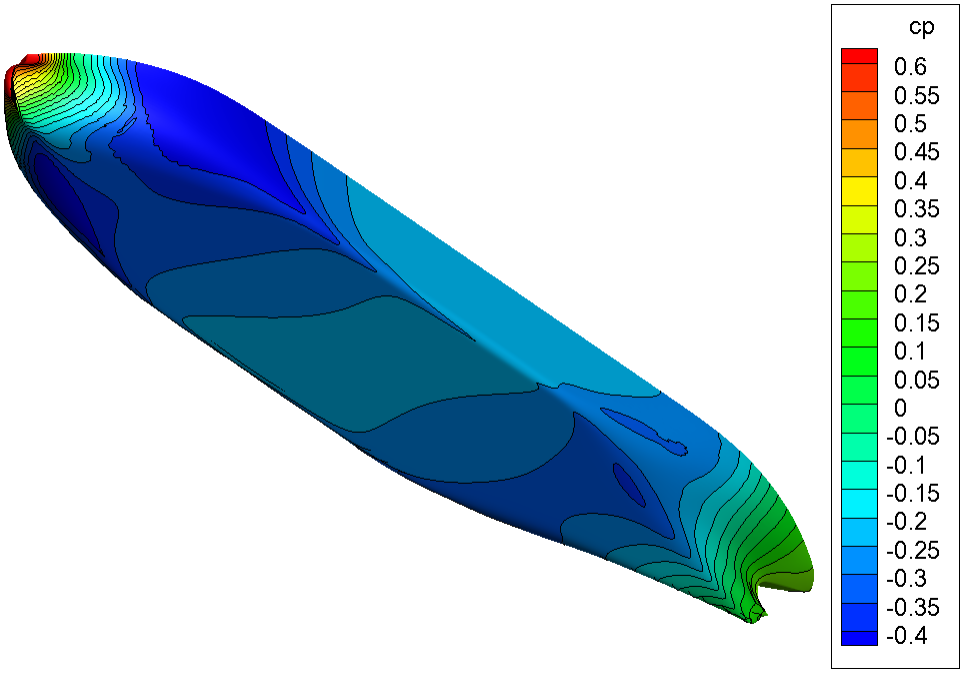

Figure 8.29: Pressure coefficient plot for KVLCC2 lee-side at $\beta = 4$ and $h = 31.2$ based on CFD calculations

ing the results from DelKelv against nearly equal values would be useless, this section presents qualitative comparison between CFD and potential flow calculations.

Figures 8.29 to 8.31 show the pressure contour plot over the hull for respectively the CFD results, the DelKelv calculation including only a wake surface at the trailing edge and the Delkelv calculation with wake surfaces attached to both the lee-side bilge and the trailing edge. For all three figures, calculations are done at a drift angle of 4 degrees and a water depth of 31.2 meter.

For all three figures, the pressure distribution in the bow region is very similar. Near the stern, were the largest difference are expected, the main difference between the two DelKelv results is the low pressure region at the portside bilge extending further towards the stern in figure 8.30. Overall, based on visual comparison, the DelKelv calculation including only a wake at the trailing edge is in best agreement with the CFD results. This is due to the larger low pressure region on portside, which is more similar to the CFD results than for the DelKelv results including the bilge wake surface. In appendix B, the pressure coefficient plots are given for the pressure side of the ship.

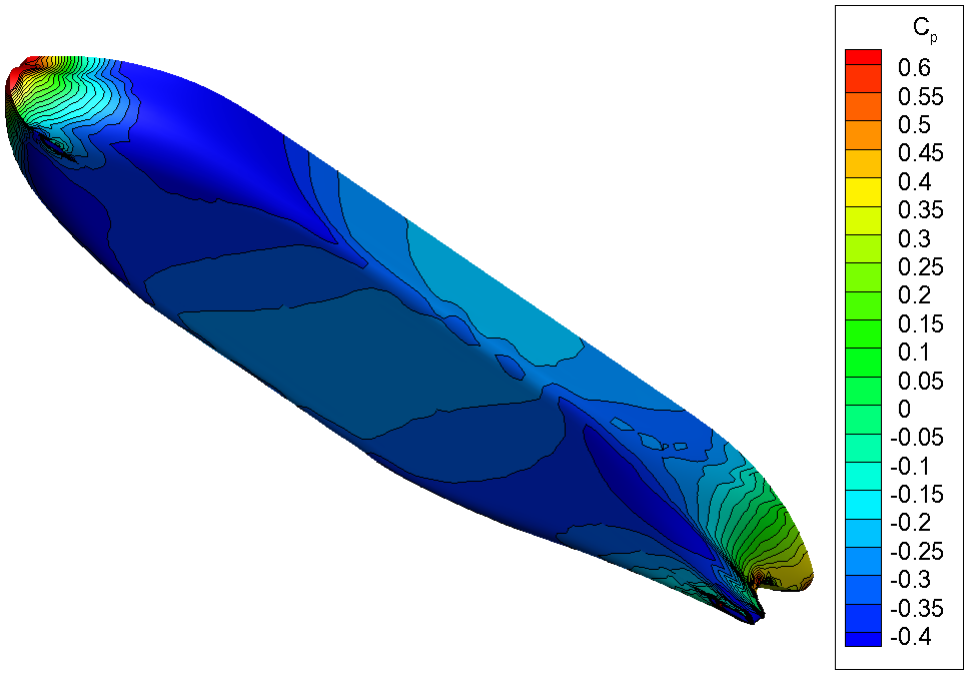

Figure 8.30: Pressure coefficient plot for KVLCC2 lee-side at $\beta = 4$ and $h = 31.2$ based on DelKelv calculations using only a wake surface at trailing edge

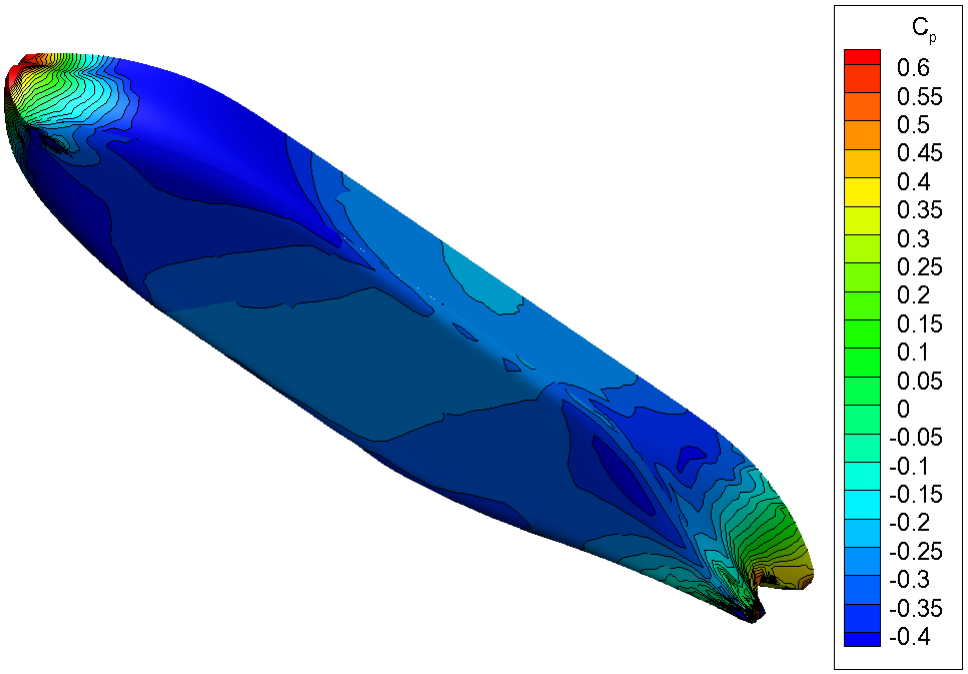

Figure 8.31: Pressure coefficient plot for KVLCC2 lee-side at $\beta = 4$ and $h = 31.2$ based on DelKelv calculations using a wake surfaces at trailing edge and lee-side bilge

8.3.3 Conclusions on KVLCC2 validation

Measurements for static drift angles and static yaw rates are compared to results from DelKelv calculations, and a comparison is made between CFD and DelKelv for a certain situation. The following conclusions can be drawn on the validation of DelKelv using KVLCC2 measurements:

- For static drift angle tests, DelKelv calculations including only a wake surface at the trailing edge result in too low forces, especially for low h/T values. For deeper water, de difference between computational and experimental results becomes smaller.
- Including a wake surface attached to the lee-side bilge results in very good agreement between measurements and calculations for shallow water. For deep water, the lateral force is overestimated due to the fact that the wake surface at the bilge enforces the flow to remain two-dimensional.
- The inclusion of a wake surface at the lee-side bilge results in non-zero forces for $\beta = 0$. This effect is absent for high drift angles, and for low drift angles an additional wake surface can attached at the windward side bilge in the aftship region.
- Inclusion of a wake surface at the lee-side bilge increases the agreement between pressure coefficient plots from DelKelv and CFD computations.
- Calculations for steady yaw rates are carried out as well. Forces determined from experiments show a large amount of scatter, and thus no conclusion can be drawn on the accuracy of DelKelv in estimating sway force during turn manoeuvres. Fortunately, the yaw moments from experiments are useful to compare with DelKelv results. For yaw moments, DelKelv shows an overall good agreement with experiments on steady yaw rates.

8.3.4 Marin Inland Ship validation

The project from which the present study originates, focuses on inland shipping. Therefore, an inland ship is also part of the validation study. It is already showed that DelKelv is able to predict manoeuvring forces acting on the KVLCC2. This

section will discuss the validation of DelKelv for an 110 m inland ship, the MARIN Inland Ship. The Marin Inland Ship is a benchmark ship as well, meaning that the design is publicly available and various organizations can use the design for validation of CFD calculations, investigate shallow water effects, etcetera. The main dimensions of the ship are given in table 8.9.

Table 8.9: Main dimensions of Marin Inland Ship

Name	Marin Inland Ship	
Length	110.00	m
Breadth	11.40	m
Draught	3.50	m
Block Coefficient	0.887	
Midship section coefficient	0.999	

Description of experiments

At MARIN, experiments were carried out to determine hull forces for the ship under drift. Yaw rates were not included during the tests. The tests have been carried out at two different water depths. Table 8.10 gives an overview of the tests.

Table 8.10: Experimental set-up for the Marin Inland Ship

Length of Basin	220.00	m
Width of Basin	15.80	m
Water depth	0.272 and 0.388	m
Model scale	18.0	
Model length	6.11	m
Model width	0.636	m
Model draught	0.194	m
h/T ratios	1.4 and 2.0	
Drift angles	0, 5, 10, 20 and 40	deg
Model speeds	0.393 and 0.917	m/s

Preparations for DelKelv

Two designs of the ship are available, a single and double screw ship. The single-screw version is used for the DelKelv calculations. The ship is equipped with tunnels to prevent the propeller from ventilating. These tunnels pose a problem in potential

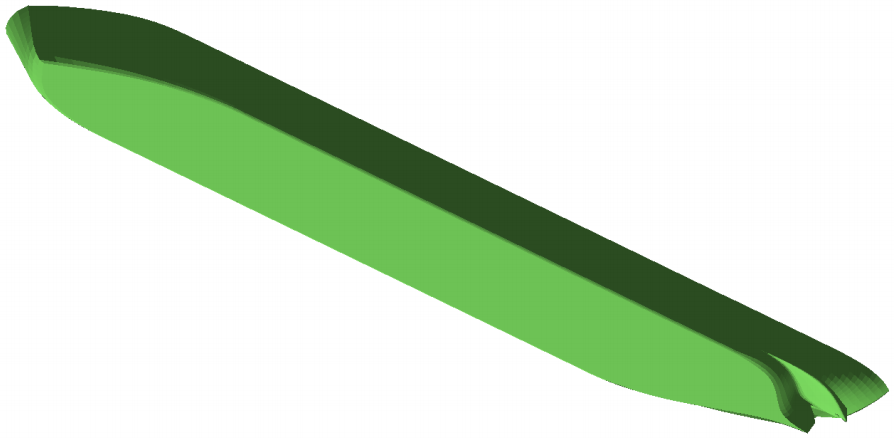

Figure 8.32: Three dimensional model of the single-screw version of the MIS

flow calculations using DelKelv, as will be shown later. A significant modification is applied to the ship hull in order to overcome these problems. The three-dimensional model of the ship is divided into a number of sub-surfaces, each having its own panel density. The bow and stern of the ship is given a more dense grid, while the grid of the parallel mid ship part is more coarse. Figure 8.32 shows the 3D model of the ship.

The channel length and channel panel size are chosen based on a grid study described in a next section. The channel width can be set at the scaled towing tank width, but this would lead to an unnecessary wide channel. From test calculations, it appeared that the influence of the channel sides is negligible for a width of over 150 meter. The channel sides can then be left out, leaving only the bottom surface to be modelled. The bottom surface is given a width of 150 meter.

For wake construction, two different wake surface models are used. The first wake model is only attached to the trailing edge of the ship, see figure 8.33. The wake extends from the keel to the free surface, meaning that the wake is also attached at the submerged transom of the ship. At this stern, the wake is attached perpendicular to the stern. A better option may be to connect the wake as shown in figure 8.34. For this wake model, no calculations are carried out due to gridding complexities. However, the modified Marin Inland Ship (described below) is equipped with a similar wake model. The other wake model for which calculations are carried out, is the model that includes wake surfaces at the bilges as well. This is shown in 8.35.

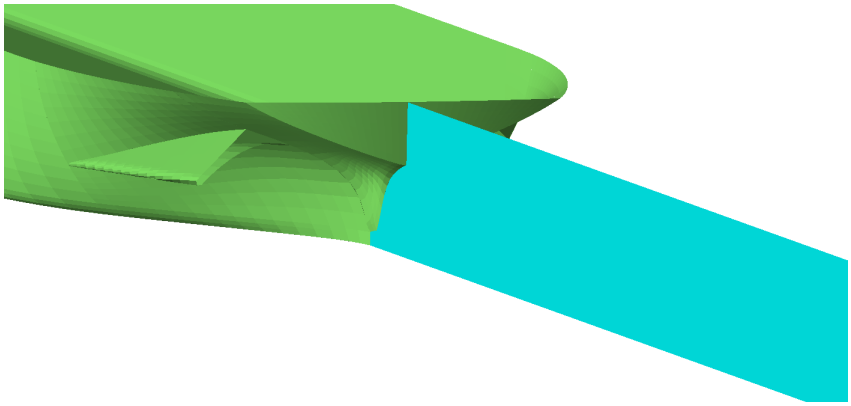

Figure 8.33: Overview of the wake surface only attached to the ship's trailing edge. Note that the wake is perpendicularly attached to the submerged transom

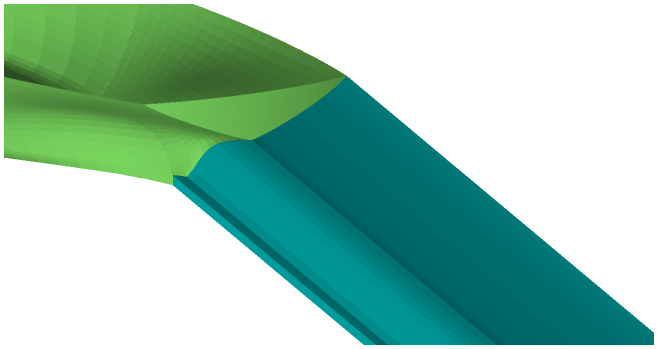

Figure 8.34: A view of the aft ship, with a wake attached to the starboard side of the stern instead of in the middle of the stern. No calculations are done for this wake in the present study

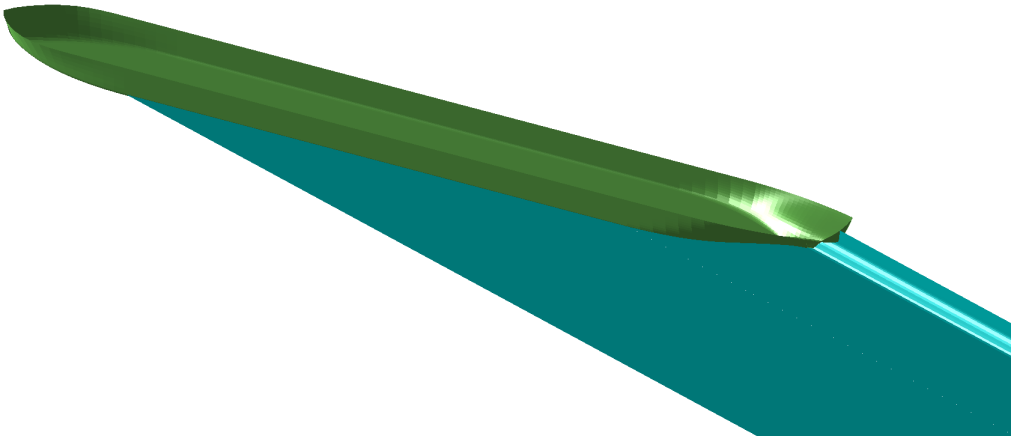

Figure 8.35: Overview of the wake surface attached to the trailing edge as well as to the ship bilges

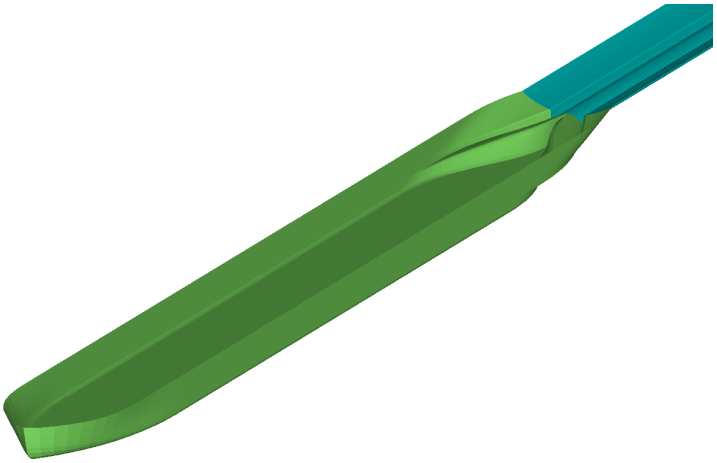

Figure 8.36: Overview shortened Marin Inland Ship, including the wake surface connected to the new stern and tunnels.

As mentioned, a significant modification is applied to the ship hull to overcome the problem that arise from the presence of the anti-ventilation tunnels. The last 2.5 meter of the ship is removed, and the surfaces at the aft end of the tunnels are removed as well. This results in a ship without a transom. Removal of the transom results in no need for two surfaces (transom and aft end of ship) to be equally spaced, and thus a wake model similar to the wake in figure 8.34 can be applied.

Using a wake surface that is attached from the edge of the 'new transom', the flow is enforced to leave the ship in flow direction and not rotating about the new ship transom. The purpose of this modification is to prevent problems arising from the wake surfaces being too close to the ship's panels, or even penetrating the ship hull. Figure 8.36 shows the shortened ship model including the wake attached to it.

For this shortened version of the Marin Inland Ship, calculations are carried out as well to investigate the effect on forces and moments of cutting the ship by 2.5 meters.

Grid study

For the MARIN Inland Ship, a numerical verification study is conducted to determine the required channel length and grid density. The study for grid panel size was conducted at a channel length of 500 meters, while the channel length study was conducted at a channel grid panel size of 4.0 meters. Values for lateral hull forces

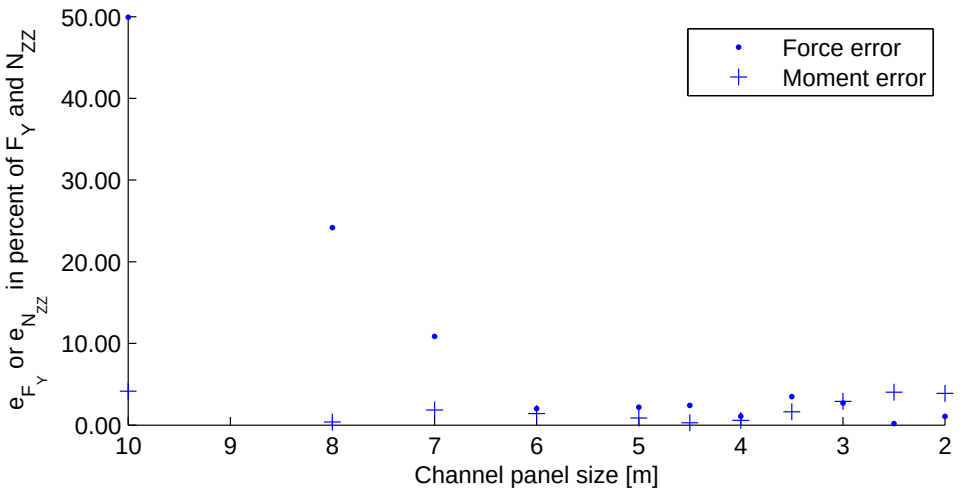

Figure 8.37: Numerical error estimate at decreasing channel panel size for MIS at $h/T = 1.4$

and yaw moments at infinite channel length of zero size panels are determined by the least squares approach as used in [19].

For all panel sizes considered, the errors for yaw moment was below five percent. However, decreasing the panel size towards 2.0 meter does not show that the error decreases towards zero, it even increases again for panel sizes below 4.0 meter. For lateral forces, the error decreases until the panel size is smaller than 5.0 meters. A panel size of 5.0 meters is chosen to be used in further calculations. The increase of forces and moments for panel sizes below this value is due to the fact that the locations of the grid points are all displaced when a different grid is used. A decrease of error magnitude can be observed if the panel size is further decreased, however this was not possible due to memory limits on the used computer.

For channel lengths considered, the error is below one percent from all channel lengths considered. Apparently, a channel length of less than three times the ship length is sufficient, while for the KVLCC2 a much longer channel was required. For furhter calculations, a channel length of 300 meters is used.

Comparison method

The same method of comparison as described in section 8.3.2 is used for the Marin Inland Ship. The lateral hull forces is converted from the earth-fixed (from DelKelv) to the ship-fixed coordinate system by:

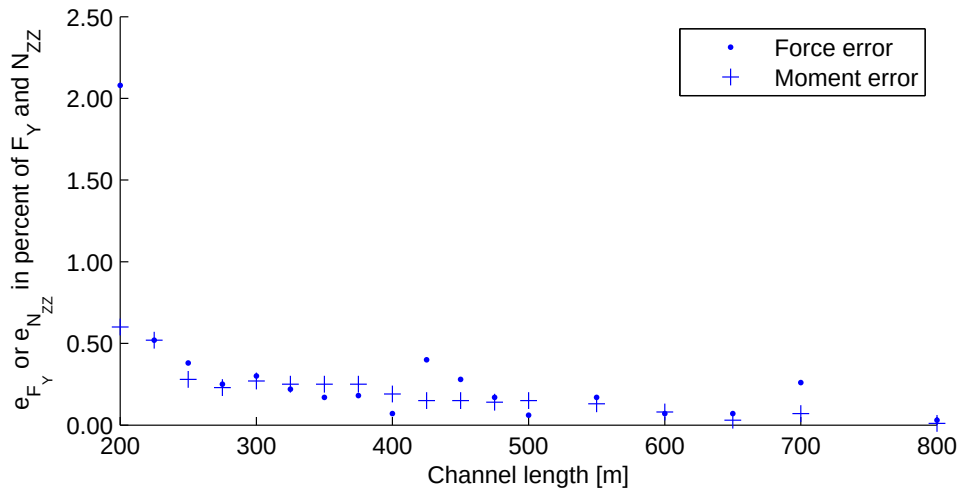

Figure 8.38: Numerical error estimate for increasing channel length for MIS at $h/T = 1.4$

$$F_{lat} = F_y cos(\beta) - F_x sin(\beta) \tag{8.7}$$

The moments are kept the same. Same as for the Beukelman wing and the KVLCC2, it is not expected that results from experiments and calculations are equal at all drift angles. In fact, the derivative of the lateral force or yaw moment at $\beta = 0$ should be equal for both experiments and calculations, as non-linear effects become negligible if the drift angle approaches zero.

Still, differences for the derivative of forces and moments at $\beta = 0$ between results from DelKelv and experiments are expected, as the experiments are conducted fully appended. Rudders and propellers are attached to the ship, and active during measurements. The results used for comparison are those from the tests where the rudder angle was zero, however the propeller were still active.

Static drift angle tests, only including a wake attached to the trailing edge of the ship

This section shows the comparison between Delkelv results and measurement results. A wake surface is applied to the trailing edge of the single-screw vessel here. Figures 8.39 and 8.40 show the comparison of lateral forces and yaw moments between calculations and measurements.

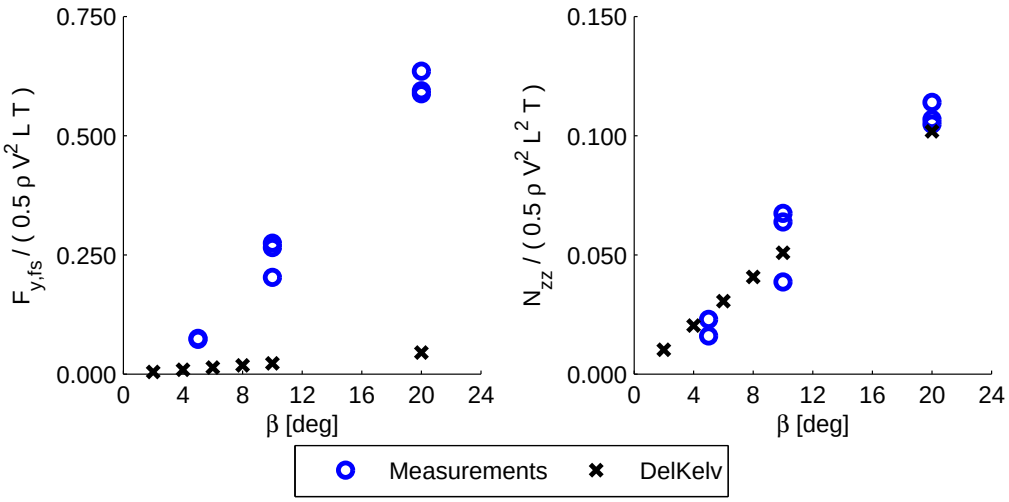

Figure 8.39: Comparison of forces and moments between measurement and DelKelv results for a simple wake and $h/T = 1.4$.

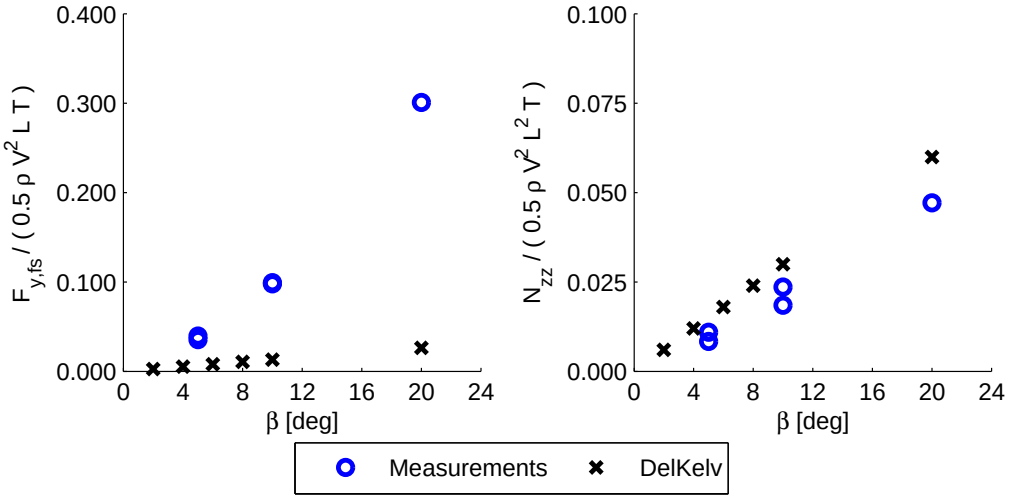

Figure 8.40: Comparison of forces and moments between measurement and DelKelv results for a simple wake and $h/T = 2.0$.

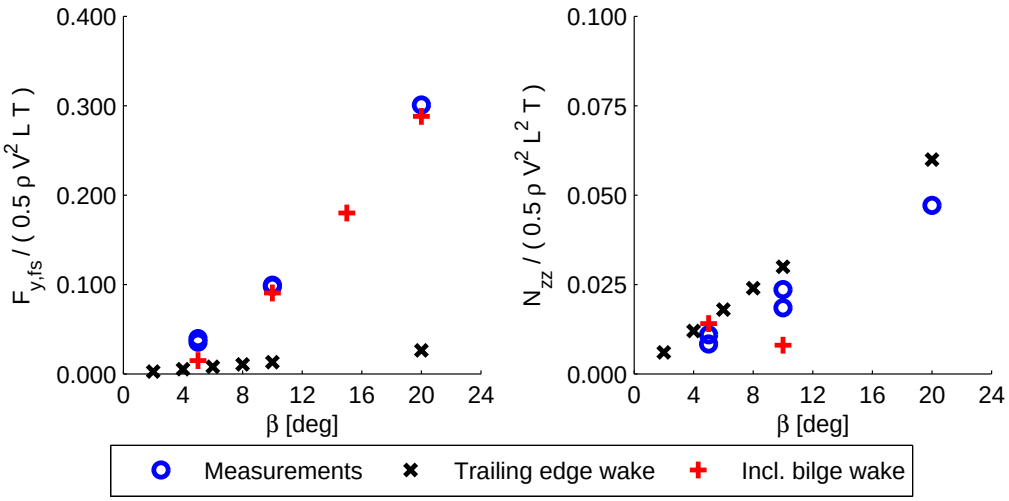

Figure 8.41: Comparison between model test results and calculations for using only the trailing wake and including the bilge wake, $h/T = 2.0$.

The graphs if figures 8.39 and 8.40 show a large difference between the force results of experiments and DelKelv calculations. At small drift angles already, the calculated forces are only a quarter of the measured forces. For moments, a relatively good agreement is found between measurements and calculations. However, as the moment is determined by the force and its center of action, there must be a large difference in the location of this center between calculations and measurements. Furthermore, a detailed view on the computed pressure distribution over the ship hull shows that the pressure at the submerged transom is very high, and also not completely continuous. This has a serious effect on the integral forces and moments.

Only attaching a wake surface to the ship's trailing edge shows to be insufficient for estimation of lateral force. A wake surface is therefore also attached to the lee-side bilge of the MARIN Inland ship, as shown in figure 8.35. The results for this wake model are discussed in the next section.

Static drift angle tests, including wake surfaces attached to the trailing edge and the bilge

The bilge wake is applied in the calculation for $h/T = 2.0$. Drift angles of 5, 10, 15 and 20 degrees are used in the calculation, of which the results are shown in figure 8.41

In figure 8.41, it is showed that the lateral forces are tremendously increased if a

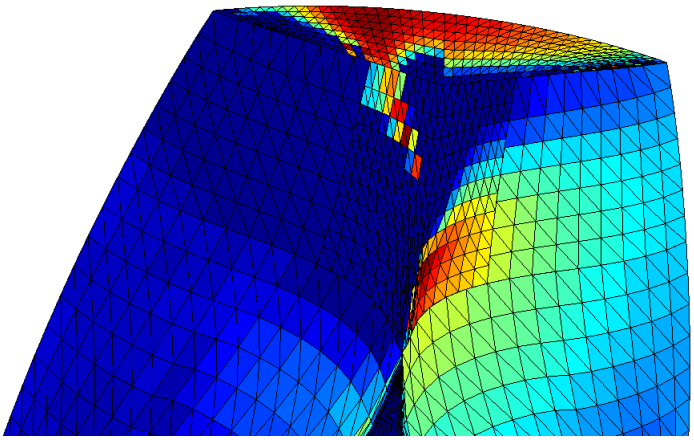

Figure 8.42: The pressure discontinuity occuring at the aft end of the ship. Normally, pressure should be equal at the trailing edge for both the leeward and windward side.

wake is attached to the lee-side bilge as well. The lateral forces show good agreement between experiments and calculations here. For the moments, however, a strange trend is seen. The moments decrease for increasing drift angle. This is not expected, and it may be due to errors in the calculation. Looking at the computational results in more detail, a large pressure discontinuity is found at the trailing edge of the ship. The effect of this on the integral forces is small for small drift angles, but it induces a strong negative moment about the midship for large drift angles. The discontinuity arises from problems in the wake construction. If the wake surface leaves the ship parallel to the ship's heading, the angle between ship panels and wake panels remains larger than 90 degrees, making sure the flow can leave the ship in a physically correct way. If the wake leaves the ship at a certain angle (which is the case in the present study when bilge wakes are included), the wake surface at the trailing edge is deformed, and wake panels that are next to hull panels will be rotated such that they approach the hull panels. The distance between the panels becomes very small compared to the panel size, resulting in numerical errors and significant pressure discontinuities. The pressure discontinuity is visualized in figure 8.42

Calculations for the shortened version of the Marin Inland Ship

The pressure discontinuities in the aft ship region of the Marin Inland Ship give significant errors in the calculation results. As the errors are mainly due to the fact that the wake surface approaches the ship panels very closely in the most aft

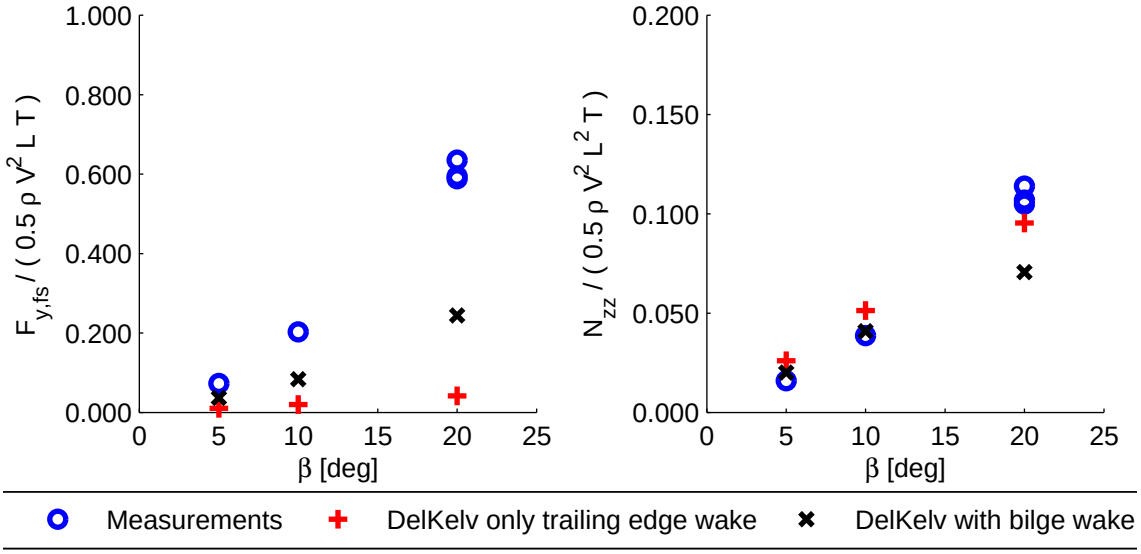

Figure 8.43: Comparison between model test results and calculations for both wake models, $h/T = 1.4$.

ship region, this region is removed from the ship. Figures 8.43 and 8.44 show the comparison between experiments and calculations for the shortened Marin Inland Ship. In both figures, calculation results for the wake model only including a trailing edge wake surface as well as results for the wake model including wake surfaces at both the trailing edge and lee-side bilge are included.

For both h/T ratios, is it observed that inclusion of the wake surface at the lee-side bilge leads to an improved agreement between measurements and calculations. Especially for yaw moments, the non-dimensional coefficients determined from DelKelv computations and measurements are very close to each other for drift angles of 5 and 10 degrees. For the lateral forces, using a bilge wake shows improvement. A better comparison can be made by evaluating equation 8.8 for all drift angles:

$$F_{lat,\beta} = \frac{F_{lat}}{\sin\beta} \tag{8.8}$$

Figure 8.45 shows the comparison for the values obtained from evaluating equation 8.8. This plot is particularly useful for distinguishing between linear and non-linear contributions. As the linear part of the lateral hull force should increase linearly with β, plotting $F_{lat,\beta}$ gives a nearly constant value for all drift angles. By drawing a trend line through the points, the intersection point of that trendline and the vertical axis

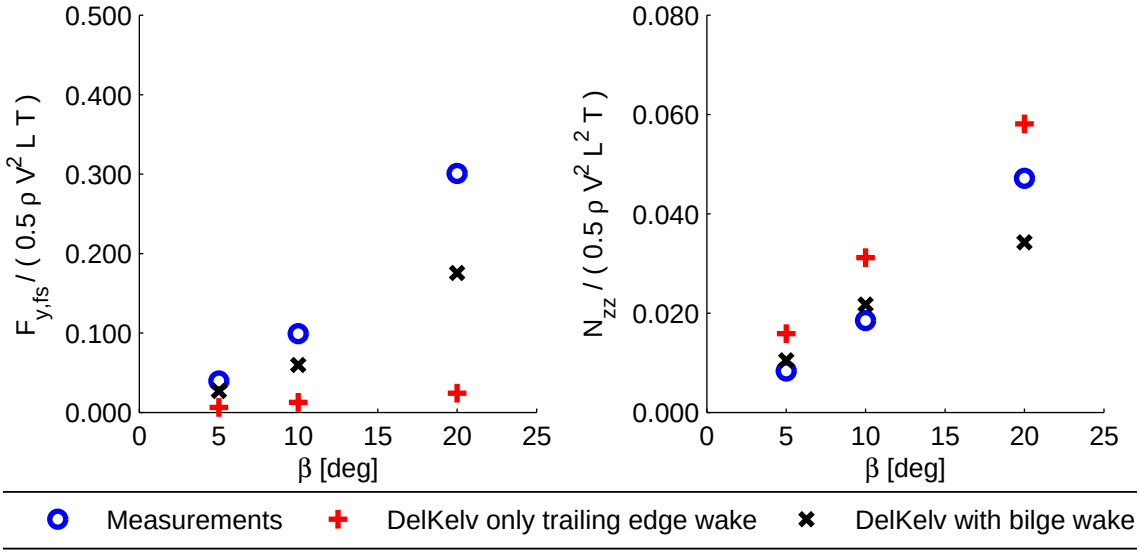

Figure 8.44: Comparison between model test results and calculations for both wake models, $h/T = 2.0$.

gives the linear hull force coefficient.

From the figure, it is observed that for the simple wake model, the value of $F_{lat,\beta}$ is constant over all drift angles. For the wake model including a wake surface at the lee-side bilge, the value is not constant. This indicates that non-linear effects are captured. This is expected as with increasing drift angle, the wake surface dimensions for the lee-side bilge wake surface increase as well. In reality, the size of the wake left behind by the ship also increases for larger drift angles, also resulting in non-linear lift force.

Viewing the trends of both DelKelv results and measurement results, particularly considering their intersection with the vertical axis, it is clear that the wake model with only the trailing edge wake surface is not sufficient. Inclusion of the lee-side bilge wake surface leads to a significantly higher values and better agreement. The difference between DelKelv calculations for that wake model and measurements is less that 25 percent. Still, the differences are relatively large compared to those seen in the validation studies of the Beukelman Wing and the KVLCC2, but the tests for the Marin Inland Ship were conducted fully-appended, which may have a significant influence on the results. The next section will give a comparison of the hull pressure distribution between CFD and potential flow.

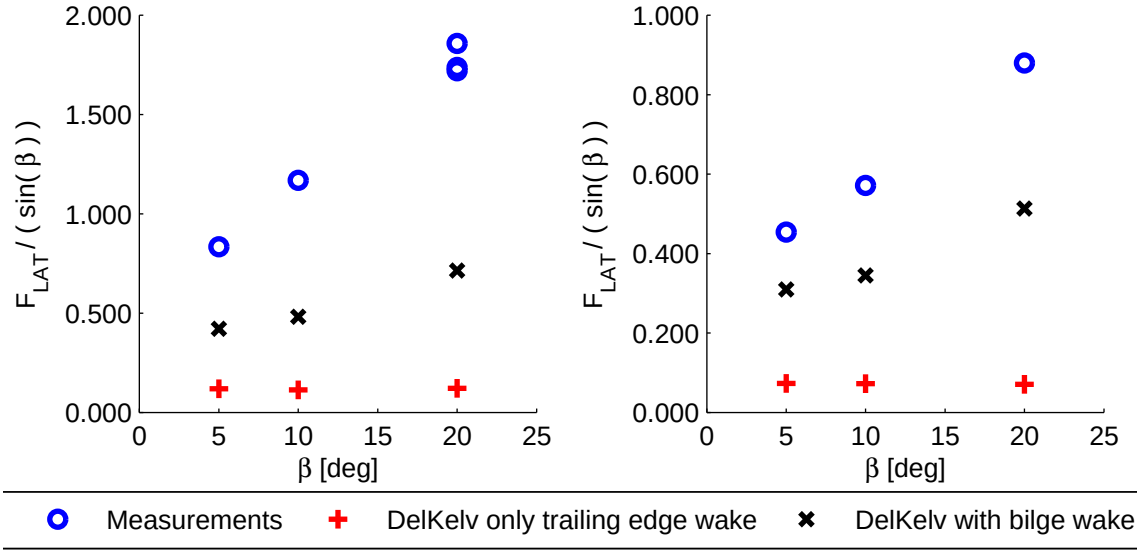

Figure 8.45: Comparison between model test results and calculations for force divided by drift angle, for $h/T = 1.4$ (left) and $h/T = 2.0$ (right).

Comparison of Potential flow and CFD calculations

A similar comparison between CFD and potential flow as done for the KVLCC2 will be made for the Marin Inland Ship. CFD calculations are carried out for one specific situation; namely a h/T ratio of 1.4 and a drift angle of 5 degrees. Figures 8.46 to 8.48 show a visual comparison, including both the wake model with only the trailing edge wake surface and the wake model with wake surfaces at trailing edge and lee-side bilge.

The figures show that - despite the better agreement of calculations using the wake model including bilge wakes with the experiments - the pressure coefficient distribution based on calculations using the simple wake model shows the best agreement with the CFD results. The main differences between the results for both wake models is seen in the aft ship region, with the bilge wake model results showing a higher pressure on average. Other pressure comparison plots can be found in appendix B.

Apart from a visual comparison, the forces and yaw moments obtained from the CFD calculations can be compared to the values from DelKelv as well. Table 8.11 shows this comparison for non-dimensional values. The DelKelv results are those from the calculations for the shortened Marin Inland Ship, as the results for these calculations are more realistic than for the full-length Marin Inland Ship.

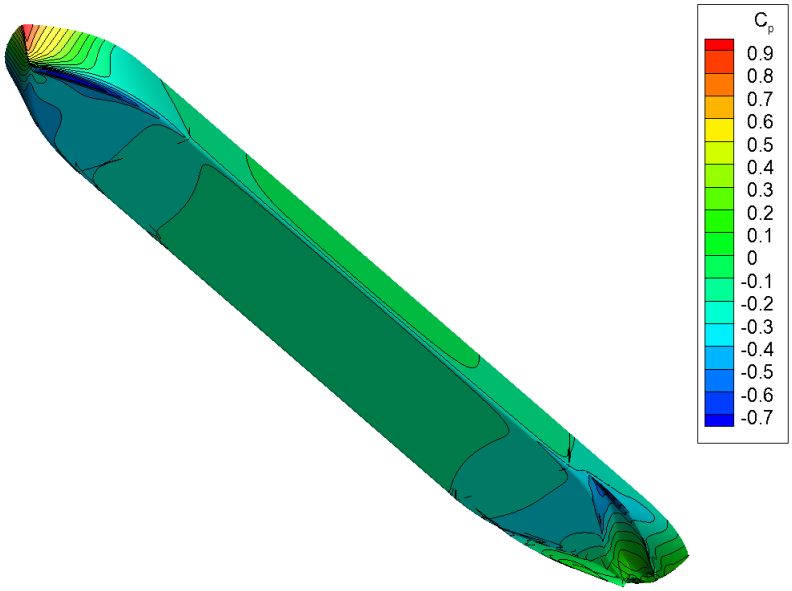

Figure 8.46: Pressure coefficient plot for MIS at $\beta = 5$ and $h = 4.90$ based on CFD calculations, viewed from pressure side

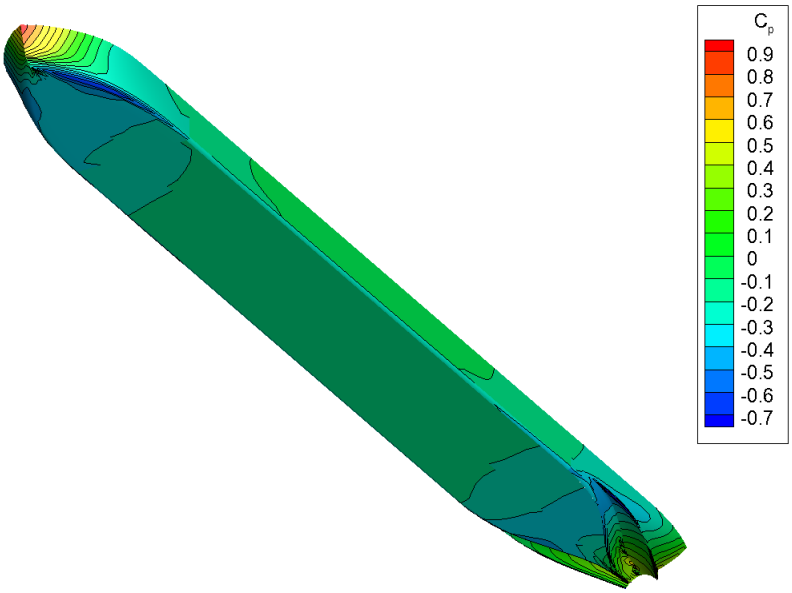

Figure 8.47: Pressure coefficient plot for MIS at $\beta = 5$ and $h = 4.90$ based on DelKelv calculations using only a wake surface at trailing edge, viewed from pressure side

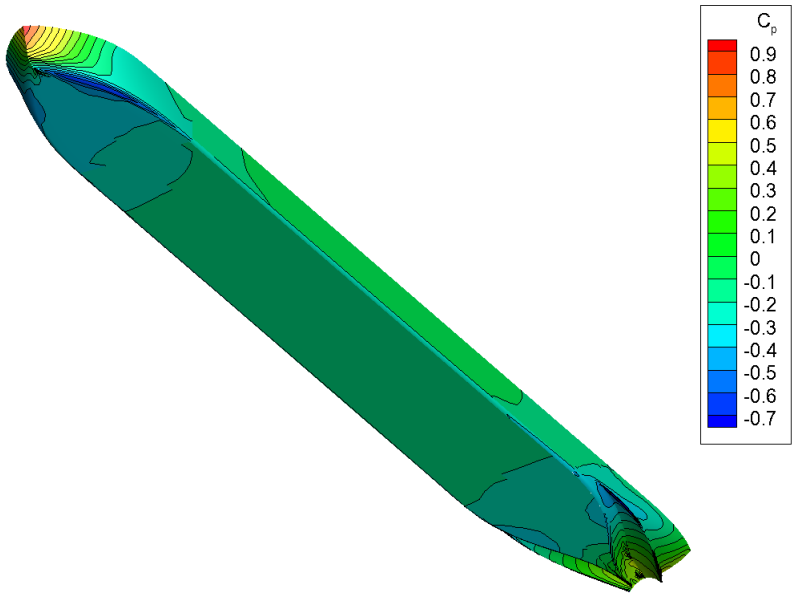

Figure 8.48: Pressure coefficient plot for MIS at $\beta = 5$ and $h = 4.90$ based on DelKelv calculations using a wake surfaces at trailing edge and lee-side bilge, viewed from pressure side

Table 8.11: Comparison between CFD and DelKelv results of non-dimensional lateral hull force and yaw moments for Marin Inland Ship at $h/T = 1.4$ and $\beta = 5$

	Lateral force [-]	Yaw moment [-]
CFD	0.0666	0.0260
DelKelv for simple wake model	0.0104	0.0260
DelKelv for bilge wake model	0.0368	0.0201

The table shows that for yaw moment, calculations with the simple wake model show good agreement with the CFD results. For the lateral hull force however, a large difference is found between DelKelv and CFD results. Using a bilge wake model increases the lateral hull force significantly. From figure 8.45, it is clear that significant non-linear effects are already present at $\beta = 5$. For a good comparison between DelKelv and CFD for lateral hull forces, CFD calculations at more drift angles are required to distinguish between linear and non-linear effects. Another remark that needs to be made here is that the CFD calculations include a certain sinkage and trim, which are not included in the DelKelv calculations.

Conclusion on Marin Inland Ship validation

Measurements for two different water depths are compared to results from DelKelv calculations, which are carried out for two different wake models. Also, the ship's three-dimensional model was modified to improve quality of results. The following conclusions can be drawn on the validation of DelKelv for the Marin Inland ship:

- First of all, a good or bad agreement between experiments and DelKelv calculations does not necessarily mean that DelKelv calculations are indeed good or bad for the Marin Inland Ship. Propellers and rudders, which are attached to the ship model, produce forces and moments and thereby influence the experimental results. Conducting bare-hull measurements would give a better view on the agreement between DelKelv and experiments. Still, from the comparisons made here, a conclusion can be drawn on whether DelKelv gives reasonable results or not.

- For the trailing edge wake surface only, forces determined by DelKelv are much lower than those from the experimental results. Moments are in relatively good agreement with the experimental results.

- Including a wake at the bilge significantly increases the forces determined by DelKelv, resulting in computed forces matching the experimental results. This indicates that the vortices leaving the ship at the bilge have a large influence on the integral forces. However, the inclusion of a horizontal bilge wake surface poses new problems, such as pressure incontinuities and unrealistically high forces.

- The heavily curved trailing edge is the reason for these problems. Shortening the ship by 2.5 meters gives better and neater pressure distributions, which lead to a better estimation of lateral hull forces and yaw moments.

- Using a shortened ship, much better agreement was found between calculations using the bilge wake model and experiments for both lateral hull forces and yaw moments. Especially for yaw moments, good agreement between DelKelv and experiments is observed.

- Comparing the pressure distributions from DelKelv to CFD results, both wake

modelling methods used in DelKelv give a pressure distribution in good agreement with the CFD results, if the shortened ship is used.

- Comparison of forces and yaw moments between DelKelv and CFD shows that the yaw moment determined from simple wake model calculations is approximately equal to the yaw moment estimated from CFD, while the lateral force is much smaller. For the bilge wake model, the difference between the lateral forces is smaller, while the difference between yaw moments increases.

Altogether, DelKelv gives good results on yaw moments, as seen from comparison with experiments and CFD calculations. For lateral hull forces, non-linear effects are already present at low drift angles, as shown in figure 8.45. Experiments at even smaller drift angles (between zero and five degrees) should be conducted to give a better insight on this. From the same figure, it can be concluded that DelKelv computes lateral hull forces reasonably, when the results are extrapolated towards $\beta = 0$.

8.4 Conclusions on potential flow theory for ship manoeuvring

The DelKelv program, as well as potential flow theory, have been tested for different three-dimensional cases. The Beukelman Wing is a very simple - and therefore robust - method to validate certain wake surface modelling methods, while for the KVLCC2 much data is available in the field of shallow water manoeuvring. The inland ship offers new and interesting tests case. Conclusions on the overall performance of potential flow theory in ship manoeuvring can be drawn and are given here.

- Overall, it is clear that inclusion of the bilge wake surface at the lee-side bilge significantly improves the agreement between calculations and experiments in shallow water.

- In deep water, the bilge wake surface preserve two-dimensionality in the flow, as was clear from validation for the KVLCC2. This lead to overestimation of lateral hull force and underestimation of yaw moment in deep water.

- For small drift angles, the longitudinal projection of the ship extends to the pressure side (starboard) as well. In case of small drift angles, a bilge wake surface needs to be attached at the pressure side as well.

- For inland ships, the aft end of the ship poses problems when it comes to inclusion of the bilge wake. Since the wake surface must leave the ship in flow direction, the wake surface is deformed and the wake surface panels approach of even penetrate the ship hull, leading to pressure discontinuities and unrealistic results.

- Inland ships usually have submerged transoms. This gives problems in wake modelling, as the attached wake surface will force the flow to leave the ship nearly perpendicular to the transom, which is impossible due to the boundary conditions applied. Removal of the transom and attaching a wake to the transom edge leads to better results.

- The tunnels on inland ships also produce significant lift force, and a wake surface should be included on these tunnels as well. This, again, can give modelling problems.

Summarizing, it can be stated that potential flow is a useful tool for use in the field of ship manoeuvring. The trailing edge of the ship should preferably consist of an line that is not curved too much, and also the ship should not be equipped with large tunnels for prevention of propeller ventilation. For inland ships, removing the transom, tunnels or even a part of the aft ship can lead to better results.

Chapter 9

Review of SURSIM model for Inland Shipping

In chapter 7, the method implemented in SURSIM for correction of lateral hull force and yaw moments are discussed, as well as methods found in literature. Chapter 8 then discussed the possibilities of potential flow calculations in the field of ship manoeuvring, showing that DelKelv is able to estimate sway force and yaw moment for the Beukelman Wing, KVLCC2 and Marin Inland Ship. For the KVLCC2, it is shown that DelKelv predicts lateral added mass accurately as well. For the MARIN Inland Ship, the ship model used in DelKelv had to be modified in order to get useful results for validation.

This chapter gives a review on the SURSIM method for estimation of respectively the added mass distribution, total added mass, sway forces and yaw moments. This sequence is chosen since the estimation of sway forces and yaw moments is done using the slender body method, in which linear hull forces and moments are determined based on the distribution of lateral added mass.

As the present study mainly focuses on inland shippping, the calculations and results given in this chapter mainly correspond to results for the Marin Inland Ship. In some cases, comparisons are given for the KVLCC2 as well. The first section gives a review on the added mass determination method in SURSIM, while the second section gives a review on the determination of sway forces and yaw moment. The last section will give an overview of the recommendations for improving the mathematical model SURSIM.

9.1 Review on the estimation of added mass

As mentioned, the distribution of added mass is the basis of the estimation of sway force and yaw moment. In SURSIM, the distribution of added mass is determined by equation 9.1. This equation is derived from two-dimensional strip theory by Papanikolaou [25].

$$m_{YY} = \frac{\rho\pi}{2} T^2 \left(C_1 \exp\left(\frac{C_2 B}{T} + C_3 \right) \right) \tag{9.1}$$

In which:

$$\begin{aligned} C_1 &= 0.388 + 0.1485 C_s - 1.3283 C_s^4 \\ C_2 &= -0.578 + 0.200 C_s \\ C_3 &= 0.7529 - 0.4677 C_s + 1.6148 C_s^4 \\ C_s &= \frac{A_T}{BT} \end{aligned}$$

The formula gives an estimation of the sectional added mass, in kilograms per meter. Based on the derivative of this function with respect to x, the sectional lift force can be determined as well.

9.1.1 Longitudinal distribution of added mass

Since the formula is based on two-dimensional strip theory, the estimation of added mass may be too high, especially for the bow and stern regions where the variation of the hull is large. In figures 9.1 and 9.2, the distribution of added mass is shown for the KVLCC2 and the Marin Inland Ship, respectively.

For the KVLCC2, comparison was made also with SHIPMO - a two-dimensional diffraction method - and PreCal, a three-dimensional diffraction method. Both the figures show a significant difference between two-dimensional and three-dimensional computations. Especially for the KVLCC2, where a difference of nearly ten percent is found in even the midship region. For both ships, the added mass distribution determined by a two-dimensional method is too high over the whole ship. The total added mass will thus be too high as well.

The differences occur because in two-dimensional added mass methods, it is assumed that flow only passes the ship underneath the keel. In real (three-dimensional) flow, however, flow also passes the ship around the bow and the stern, resulting in

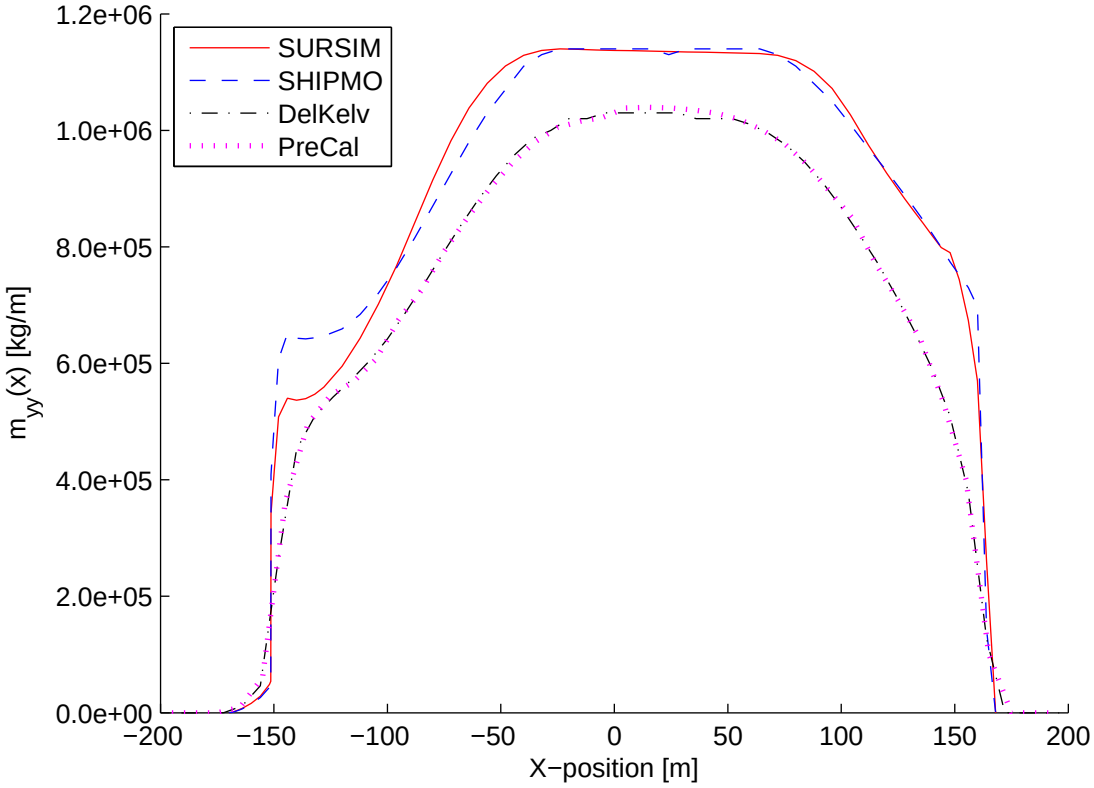

Figure 9.1: Comparison of various methods for determination of lateral added mass distribution. SHIPMO is an two-dimensional diffraction method, PreCal is a three-dimensional diffraction method. Calculations are done for $h/T = \infty$.

longitudinal flow. The fact that flow thus has more methods or space to pass the ship towards the other side, results in lower added mass.

Three-dimensional effects can be taken into account in the SURSIM method by altering Papanikolaou's method. Parameters such as x/L_{pp} or B/L_{pp} are expected to have a significant influence on the difference between two-dimensional and three-dimensional added mass. A derivation of a new, improved method for the estimation of the longitudinal added mass is not made in this study.

The distribution of added mass in shallow water

In shallow water, the three-dimensional effect on the distribution of added mass is increased even more. This is shown in figure 9.3. The figure shows the longitudinal distribution of lateral added mass for the MIS determined by DelKelv for several h/T

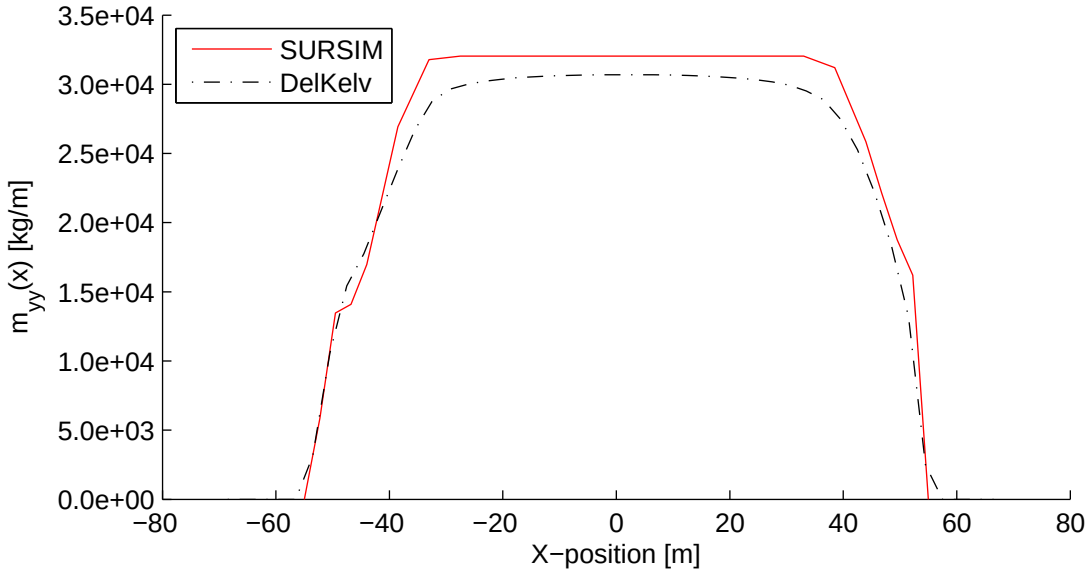

Figure 9.2: Comparison of various methods for determination of lateral added mass distribution. Calculations are done for $h/T = \infty$.

ratios.

The increase of three-dimensional effect on the distribution of added mass is expected. In shallow water, less water can pass the ship underneath. Therefore, more water is forced to pass the ship at the bow and stern, resulting in larger flow velocities in longitudinal direction. At a point near midship, the flow velocity in x-direction is zero, yielding maximum added mass at that point.

Using a method to estimate the increase of three-dimensional effects for added mass in shallow water, the estimate for sway force and yaw moment can be improved. A proposition for this method is given in equation 9.2.

$$\begin{aligned} C_{m_{yy},3D}(h,x) &= C_{M_{yy}}(h) \cdot C_{3D}(a,x) \\ C_{3D}(a,x) &= a\left(\frac{x}{L}\right)^2 + \left(1 - \frac{1}{12}a\right) \\ a(h) &= -0.55 \cdot \left(\frac{T}{h-T}\right)^{0.5} \end{aligned} \tag{9.2}$$

The proposed method is derived based on results of a series of systematic calculations for different inland ships, some at various draughts. It basically alters a single-factor added mass increase factor using the x/L_{pp} parameter. An overview of the ships used in the systematic series is given in table 9.1.

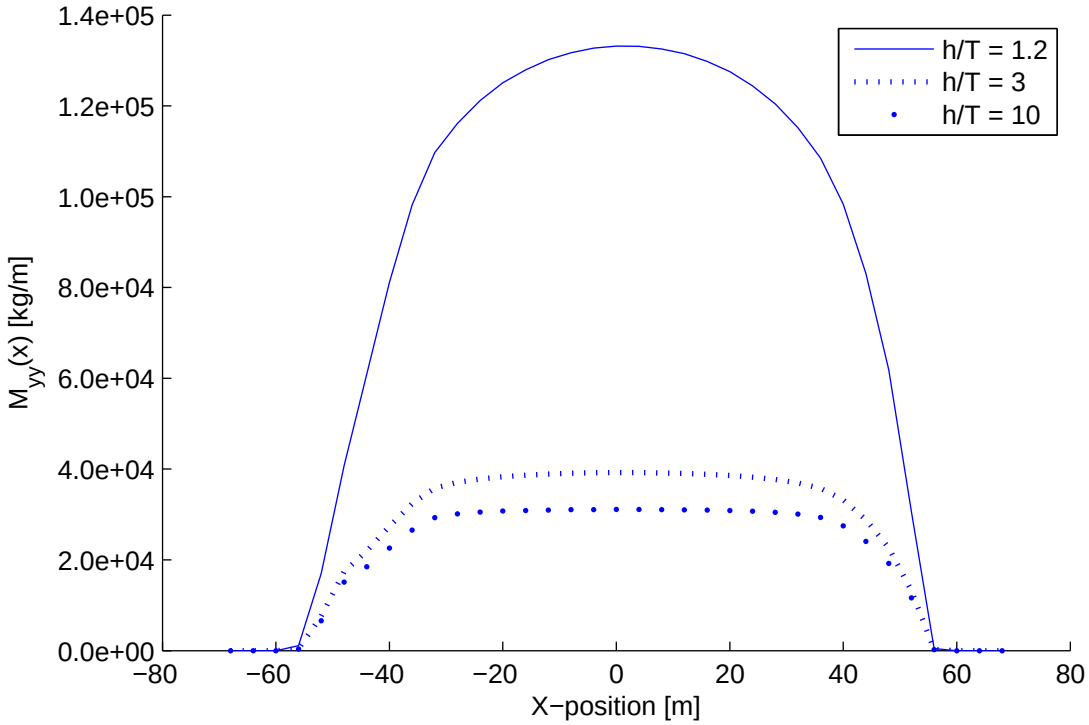

Figure 9.3: Distribution of added mass [kg/m] for the Marin Inland Ship at various h/T values.

9.1.2 Total added mass in shallow water

From the preceding section, we know that the two-dimensional method for estimation of sectional added mass gives too high results. The total added mass is obtained from integration of the sectional added mass, and will be too high as well. Using DelKelv, the total added mass is determined for various water depths and ships shown in table 9.1. The shallow water corrections are determined by dividing each of results by the result for deep water. The corrections obtained from the DelKelv study are compared to the method implemented in SURSIM. The comparison is shown in figures 9.4 to 9.6.

From the figures, the following observations can be made. First, it appears that for increasing B/T ratio, SURSIM is increasingly overestimating the shallow water correction of lateral added mass. As high B/T ratios are not rarely seen in inland shipping, the SURSIM correction used for lateral added mass can lead to too high estimates of lateral added mass. Second, SURSIM gives a too low shallow water

Table 9.1: Ship database for new added mass correction method

Ship	Length	Breadth	Draught
Marin Inland Ship	110	11.40	3.5
Marin Inland Ship	110	11.40	3.0
Rhine-Donau RoRo vessel	130	22.60	1.5
Rhine-Donau RoRo vessel	130	22.60	2.2
HKG Inland Ship	130	17.00	3.8
HKG Inland Ship	130	17.00	3.3
HKG Inland Ship	130	17.00	3.0
KLVCC2	320	58.00	20.80

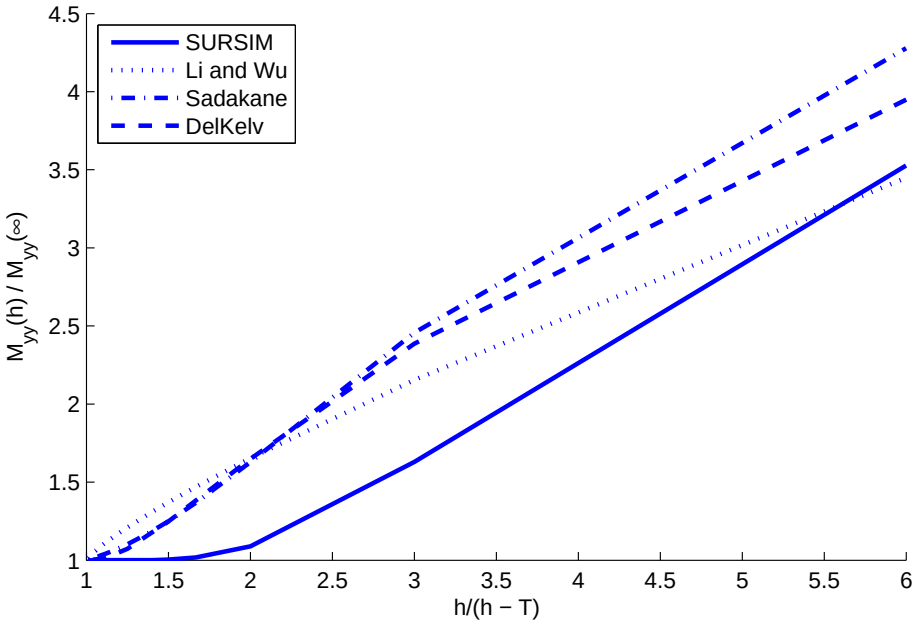

Figure 9.4: Comparison of DelKelv results and empirical methods for the MARIN inland ship

correction for non-extreme situations. Approximately no correction is given up to $h/T = 2.0$. The DelKelv results clearly show a significant shallow water effect is present for $h/T = 2.0$ already.

Based on results of the systematic study, a new method for correction of lateral added mass is proposed. The new method is shown in equation 9.3.

$$\frac{M_{yy}(h)}{M_{yy}(\infty)} = 1 + 0.9785 \left(\frac{h}{T}\right)^{-0.5} \left(\frac{A_M}{h^2}\right) C_B^{-0.5} \tag{9.3}$$

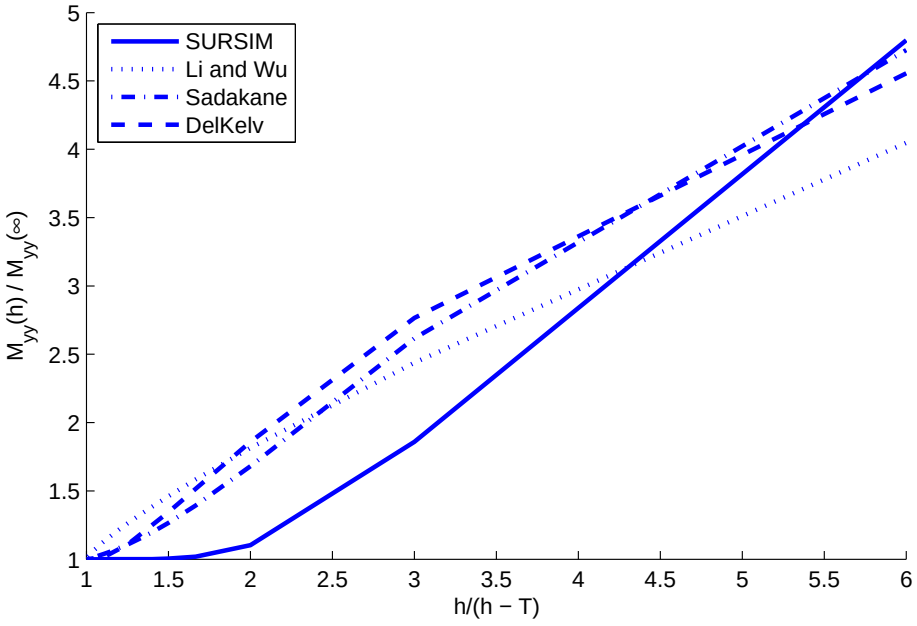

Figure 9.5: Comparison of DelKelv results and empirical methods for the HKG inland ship ($L_{pp} = 130$, $B = 17$, $T = 3.8$)

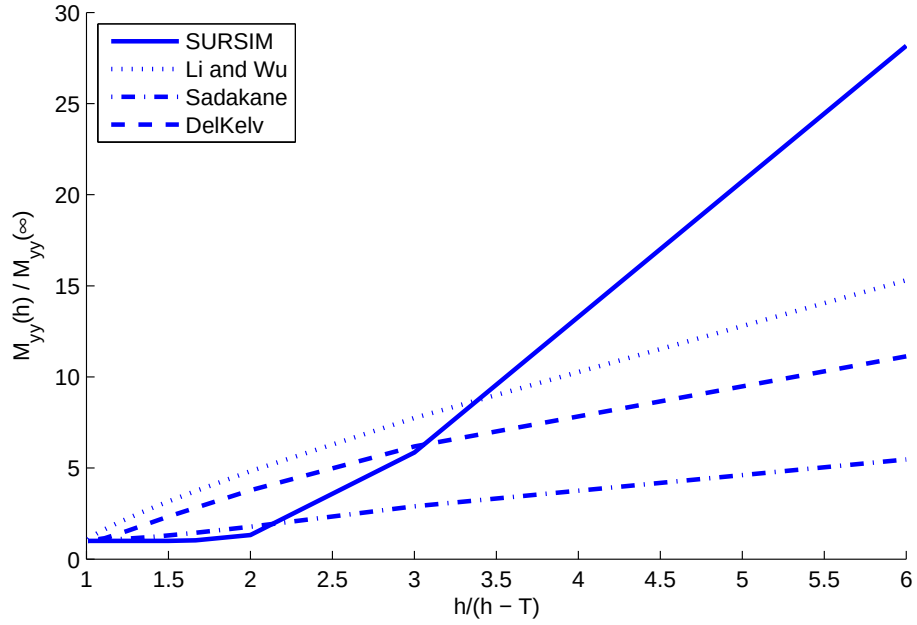

Figure 9.6: Comparison of DelKelv results and empirical methods for the RoRo inland ship ($L_{pp} = 130$, $B = 22.6$, $T = 1.5$)

The proposed method especially gives better results until $h/T = 1.5$. For lower h/T ratios, the difference between the new method and DelKelv results increases. A non-linear effect is observed as well. This effect could be captured by using a more complex correction formula, but an h/T value of 1.2 is considered to be a very extreme situation. In these situations, much more effects arise from shallow water, such as significantly increased sinkage and trim. Figure 9.7 shows the comparison between the SURSIM method, DelKelv results and the new method. The new method can be used for determination of the $C_{M_{yy}}$ value in equation 9.2.

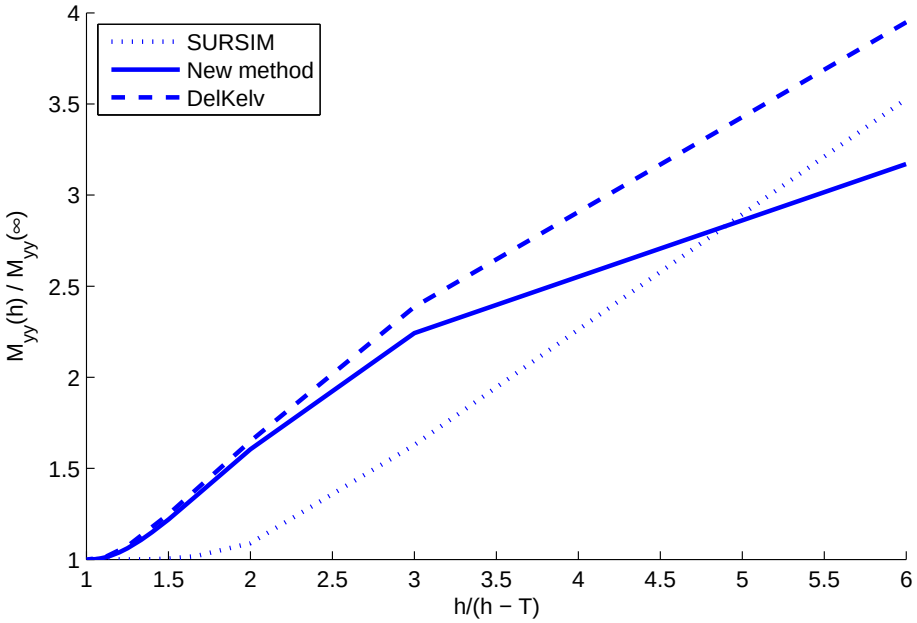

Figure 9.7: Comparison of new added mass correction method applied on MIS with original SURSIM method and DelKelv results

9.2 Review on sway force and yaw moment estimation

The previous section discussed the determination of the added mass distribution as well as the total sway added mass. It appeared that the method used for the estimation of the added mass distribution, Pananikolaou's formula, gives to high estimates for the sectional added mass because the method is based on two-dimensional strip

theory. Further, it appeared that SURSIM's added mass correction for total sway added mass yields too low corrections for non-extreme shallow water, but yields to high values in case of significant shallow water effects and a high B/T ratio.

This section investigates the sway force distribution, as well as the sway force itself and yaw moments acting on an inland ship. The method used in SURSIM - described in chapter 7 - is compared to DelKelv results. A comparison with CFD results is made for the KVLCC2.

9.2.1 Sway force distribution

SURSIM estimates the sway force distribution from the distribution of added mass by taking the derivative of added mass in x-direction, $\partial M_{yy}/\partial x$, and multiplying it with the section size. Using MATLAB, it is also possible to determine the distribution of sway force from DelKelv results. A comparison between the SURSIM approach and DelKelv results for the MIS is shown in figure 9.8. The Slender Body approach as used in SURSIM is also applied to the DelKelv added mass distribution, designated by 'DelKelv, SB method'.

The figure shows that for the bow section, all three sway force distributions that are based on DelKelv results yield approximately the same sway force magnitude. Furthermore, we note that in the aft ship region, the results from slender body approach applied to DelKelv results yield the same distribution as the simple wake model calculation, apart from the large negative peak. This peak is closer to the distribution calculated by the SURSIM method. The difference between the simple wake model calculation and the SB method applied to the DelKelv added mass distribution is due to the fact that the slender body method in this case yields zero force (paradox D'Alembert).

Looking at the distribution from the bilge wake model calculation, we see that the calculated sway force at the midship section is non-zero, while all other distributions are, on the other hand, nearly zero. This is due to the bilge wake surface that preserves two-dimensionality in the flow, even for deep water. One could state that using this wake surface, shallow water effects are modelled even in deep water.

For the aft ship region, the bilge wake model yields unexpected results. Whereas one would expect the sway force distribution to be negative here (for example, see [32]), the bilge wake model yields positive forces only. Positive forces in the aft ship

region result in a decreased yaw moment.

A similar figure is made for the KVLCC2. For the KVLCC2, CFD calculations were also carried out to determine the sway force distribution on the ship hull. The comparison between the various methods to estimate the sway force distribution is visualized in a bar plot, shown in figure 9.9

Figure 9.9 shows that the slender body method applied to an added mass distribution from DelKelv gives the best comparable result to the CFD results, apart from the large negative peak at the aft end of the ship. The large peak is due to the fact that added mass decreases to zero at the aft end, resulting in large negative $\partial m_{yy}/\partial x$. The slender body method applied to the DelKelv added mass distribution also yields zero force. The results from the slender body method applied to the DelKelv added mass distribution are in better agreement with the CFD results than the sway force distribution obtained using SURSIM. This indicates that using a three-dimensional added

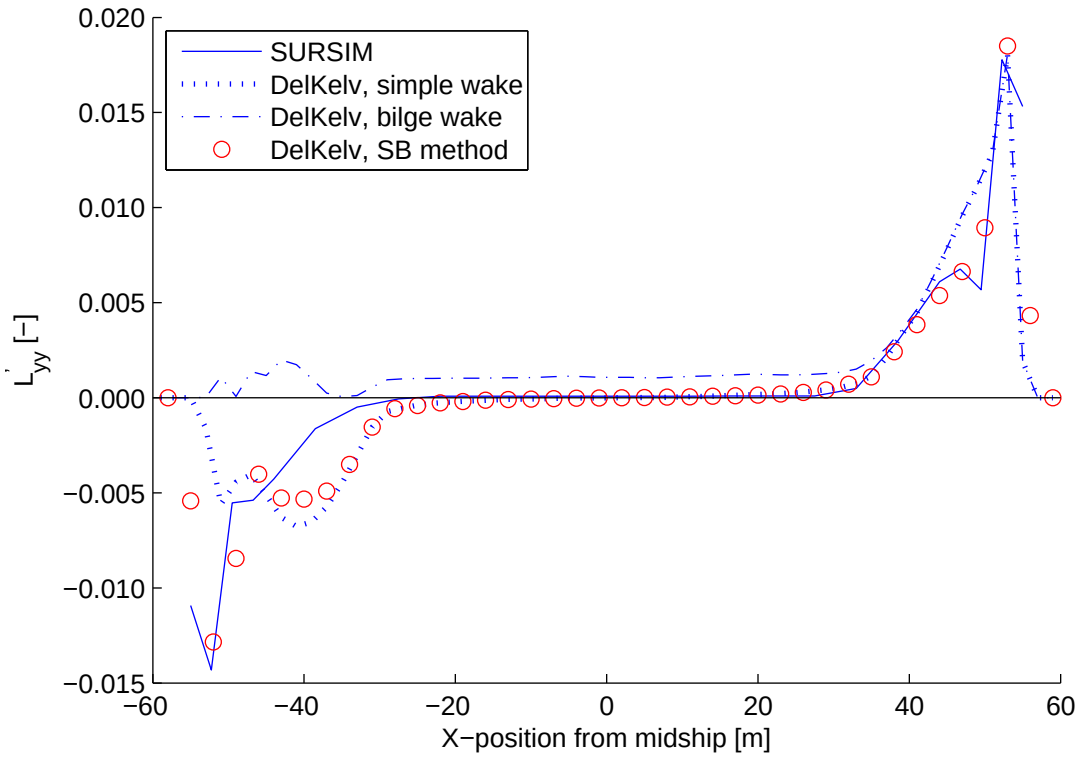

Figure 9.8: Comparison of various methods to determine the distribution of sway force for the Marin Inland Ship at $h/T = \infty$. X-axis is defined forward

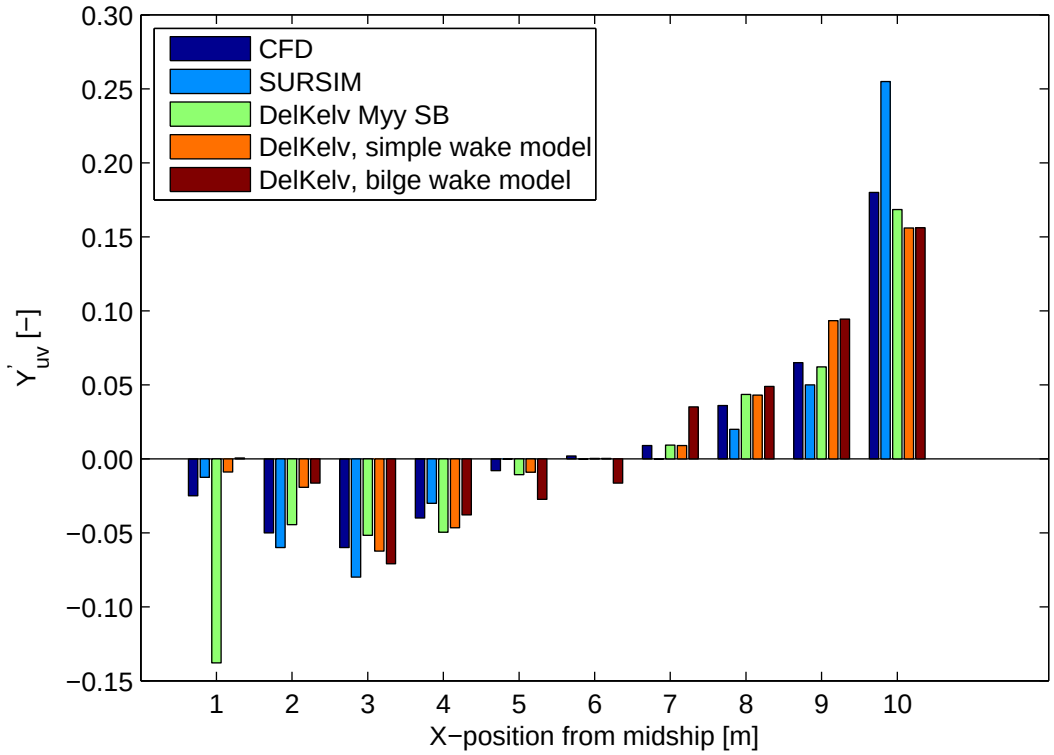

Figure 9.9: Comparison of various methods to determine the distribution of Y_{uv} for the KVLCC2 at $h/T = \infty$. The segment number on the horizontal axis increases towards the bow

mass distribution may be an improvement to the SURSIM mathematical model.

9.2.2 Total sway force and yaw moment

The previous section discussed and reviewed the methods to determine the sway force distribution. It was shown that using a three-dimensional added mass estimate yields better results when compared to CFD, except for the aft end of the ship. Furhter, it is shown that using a bilge wake model yields some unexpected results for the distribution of sway force. This section discusses the estimation of total sway force and yaw moment, which can be determined from the pressure distribution from DelKelv or by integration of the sway force distributions given in the preceding section.

Table 9.2 shows a comparison of total sway force coefficient and yaw moment coefficient, Y'_{uv} and N'_{uv}.

The table shows that results from SURSIM are very similar to the results from

Table 9.2: Non-dimensional sway force coefficient and yaw moment coefficient determined by various methods for the Marin Inland Ship at $h/T = \infty$, $V_S = 1$.

Calculation method	Y'_{uv} [N]	N'_{uv} [Nm]
SURSIM method	0.0391	0.1159
DelKelv with simple wake model	0.0473	0.1134
DelKelv with bilge wake model	0.2521	0.0647
Slender Body Method on DK M_{YY}	0.0000	0.1414

DelKelv using the simple wake model. From the validation study described in section 8.3.4, it is known that this wake model probably gives incorrect results when it comes to sway forces. According to the same validation study, using the bilge wake model results in a significant improvement of agreement for sway forces between calculations and measurements. This indicates that using DelKelv (or similar potential flow solvers) calculations, a correction method for the slender body approach or a whole new lateral force estimation method may be derived for the estimation of linear lateral hull forces acting on inland ships. For yaw moments, the results obtained by the SURSIM method are already sufficiently accurate, as the validation study for the MARIN inland ship showed that yaw moments determined from simple wake model calculations are in good agreement with results from both experiments and CFD calculations.

Applying the slender body method to the added mass distribution derived from DelKelv yields zero force, as expected. The yaw moment is higher than for other methods. The yaw moment should equal the Munk moment, which is the yaw moment that is obtained from non-viscous calculations.

9.3 Shallow water corrections for sway force and yaw moment

The previous section reviewed the SURSIM method on predicting the lateral hull force and yaw moment in deep water. It was showed there that the method used in SURSIM, the slender body method, gives significantly different results from DelKelv when a bilge wake model is used. It is concluded that moments can be estimated reasonably accurate using the simple wake model or SURSIM method. For forces, it appears that the SURSIM method is sufficient for the KVLCC2, but is insufficient

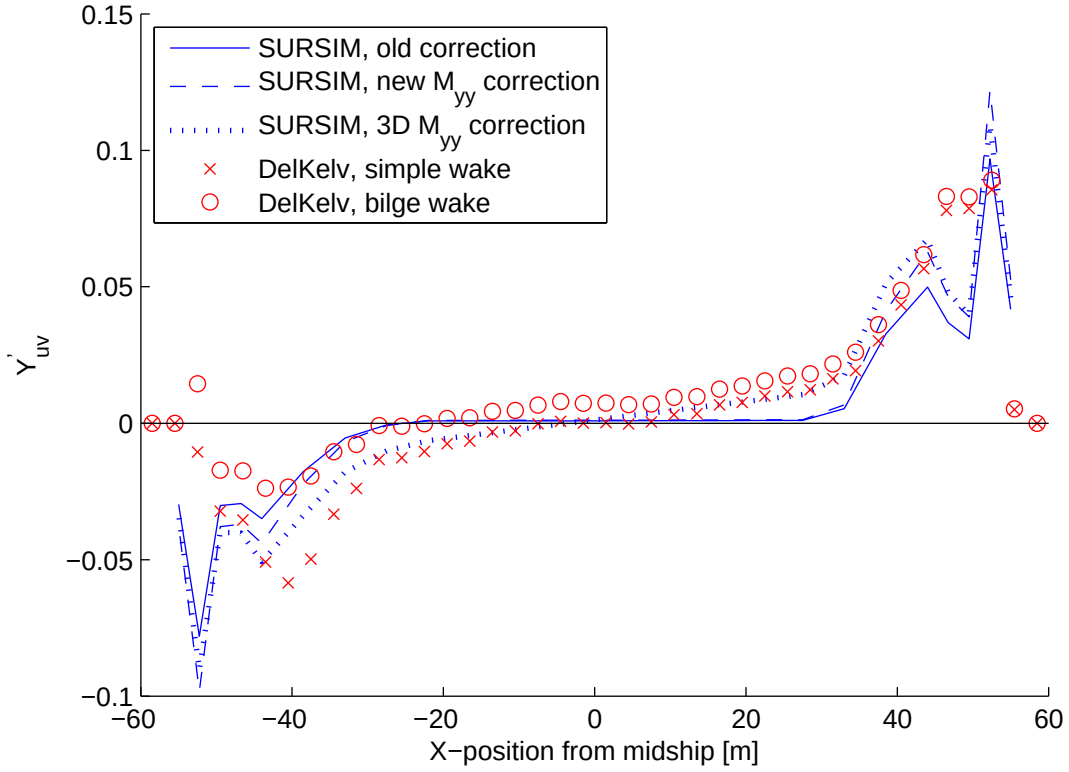

Figure 9.10: Comparison of various methods to determine the distribution of Y_{uv} for the Marin Inland Ship at $h/T = 1.4$. X-axis is defined forward

for the Marin Inland Ship. This section deals with the shallow water corrections for lateral hull force and yaw moment.

As mentioned in chapter 7, SURSIM currently applies a correction factor to the sway force and yaw moment for application in shallow water. The main aim of this section is thus to review these correction factors, however it is also interesting to investigate the change of the lateral force distribution in shallow water. Figure 9.10 shows a comparison of this distribution for $h/T = 1.4$, for two different DelKelv calculations and three different shallow water corrections applied to the SURSIM distribution seen in figure 9.8.

Figure 9.10 shows a similar picture to that for deep water when looking at the bow region. Both DelKelv calculations yield the same values, while values from SURSIM methods are significantly higher. For the midship section, the first two SURSIM methods yield a constant, nearly zero value. The SURSIM method including the 3D

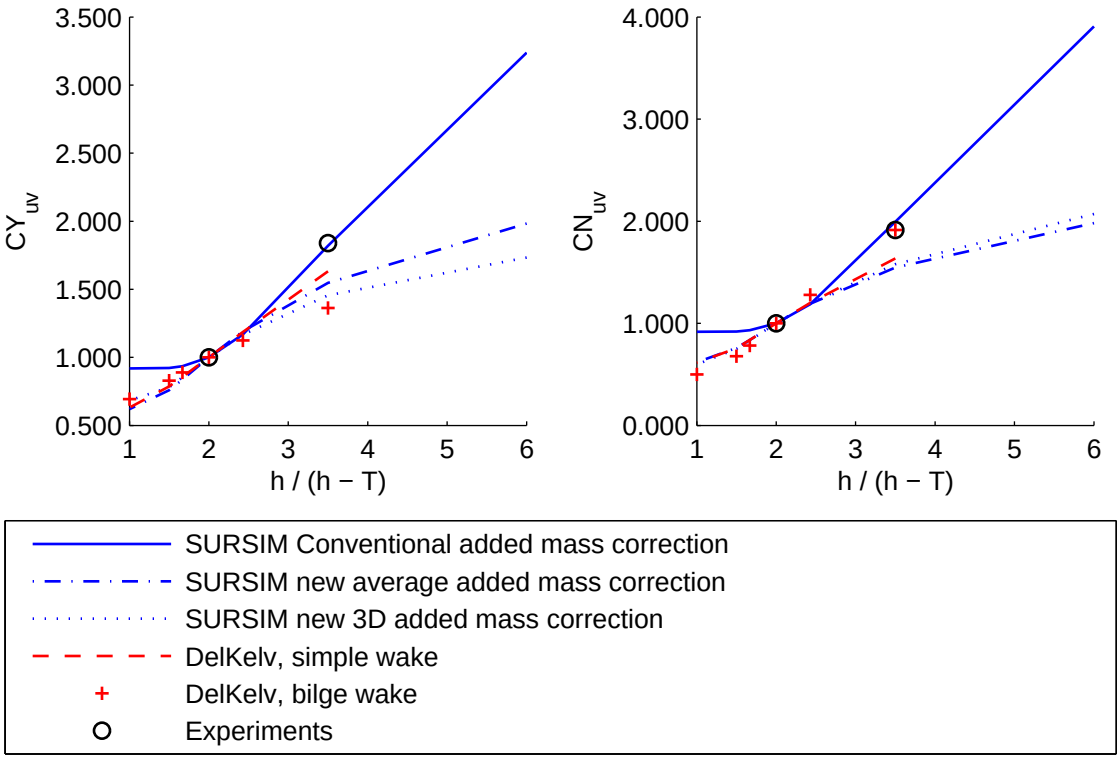

Figure 9.11: Comparison of various methods to determine the shallow water correction for lateral forces and yaw moments. Correction factors relative to $h/T = 2$

correction for sway added mass, as well as the DelKelv methods, give a non-constant value in the mid ship region. It appears that in shallow water, the parallel midship still produces lift forces. For the aft ship region, the figure shows that the value of Y'_{uv} determined from DelKelv calculations using a bilge wake, is negative in shallow water, where it was positive in deep water. The effect of shallow water is - when the bilge wake is included - particularly affecting the pressure side where no bilge wake surface is attached. At the lee-side, pseudo-shallow water effects are present in deep water due to the wake surface attached to the bilge. Thus, in shallow water, flow velocities increase at the pressure side, leading to sway forces in starboard (pressure side) direction, which are negative in the used coordinate system.

From the distribution of lateral force along the hull, the total lateral hull force and yaw moment can be computed. Computed for various water depths, the correction of forces and moments can be determined as well. In figure 9.11, correction factors relative to $h/T = 2.0$ are plotted. The choice to set the correction at 1 for $h/T = 2.0$ is made because the experiments only provide with data for $h/T = 2.0$ or $h/T = 1.4$.

The figure shows that for the relative correction with respect to $h/T = 2.0$, the method implemented in SURSIM gives a good approximation of increase factor for both lateral forces and moments. However, looking at deep water ($h/(h-T) = 1$), SURSIM significantly deviates from DelKelv results and the two new correction methods (which are derived from DelKelv results). With respect to deep water, SURSIM may thus give a too low correction for both $h/T = 2.0$ and $h/T = 1.4$.

The figure also shows that agreement between calculations and experiments is best for the simple wake model when it comes to shallow water correction of lateral hull forces. The new average added mass method - which can be easily implemented in SURSIM - gives approximately the same results as the DelKelv simple wake model, up to $h/(h-T) = 3$, at which point $h/T = 1.5$. The new average added mass correction - described in 9.1 - can thus be used as an alternative method to correct for lateral hull forces. Still, a deviation between measurements and calculations seems to occur at very shallow water. This is also seen for added mass itself. By using quadratic terms in the correction method, the correction remains accurate for very shallow water as well.

Looking at the right-hand side plot, which shows the correction of yaw moments, the DelKelv results for the bilge wake model are in very good agreement with the experimental results. As SURSIM probably gives a too low correction for the corresponding h/T ratios according to explanation above, a new yaw moment correction method may be derived based on DelKelv calculations using a bilge wake model. This is not done in the present study, due to the large effort required for such calculations because of inland ship wake modelling problems. Another choice thus needs to be made.

Figure 9.12 shows a comparison of the shallow water correction for Y_{uv} and N_{uv}, relative to deep water. For the correction of forces, figure 9.11 shows that the simple wake model gives results that are most close to the experimental results. The corrections of total added mass is very close to the simple wake model results, indicating that the total added mass correction is probably a good method to correct sway forces in shallow water as well. In SURSIM, the correction for lateral added mass and sway force were already the same, only the correction itself did not apply very well to inland ships. Using the new added mass correction method described in section 9.1, the accuracy of simulations for inland ship manoeuvring in shallow water can be improved.

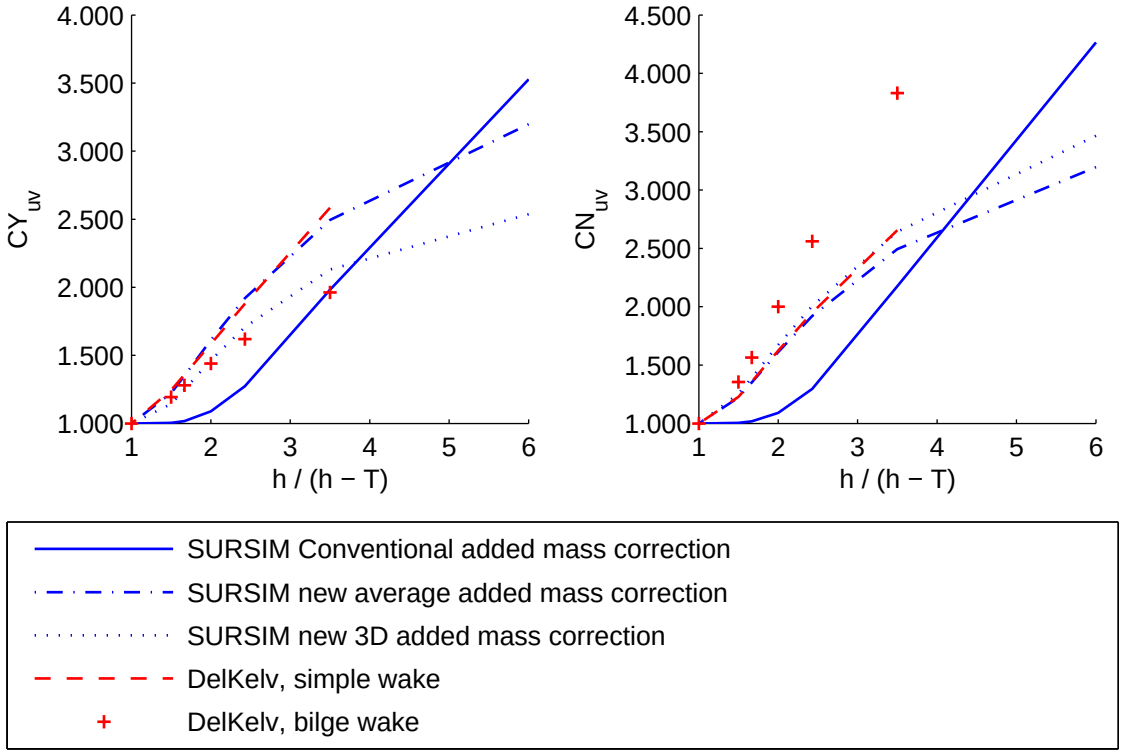

Figure 9.12: Comparison of various methods to determine the shallow water correction for lateral forces and yaw moments.

The right-hand side of figure 9.12 shows the correction for yaw moments. The bilge wake model was closest to the model experiments in estimating the shallow water correction relative to $h/T = 2.0$, and the present figure shows that this correction is significantly higher than the other corrections presented in the graph. However, results from the DelKelv bilge wake model are approximately a constant factor higher than corrections determined by the new total added mass correction. By altering this correction (discussed in section 9.1), into equation 9.4, a relatively good correction is obtained.

$$\frac{N_{uv}(h)}{N_{uv}(\infty)} = 1 + 1.63 \left(\frac{h}{T}\right)^{-0.5} \left(\frac{A_M}{h^2}\right) C_B^{-0.5} \tag{9.4}$$

Summarizing the previous, the sway force can be corrected for shallow water using the added mass correction method presented in section 9.1. The yaw moment can be corrected in a similar manner, only altering the coefficient of 0.9875 used in the added mass correction into 1.63. Figure 9.13 shows the new correction methods along

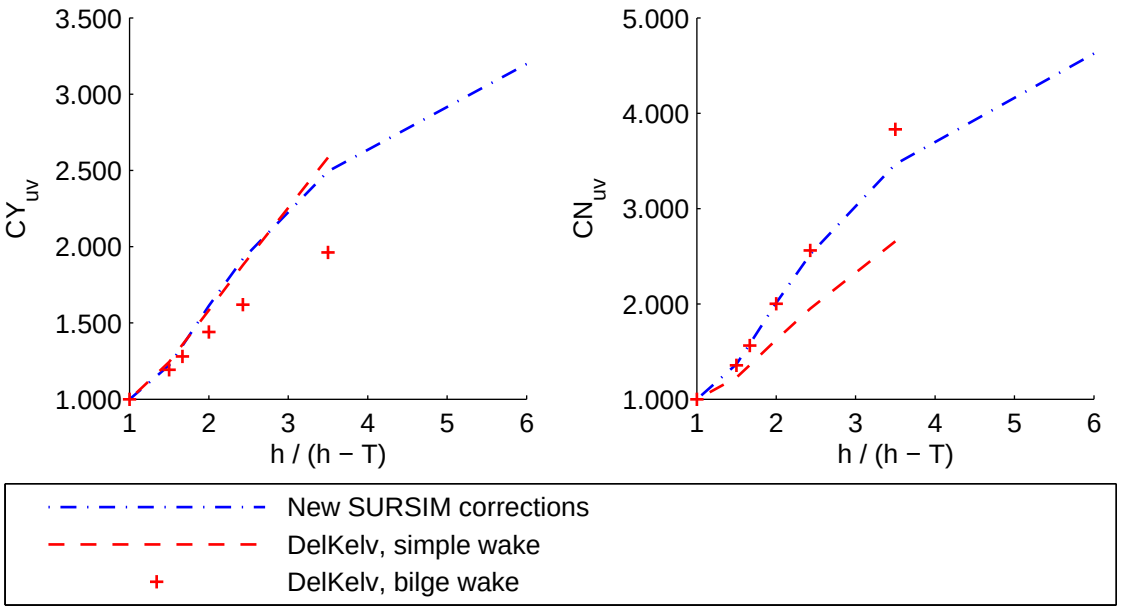

Figure 9.13: Proposed SURSIM corrections, applied to the Marin Inland Ship, presented along with the DelKelv results for both wake models

with the DelKelv results.

An important remark that needs to be made here corresponds to the validity of the proposed method for the correction of yaw moment. The correction is only based on calculations for the MARIN Inland Ship. The bilge wake model is not applied to other inland ships, as the modelling of wake surfaces at inland ships is relatively difficult due to their aft ship forms.

9.4 Propositions for improvements to the SURSIM model

The previous sections give a review on the SURSIM method used for determination and correction of sway added mass, sway forces and yaw moments. This section gives a short summary on the methods that have been proposed in the preceding sections.

For correction of sway added mass, equation 9.3 is proposed:

$$\frac{M_{yy}(h)}{M_{yy}(\infty)} = 1 + 0.9785 \left(\frac{h}{T}\right)^{-0.5} \left(\frac{A_M}{h^2}\right) C_B^{-0.5} \tag{9.5}$$

The same equation can be used to determine the correction of sway force acting

on the ship hull. For yaw moments, the following equation is proposed, which is only a slight modification of the method proposed for correction of sway force:

$$\frac{N_{uv}(h)}{N_{uv}(\infty)} = 1 + 1.63 \left(\frac{h}{T}\right)^{-0.5} \left(\frac{A_M}{h^2}\right) C_b^{-0.5} \tag{9.6}$$

Again, it needs to be noted that especially the method for correction of yaw moment is derived only on basis of calculations involving the Marin Inland Ship. However, the yaw moment correction which is currently implemented in SURSIM is also equal to the method for correction of sway force, apart from different coefficients. The method originally implemented in SURSIM for correction of yaw moment has been tested for a variety of cases, indicating the method is good. This gives reason to assume that also for inland ships, the methods for correction of sway force and yaw moment must be quite similar.

This chapter does not only describe the new corrections mentioned above, it also investigates the added mass distribution as well as the distribution of sway force. For the added mass distribution in particular, large differences between distributions from two-dimensional methods and three-dimensional methods are observed. It is also shown that using a three-dimensional added mass distribution to estimate the distribution of sway force for the KVLCC2 (see figure 9.9) results in a sway force distribution in closer agreement to CFD results (apart from the aft end of the ship). Furthermore, the three-dimensional effect on sway added mass increases for decreasing water depth. Therefore, an correction method for the added mass distribution was developed:

$$\begin{aligned} C_{m_{yy},3D}(h,x) &= C_{M_{yy}}(h) \cdot C_{3D}(a,x) \\ C_{3D}(a,x) &= a\left(\frac{x}{L}\right)^2 + \left(1 - \frac{1}{12}a\right) \\ a(h) &= -0.55 \cdot \left(\frac{T}{h-T}\right)^{0.5} \end{aligned} \tag{9.7}$$

The above set of equations is derived based on comparison of deep-water three-dimensional added mass with shallow-water three-dimensional added mass. Both deep-water and shallow-water added mass distributions are determined using DelKelv calculations. A method to determine three-dimensional added mass itself is not developed during the present study, as this would require as much larger database of ships. However, developing an improved method to estimate the added mass distri-

bution could significantly increase the accuracy of SURSIM simulations. A suitable method would be to use the added mass distribution from Papanikolaou as a basis, and using a alteration formula to obtain a three-dimensional added mass distribution. This correction method would include parameters such as L/B and x/L, for example.

Chapter 10

Conclusions and recommendations

A literature study is carried out into shallow water resistance and propulsion. Further, various methods found in literature for linear manoeuvring forces in shallow water are compared to each other, as well as to the methods used in SURSIM. Apart from literature study, the possibilities of potential flow calculations in the field of ship manoeuvring are investigated using DelKelv. A validation study is carried out using DelKelv for three test cases: the Beukelman Wing, the KVLCC2 and the MARIN inland ship. Further, potential flow calculations are used to review the shallow water corrections of linear lateral hull forces, linear hull moments and added mass by comparing empirical and computational results. Conclusions emerging from the present study are summarized in the following. After the conclusions, recommendations are given on subjects in need of more research.

10.1 Conclusions

Inland ship resistance

- For deep-water resistance estimation, large differences are found between various methods. The more modern methods yield much lower resistance, as does the method by Holtrop & Mennen. This method is considered to be useful for quick estimation of inland shipping, especially since it is regularly updated and inland ships are more often included now as well.

- Estimation methods for shallow water resistance are roughly divided into two groups: The SURSIM method belongs to the group of methods that do not sep-

arate between frictional and wave resistance. It is now more widely known that the lack of this separation can result in wrong resistance corrections. Methods that do separate between wave and frictional resistance yield much lower corrections and are considered a good alternative for the method currently being implemented.

- Part of the answer to the first sub-question given in chapter 3 is hereby given. The SURSIM correction method for shallow water does not separate between wave and frictional resistance, leading to significantly higher corrections compared to more modern methods.

Inland ship propulsion

- From literature, it becomes clear that very little is known on the effects of shallow water on propulsion performance. It is known that shallow water has a significant effect on the wake fraction, but no empirical formula is available.

- Based on the results from shallow water tests using an inland ship [27], an equation is derived for correction of wake fraction in shallow water. Also, correction of wake fraction for a ship under drift can be estimated by the method of Hirano [10]. Both equations, given in chapter 6 can be implemented in SURSIM.

- By the previous two paragraphs, the propulsion part of the first sub-question is answered as well.

Inland ship manoeuvring

- Overall, the shallow water correction methods implemented in SURSIM usually give lower corrections than other empirical methods investigated for non-extreme shallow water. However, corrections from the SURSIM method can be very large for ships having a high B/T ratio.

Potential flow for ship manoeuvring

- DelKelv is used to solve potential flow problems. The program is validated for three different test cases (Beukelman Wing, KVLCC2 and Marin Inland Ship). Wake models are used to capture lift forces acting on the ship.

- Using the bilge wake model, better agreement is found between experiments, CFD and DelKelv results compared to the simple wake model. This especially applied to sway forces. Yaw moments are estimated accurately using the simple wake model as well.
- The bilge wake model conserves two-dimensional behaviour in deep water. Overestimation of sway force may be the result.
- For ships having a highly curved trailing edge or ships that are equipped with anti-ventilation tunnels, wake construction when using the bilge wake model is difficult, since the wake surface cannot leave the ship parallel to the ships heading here. Problems can be overcome by removing a part of the aft ship region.
- Overall, potential flow shows to be useful in determining forces and moments acting on a ship under drift, at several water depths. Using some adaptations for inland ships, the DelKelv program (or any other potential flow solver) can be of great use in estimating manoeuvring behaviour of inland ships.
- Given the above, the second sub-question is also answered. Potential flow is indeed a useful and accurate method to estimated manoeuvring force such as sway force and yaw moment, for deep as well as shallow water.

Review of the SURSIM mathematical model

- In chapter 9, methods for estimation of sway force and yaw moment for deep as well as for shallow water are reviewed. It appeared that the slender body approach is very accurate on estimation of yaw moment. For sway forces, on the other hand, the slender body method yields too low values.
- Improvements to the slender body approach can be done by using a three dimensional added mass distribution. In shallow water, the added mass distribution becomes even more three dimensional, indicating even larger improvements may be achieved for shallow water.
- Comparing the shallow water correction methods currently implemented in SURSIM with DelKelv results, significant differences are found for sway added mass, sway force and yaw moment. New methods have been derived based on

systematic calculations for few inland ships. The new methods give a better estimate of shallow water manoeuvring for inland ships.

- The above three point yield the answer to the third sub-question. The most important difference found is that the SURSIM method does not give any significant correction for $h/T > 2.0$, while increase of sway force or yaw moment is clearly observed for this region already.

- The last sub-question can be answered as well. On basis of the systematic study, it is found that the block coefficient C_b (which is significantly changed when a ship is not loaded to its design draft), h/T ratio and the Am/h^2 ratio are of main importance to single factor manoeuvring force corrections for shallow water. When one would apply corrections to the base of the SURSIM method - the added mass distribution - corrections are required to take three-dimensional behaviour of flow into account. Parameters such as x/L and B/L are of importance in that case.

Answer to the main research question

Finally, the main research question can be answered as well: *"How should a mathematical model that bases on empirical methods for manoeuvring simulation be improved for application to inland ships in their normal operational conditions, using both literature study and potential flow calculations?"*

- For ship resistance, the deep water resistance estimate used in SURSIM is probably sufficient already, as the method usually applied is updated regularly, and inland ships are included in the database as well. Shallow water resistance is clearly based on the single-factor approach from Lackenby, which can be replaced by a method that separates between wave and frictional resistance.

- The estimates regarding propulsion performance can be improved by using a shallow water correction for the wake fraction. This parameter is widely known to be affected by shallow water, however no empirical method is found in literature. A very simple method is proposed in chapter 6, however the validity for a wide range of ships is unknown.

- Estimates of ship manoeuvring forces can be improved by using a three-dimensional added mass estimation method, as appeared from systematic potential flow calculations. For use of a three dimensional added mass, a new method needs to be developed. As a basis for the method, Papanikolaou's method can be used. The correction formulas presented in chapter 9 can be used to correction sway force and yaw moment for an inland ship under drift, but using potential flow calculations the systematic study can be extended to yaw rates as well.

10.2 Recommendations

10.2.1 Investigation of manoeuvring forces for yaw rates

In chapter 8, section 8.3.2 it is shown that DelKelv is able to predict yaw moment relatively accurate for the KVLCC2 under a certain yaw motion. As is also stated in [33], relatively little research is done to investigate the effects of yaw motion at ships. In order to have a complete and accurate simulation model, accurate estimation of forces and moments during yaw motion is important as well.

10.2.2 Derivation of a three-dimensional added mass distribution

As already mentioned in chapter 9, more accurate estimations of forces and moments using the Slender Body Method can be achieved if a three-dimensional added mass method is used. The three-dimensional added mass method has yet to be developed, and the estimation method from Papanikolaou [25] can be used as a base for this method.

The first correction that should be made is to derive the three-dimensional added mass distribution from the two dimensional distribution given by Papanikolaou. Parameters such as x/L and B/L are probably of great importance here.

From here, one can go further in two ways: first, determine the sway forces and yaw moments using the newly developed added mass distribution and apply shallow water corrections to the obtained forces and moments for simulation on shallow water. Second, probably better but more complex to implement, is to use first correct the added mass distribution for shallow water, and then determine sway forces and yaw

moments from the shallow water added mass distribution. The correction of the distribution is three-dimensional as well, since calculations in chapter 9 showed that the added mass becomes more three-dimensional in shallow water.

10.2.3 Potential flow calculations on inland ships

During the validation study, difficulties arose from construction of the wake surface behind an inland ship. Especially if one needs the wake surface to leave the ship parallel to the flow, panels of the wake surface and the ship body will closely approach each other, with pressure discontinuities and unrealistic forces as the result. In the present study, the aft end (2.5 meter) was cut off the ship in order to overcome these problems. In doing so, the trailing edge line of the ship becomes more straight and the wake surface panels can no longer approximate panels in the stern region.

From the validation study for the Marin Inland Ship, it appeared that the calculated force only drop by a very small amount. It is therefore recommended to use this approach for potential flow calculations applied to inland ships. Probably, the method also works for other ships having a complex aft end, as long as the part that is to be cut off is not too long.

10.2.4 Inland ship resistance and propulsion estimation

Literature showed that first of all, no detailed method is available for resistance prediction of inland ships. The method of Holtrop and Mennen can be used an may give accurate results since inland ships are also part of the database, but the significant differences in dimensions, hull form and appendages ask for a method specifically developed for inland ships. The same applies to propulsion, since it is already known that shallow water has an significant effect on propulsion performance. The absence of an empirical estimation method of shallow water propulsions indicates that more research is required in this field.

Bibliography

[1] W. Beukelman. Lift and drag for a low aspect-ratio surface piercing wing-model in deep and shallow water. Technical report, TU Delft, 1993.

[2] E. Campana, L. Fabbri, and Claus D. Simonsen. An experimental study of the water depth effects on the kvlcc2 tanker. In *NATO RTO AVT-189 Specialists Meeting on Assessment of Stability and Control Prediction Methods for NATO Air and Sea Vehicles*, number RTO-MP-AVT-189-9, Portsdown West, UK, October 2011.

[3] W. Górski. The effect of limited depth and width of waterway on performance of ducted propeller. *Polish Maritime Research*, 2005.

[4] H. Graewe. Die querschnittgrößeines wasserführenden großschiffahrtskanals. *Die Wasserwirtschaft*, 1966.

[5] F. van der Knaap H. Blaauw. *Prediction of squat of ships sailing in restricted water*. Delft Hydraulics Laboratory, 1983.

[6] R.H.M. Huijsmans H. de Koning Gans and J. Pinkster. A method to predict forces on passing ships under drift. In R.F. Beck, editor, *proceeding of the NSH*, pages pp. 1–13, 2007.

[7] Y. Lee H. Sadakane, Y. Toda. The simplified formulas to predict the coefficient of added mass and yaw added moment of inertiaof ship in shallow water. *Journal of Japan Institute of Navigation*, 105:pp. 11–20, 2001.

[8] S. Harvald. Wake and thrust deduction at extreme propeller loadings for a ship running in shallow water. Technical report, Royal institution of naval architects, 1977.

[9] R. Hekkenberg. *Inland ships for efficient transport chains*. PhD thesis, TU Delft, 2013.

[10] M. Hirano. A practical calculation method of ship maneuvering motion at initial design state. *J.S.N.A.*, 147:pp. 68–80, June 1980.

[11] J. Holtrop and F. Mennen. An approximate power prediction method. *International Shipbuilding Progress*, 29:166–171, 1982.

[12] J. Holtrop, F. Mennen, and T. van Terwisga. Een empirisch model voor de weerstandspredictie van bakken. Technical Report 49791-1-RD, MARIN, August 1990.

[13] J. Hooft and F. Quadvlieg. Non-linear hydrodynamic hull forces derived from segmented model tests. In *MARSIM*, 1996.

[14] J. P. Hooft. The cross flow drag on a manoeuvring ship. *Ocean Engineering*, 21(3):329–342, April 1994.

[15] J. P. Hooft and U. Nienhuis. The prediction of the ship's manoeuvrability in the design stage. *SNAME Annual Meeting*, 102:1–24, November 1994.

[16] T. Jiang. A new method for resistance and propulsion prediction of the ship performance in shallow water. In *8th PRADS Symposium*, 2001.

[17] Tsutsui Y. Kijima K., Nakiri Y. and Matsunaga M. Prediction method of ship manoeuvrability in deep and shallow waters. In *MARSIM & ICSM 90*, pages pp. 311–318, Tokyo, Japan, 1990.

[18] E. Kobayashi. The development of practical simulation system to evaluate ship maneuverability in shallow water. In *Proceedings, PRADS95*, pages pp. 1712–1723, 1995.

[19] M. Hoekstra L. Eca. An evaluation of verification procedures for cfd applications. In *24th Symposium on Naval Hydrodynamics*, Fukuoka, 2002.

[20] H. Lackenby. The effect of shallow water on ship speed. *The ship builder and the marine engine builder*, september 1963.

[21] M. Li and X. Wu. Simulation calculation and comprehensive assessment on ship maneuverabilities in wind, wave, current and shallow water. In *Proceedings of MARSIM & ICSM 90*, pages pp 403–411, 459–465, 1990.

[22] S. Moriya M. Hirano, J. Takashina and Y. Nakamura. An experimental study on manoeuvring hydrodynamic forces in shallow water. *TWSNA*, 69:pp. 101–110, 1985.

[23] H. Munoz. A potential approach for drift angle viscous effects applied to passing ship events. Master's thesis, TU Delft, 2012.

[24] J.N. Newman. *Marine Hydrodynamics*. MIT, 1977.

[25] A. Papanikolaou. Hydrodynamische koeffizienten fr die linearen schwingungen von schwimmenden zylindern. Technical report, Techn. Univ., Inst. fr Schiffstechnik, 1979.

[26] P. Pompe. Some aspects about modeling inland shipping resistance and propulsion to estimate fuel consumption. *MoveIT presentation*, 2013.

[27] H. Raven. Invloeden van beperkt water op viskeuze weerstand en voortstuwingsfactoren van een schip. Technical report, MARIN, 1981.

[28] H. Raven. A computational study of shallow-water effects on ship viscous resistance. In *29th symposium on naval hydrodynamics*, Gothenburg, 2012.

[29] H. C. Raven. Towards a new shallow-water correction method for ship speed-power relations. Technical report, MARIN, 2012.

[30] K. Kijima S. Inoue, M. Hirano. Hydrodynamic derivatives on ship manoeuvring. In *International shipbuilding progress*, volume 28, May 1981.

[31] T. van Terwisga. Weerstand en voorstuwing van bakken; een literatuurstudie. Technical report, MARIN, 1989.

[32] S. L. Toxopeus. Validation of slender-body method for prediction of linear manoeuvring coefficients using experiments and viscous-flow calculations. In 7^{th} *ICHD International Conference on Hydrodynamics*, pages 589–598, Ischia, Italy, October 2006.

[33] S. L. Toxopeus. *Practical application of viscous-flow calculations for the simulation of manoeuvring ships*. PhD thesis, Delft University of Technology, May 2011.

[34] S. L. Toxopeus and S. W. Lee. Comparison of manoeuvring simulation programs for SIMMAN test cases. In *SIMMAN*, pages E56–61, Copenhagen, Denmark, April 2008.

[35] Serge Toxopeus. Viscous-flow calculations for kvlcc2 in deep and shallow water. In *International Conference on Computational Methods in Marine Engineering*, 2011.

[36] H. Verheij. Aantasting van dwarsprofielen in vaarwegen. Technical report, Delft Hydraulics Laboratory, 1986.

[37] D.G.M. Watson. *Practical ship design*. Gulf Professional Publishing, 2002.

Appendix A

Description of the DelKelv program

The program DelKelv, used for potential flow calculations described in chapters 8 and 9, is used as it is, so an extensive explanation of the program is omitted in the report itself. This appendix gives a slightly detailed described of the Delkelv program for interested readers. Brief descriptions are given here on the potential flow theory, panel method, involved boundary conditions, the Kutta condition and the determination of forces, moments and added mass.

A.1 Potential flow theory

In potential theory, the velocity field within a fluid domain is described as the gradient of a scalar function, the potential ϕ. This is only possible if the flow is irrotational:

$$\frac{\partial}{\partial \vec{x}} \times \vec{u} = \vec{0} \tag{A.1}$$

This leads to the definition of the potential function, of which the gradient gives the velocity field:

$$\frac{\partial \phi}{\partial x_i} = u_i \tag{A.2}$$

Which satisfies equation A.1. Then, from the fact that a potential flow is also incompressible, the potential function must satisfy the Laplace-equation:

$$\Delta\phi = \frac{\partial^2\phi}{\partial x^2} + \frac{\partial^2\phi}{\partial y^2} + \frac{\partial^2\phi}{\partial z^2} = 0 \tag{A.3}$$

The last assumption that should be made is that the flow must be inviscid; which is a result of the fact that the flow is, and remains, irrotational. This is directly one of the main drawbacks of potential theory, since it principally results in zero force for all calculations. Luckily, certain boundary conditions and modelling methods allow us to still derive non-zero forces from potential flow calculations. This is discussed in section A.4.

A potential flow problem can be solved in two ways; first, it is possible to discretize the full domain, resulting in a three-dimensional grid. This is a very straightforward method to solve potential flow problems, as it is only a simplification of a viscous CFD calculation. Another, more efficient, method, is to convert the three dimensional problem into a two-dimensional problem using Green's Theorem. This is the basis for the panel method, which is explained in the next section.

A.2 The panel method

The panel method is a very strong tool to solve potential flow problems, since the complexity of the calculations is greatly reduced (apart from the fact that viscous effects were already neglected). As mentioned in the previous section, the basis of the panel method is that the three-dimensional potential flow problem is converted to a two-dimensional problem using Green's theorem:

$$\iiint_V (\phi\Delta\Psi - \Psi\Delta\phi)\, dV = \iint_\Omega \left(\phi\frac{\partial\Psi}{\partial n} - \Psi\frac{\partial\phi}{\partial n}\right) d\Omega \tag{A.4}$$

In which ϕ is a potential function, and

$$\Psi = \frac{-1}{4\pi r} \tag{A.5}$$

Equation A.5 applies in this case, since the free surface is omitted in this study. If a free surface is included in the problem Ψ will be a more complex function. Including the free surface may cause complex, non-linear effects, and is therefore omitted in this study. Since ϕ is a potential function, the second term on the left hand side will vanish according to equation A.3. Now, it is possible to rewrite equation A.4 into:

$$p\phi(P) = \frac{1}{4\pi} \iint_{\Omega} \left(\phi(Q) \frac{\partial}{\partial n_Q} \left(-\frac{1}{r} \right) - \frac{-1}{r} \frac{\partial \phi}{\partial n_Q} \right) d\Omega \tag{A.6}$$

In which

$$p = \begin{cases} 0 \text{ For } P \text{ outside } V \\ \frac{1}{2} \text{ For } P \text{ on } \Omega \\ 1 \text{ For } P \text{ inside } V \end{cases} \tag{A.7}$$

A source term and a dipole can be recognized in equation A.6, which are $\partial\phi/\partial n = \sigma$ and ϕ respectively. In the present study, the source term distribution over the geometry is known ($\sigma = \vec{V} \cdot \vec{n}$ so by solving A.6 for the dipole terms, the potential distribution in the whole domain can be computed. Off course, interest is present for solving the potential on the ship hull specifically.

Equation A.6 is rewritten into the Fredholm equation of the second kind, then discretized over panels, which together form the ship body and the boundaries of the fluid domain. Each of the panels in the computational domain is assigned a collocation point, which in this case is located at the center of the panels. DelKelv determines the 'Hydrodynamic Influence Coefficients' for all of these collocation points, for both the sources and the dipoles. A hydrodynamic influence coefficient is a coefficient of the influence one panel has at another panel. A certain point is influenced by all panels, however the panels at great distance from the point have less influence than panels close to the point's location.

After discretization, a system of equations is the result, where hydrodynamic influence coefficients are denoted by hic_{ij}. The system of equations is shown in A.8. An infinite number of solutions would exist if the system is not subject to various boundary conditions, which are explained in the next section.

$$\frac{1}{2}\begin{bmatrix}\phi_1\\ \vdots\\ \phi_N\end{bmatrix} + \begin{bmatrix} hic_{11} & \dots & hic_{1N}\\ \vdots & \ddots & \vdots\\ hic_{N1} & \dots & hic_{NN}\end{bmatrix}_{dip}\begin{bmatrix}\phi_1\\ \vdots\\ \phi_N\end{bmatrix} = \begin{bmatrix} hic_{11} & \dots & hic_{1N}\\ \vdots & \ddots & \vdots\\ hic_{N1} & \dots & hic_{NN}\end{bmatrix}_{src}\begin{bmatrix}\frac{\partial\phi}{\partial n_1}\\ \vdots\\ \frac{\partial\phi}{\partial n_N}\end{bmatrix} \tag{A.8}$$

A.3 Boundary conditions

The problem is subject to a single type of boundary condition; only von Neumann boundary conditions are applied at the ship hull, the channel bottom and the channel sides. This boundary condition essentially stands for the no-leakage condition (normal velocity on a panel equal to the panel velocity):

$$\frac{\partial\phi}{\partial n_P} = \vec{V}_P \cdot \vec{n}_P \tag{A.9}$$

For the channel bottom and sides, the right hand side of equation A.9 is zero. For the ship, the velocity on the right hand side is equal to the ship speed.

With only the channel bottom, sides and the ship body, the fluid domain is not fully enclosed yet. At the front and aft end of the domain, the potential value at infinity is applied. In the present study, the potential is zero at infinity: $\phi = 0$ for $r \to \infty$. This means that the fluid domain needs to be long enough, so that the hydrodynamic influence of the panels at the channel ends on the ship body panels is practically zero.

Then, the free surface remains. This free surface is omitted, as stated in section A.2, so the free surface with panels will not close the fluid domain. It is not possible to use the condition at infinity here as well, since the top panels of the ship are located against the free surface. Another method is chosen instead, namely using two symmetrical solutions. The whole fluid domain is mirrored about the horizontal plane at $z = 0$, resulting in a closed domain in all directions. Mirroring does not increase the amount of equations to be solved, as the solution of the mirrored part of the problem is exactly the same as the original one. In fact, it can increase the quality of the results, since there are no discretization errors arising from the free

surface now. The ends of the channel are still open, but the condition at infinity can be applied here.

Now that there is a closed fluid domain, the problem can be solved. However, the problem as described so far will not yield any forces. To overcome this, a wake surface must be modelled. This is explained in A.4.

A.4 The Kutta condition in potential flows

As mentioned, a potential flow calculation will normally not result in forces acting on the body, apart from the so-called Munk Moments. This is due to the fact that in an inviscid flow, the flow is able to leave the body at a location such that the integral of the pressure on the body becomes zero. In a real, viscid flow, the flow will leave the body at the trailing edge (the aft tip of a wing, for example), since the flow is not able to move around the sharp tip and leave the body elsewhere. When the flow leaves the body at the trailing edge, the Kutta condition is established. As the flow is not able to leave the body at a point other than the trailing edge, circulation around the body is generated if the body is given a certain drift angle. This circulation results in a lift force.

In potential flows, the Kutta condition can be established at the trailing edge of a body by modeling a wake surface attached to that location. At this wake surface, the no-leakage condition ($\partial\phi/\partial\vec{n} = 0$) applies, meaning the flow must be parallel to the wake surface. This means the flow will leave the body at exactly the location where the wake is attached.

The location where the wake is to be attached depends on the shape of the body. For a two-dimensional wing, a wake surface attached to only the trailing edge is usually sufficient. For ships under drift - which in practice may be seen as low-aspect ratio wings - a wake surface could also be attached at the bilges since a significant amount of circulation is lost by flow passing the ship underneath.

A.5 Determination of forces and moments

After the problem is solved, a potential distribution over the channel bottom, sides and the ship hull is determined. From this distribution, the pressures on the ship hull

need to be determined in order to obtain forces. First, the pressures are obtained from Bernouilli's formula:

$$\frac{p}{\rho} + \frac{\partial \phi}{\partial t} + \frac{1}{2} < \nabla\phi \cdot \nabla\phi > + gz = \frac{p_\infty}{\rho} \tag{A.10}$$

Integrating the pressure obtained using equation A.10, forces and moments can be determined:

$$\begin{aligned} < F_X, F_Y, F_Z > &= -\iint\limits_\Omega p\vec{n} d\Omega \\ < M_{XX}, M_{YY}, M_{ZZ} > &= -\iint\limits_\Omega p < \vec{x}_\Omega \times \vec{n}_\Omega > d\Omega \end{aligned} \tag{A.11}$$

A.6 Determination of added mass

Apart from forces and moments, of which the determination methods are described in the previous section, it is also possible to determine added mass using potential flow calculations. Added mass is an inertial effect, so the absence of viscous effects does not affect added mass significantly (although it is known that lateral added mass slightly changes with forward speed). Determination of added mass using potential flow is not new, there exist a variety of diffraction codes that can determine added mass. But it is also interesting to investigate the possibilities of added mass estimations in the present method of potential flow solving.

Newman [24] already mentioned how added mass can be determined from the time-derivative of the potential distribution:

$$m_{yy} \cdot \dot{\vec{u}}_S = \rho \iint\limits_\Omega \frac{\partial \phi}{\partial t} n_y d\Omega \tag{A.12}$$

For $\dot{\vec{u}}_S =< 0, 1, 0 >$. Other added mass values like m_{xy} or m_{xx} can be determined by taking a different $\dot{\vec{u}}_S$ or changing the normal n_y. For rotational added mass, m_{rx}, m_{ry} or m_{rr}, a different approach is required:

$$m_{rr} \cdot \dot{\vec{u}}_S = \rho \iint\limits_\Omega \frac{\partial \phi}{\partial t} \begin{vmatrix} r_{xx} & r_{yy} \\ n_x & n_y \end{vmatrix} d\Omega \tag{A.13}$$

For $\dot{\vec{u}}_S =< 0, 0, 1 >$. In this report, the added mass values obtained using the

methods described above are validated against diffraction code results that are known to be correct. The only added mass values of interest in this report are m_{yy} and m_{rr}, as the other added mass values do not have a large effect on ship manoeuvring.

Obtaining added mass values from DelKelv required a different interpretation of the program input and results. Normally, the input for DelKelv is a steady velocity, while the result is a distribution of the potential value over the modelled surfaces. For added mass, the input should be interpreted as acceleration ($\dot{\vec{u}}_S$), which will give the distribution time derivative of the potential ($\partial\phi/\partial t$) as result. Now, the required parameters to evaluate equations A.12 and A.13. This all is possible, since the potential problem is a geometrical problem.

This method of added mass determination is very useful for nonsteady potential calculations, like the simulation of a complete ship manoeuvre in a potential flow. Results of potential flow calculations for added mass are shown in chapter 9.

Appendix B

Comparisons between CFD and Potential flow

This appendix shows the remaining comparisons between CFD calculations and potential flow calculations for the KVLCC2 and the MARIN Inland Ship.

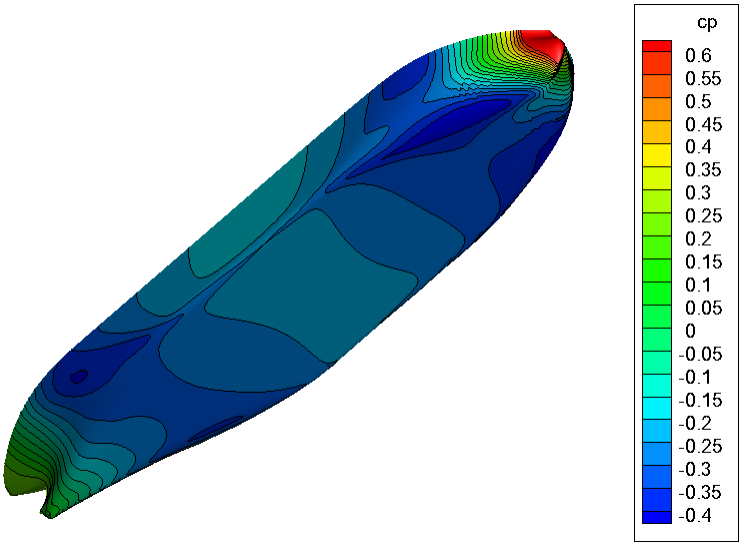

Figure B.1: Pressure coefficient plot for KVLCC2 pressure side at $\beta = 4$ and $h = 31.2$ based on CFD calculations

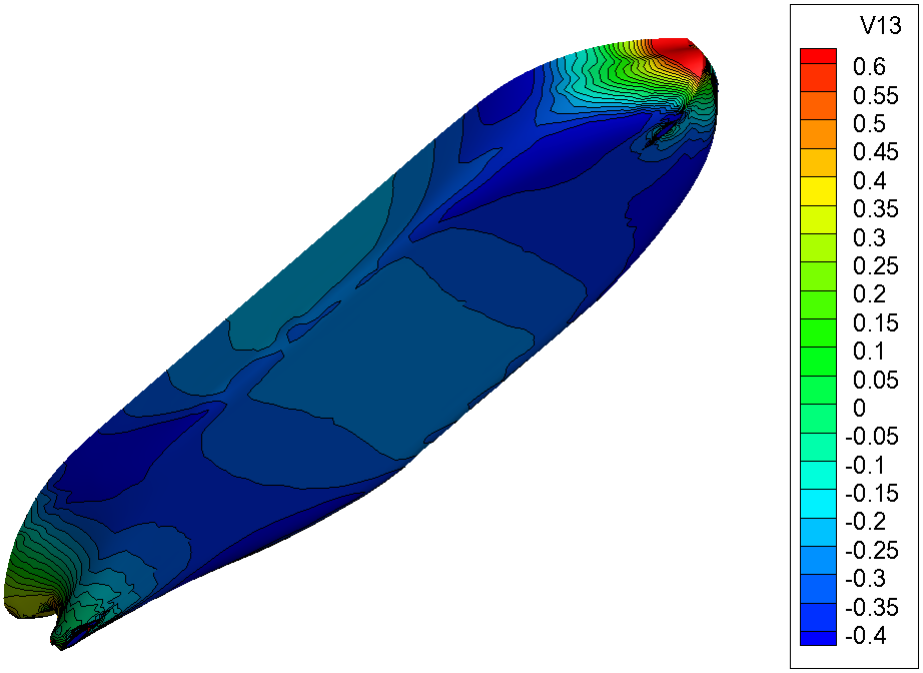

Figure B.2: Pressure coefficient plot for KVLCC2 pressure side at $\beta = 4$ and $h = 31.2$ based on DelKelv calculations using only a wake surface at trailing edge

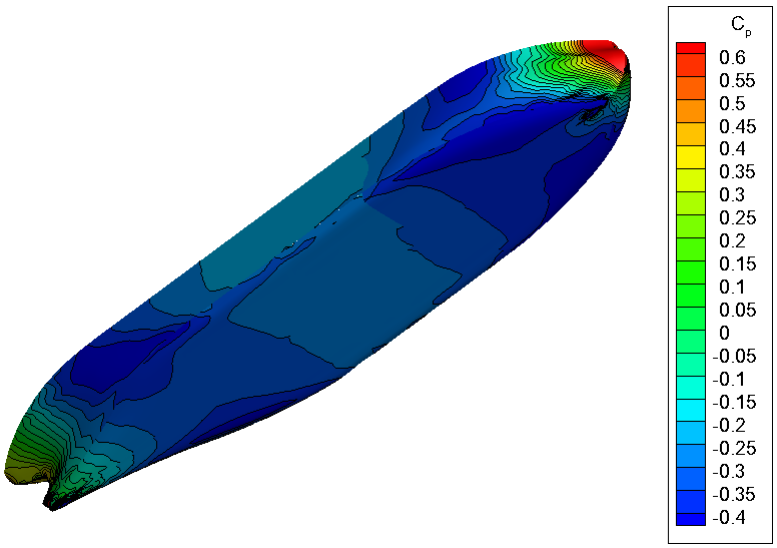

Figure B.3: Pressure coefficient plot for KVLCC2 pressure side at $\beta = 4$ and $h = 31.2$ based on DelKelv calculations using a wake surfaces at trailing edge and lee-side bilge

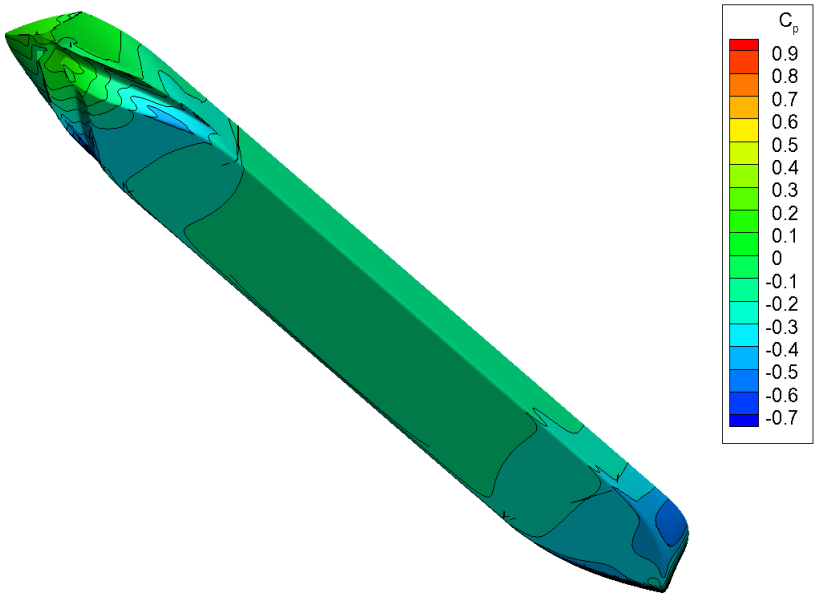

Figure B.4: Pressure coefficient plot for MIS at $\beta = 5$ and $h = 4.90$ based on CFD calculations, viewed from lee side

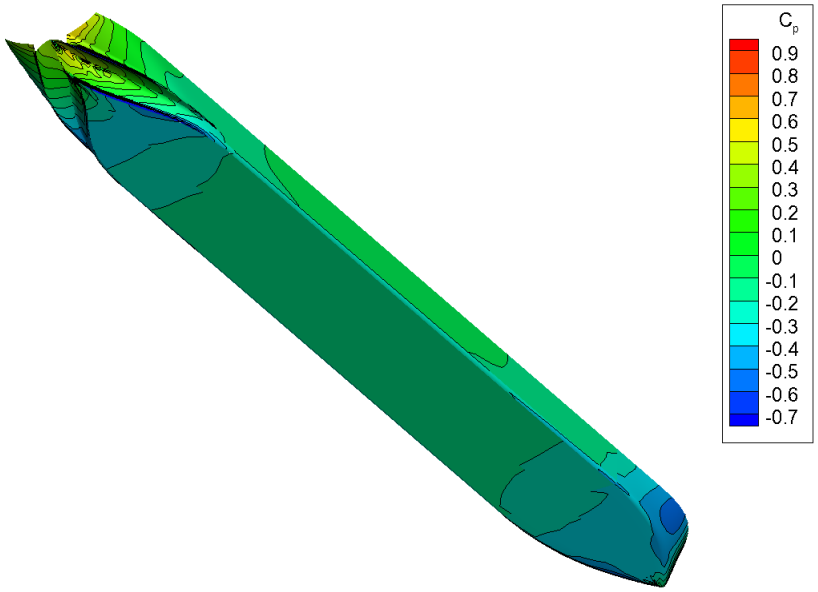

Figure B.5: Pressure coefficient plot for MIS at $\beta = 5$ and $h = 4.90$ based on DelKelv calculations using only a wake surface at trailing edge, viewed from lee side

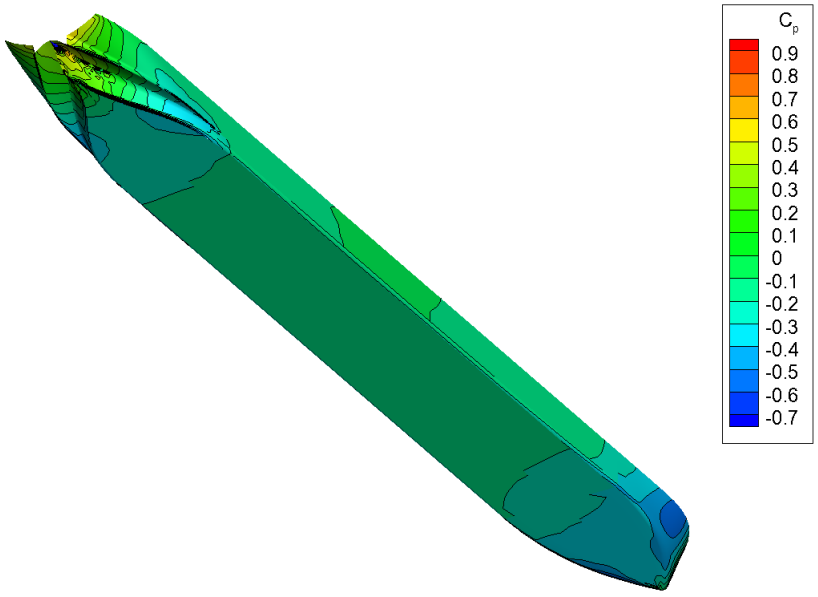

Figure B.6: Pressure coefficient plot for MIS at $\beta = 5$ and $h = 4.90$ based on DelKelv calculations using a wake surfaces at trailing edge and lee-side bilge, viewed from lee side